

Learning to control non-equilibrium dynamics using local imperfect gradients

Carlos Floyd,* Aaron R. Dinner, and Suriyanarayanan Vaikuntanathan†

The Chicago Center for Theoretical Chemistry, The University of Chicago, Chicago, Illinois 60637, USA

Department of Chemistry, The University of Chicago, Chicago, Illinois 60637, USA and

The James Franck Institute, The University of Chicago, Chicago, Illinois 60637, USA

(Dated: April 8, 2024)

Standard approaches to controlling dynamical systems involve biologically implausible steps such as backpropagation of errors or intermediate model-based system representations. Recent advances in machine learning have shown that “imperfect” feedback of errors during training can yield test performance that is similar to using full backpropagated errors, provided that the two error signals are at least somewhat aligned. Inspired by such methods, we introduce an iterative, spatiotemporally local protocol to learn driving forces and control non-equilibrium dynamical systems using imperfect feedback signals. We present numerical experiments and theoretical justification for several examples. For systems in conservative force fields that are driven by external time-dependent protocols, our update rules resemble a dynamical version of contrastive divergence. We appeal to linear response theory to establish that our imperfect update rules are locally convergent for these conservative systems. For systems evolving under non-conservative dynamics, we derive a new theoretical result that makes possible the control of non-equilibrium steady-state probabilities through simple local update rules. Finally, we show that similar local update rules can also solve dynamical control problems for non-conservative systems, and we illustrate this in the non-trivial example of active nematics. Our updates allow learning spatiotemporal activity fields that pull topological defects along desired trajectories in the active nematic fluid. These imperfect feedback methods are information efficient and in principle biologically plausible, and they can help extend recent methods of decentralized training for physical materials into dynamical settings.

I. INTRODUCTION

Modern machine learning techniques have enabled unprecedented advancements in pattern recognition, decision making, generative data synthesis, and numerous other tasks [1]. Efficiently training models with a large number of parameters has been key for this progress, and the predominant training method involves recursively computing gradients of a global error function through automatic differentiation algorithms like backpropagation. There is a conceptual tension, however, between this successful procedure for training artificial neural networks and our current knowledge of how synaptic weights in the brain are updated [2]. Automatic differentiation of a global cost function requires knowing weights which are arbitrarily far downstream of a given unit. This represents a top-down approach to training which is not biologically plausible given the local connectivity and plasticity mechanisms of actual neurons.

This tension has motivated research into alternative training algorithms which avoid exact computation of a global cost function’s derivatives [2, 3]. In the context of a feedforward neural network architecture, recent work has shown that severe approximations to the “correct” gradient signal, even including a fixed random backward weight layer, can successfully be used during training if combined with accurate forward passes through the model [4]. This principle of using imperfect, but easily accessible, error gradients has recently been leveraged

to train real physical systems to act as machine learning models by using approximate differentiable simulations of the forward path to compute the error gradient [5]. More broadly, the feedforward architecture can be replaced with distributed systems, such as heterogeneously parameterized networks of springs or resistors [6–8]. These systems evolve under physical dynamics to minimize some variational quantity, such as the total elastic energy or steady-state power dissipation [9]. The steady-states of these physical systems can be interpreted as outputs which represent computations done on a set of input variables of the system, and this computation can be trained by iteratively nudging the parameters to lower the variational quantity for the desired output in response to a given input.

Although recent works have studied how local update rules based on variational quantities can compute functions on static sets of data in non-equilibrium settings [10, 11], they have not explored how these local update rules can be used to control non-equilibrium dynamics (Figure 1A). One can draw a parallel between backpropagation for training machine learning models, which requires a global cost function and non-local propagation of information, and optimal control [12], which similarly uses numerical descent of a global cost function and requires complete model specification to work (Figure 1B). Much recent progress has been made in formulating and solving optimal control strategies for non-equilibrium dynamics, often with the aim of minimizing the heat dissipated by the trajectory [13–22]. Additionally, related works have successfully leveraged reinforcement learning (RL) to find control policies that guide active matter systems into desired dynamical states [23, 24]. These

* csfloyd@uchicago.edu

† svaikunt@uchicago.edu

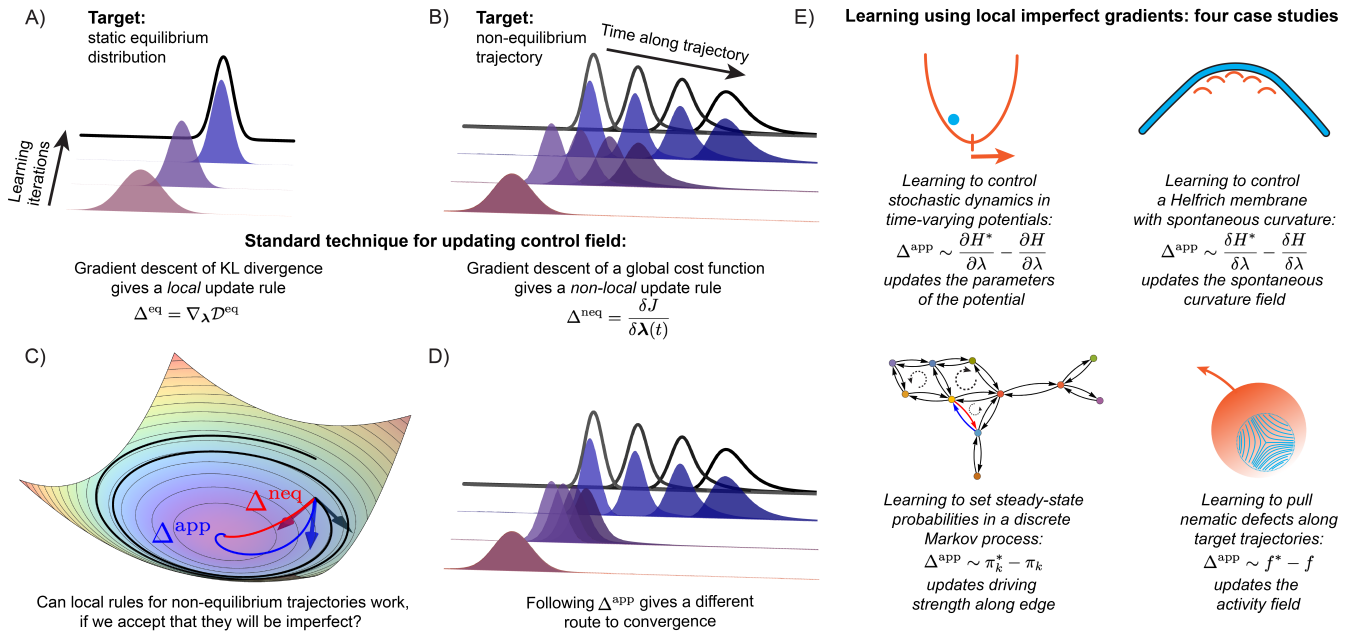


FIG. 1. Using imperfect gradients to solve inverse problems of non-equilibrium control. A) A classic learning problem is to fit the parameters of a model distribution (purple-blue) to that of a target (black). This can be solved by flowing the parameters down the gradient of the Kullback-Leibler divergence between the two distributions. B) In a dynamical setting, the objective is to fit a non-equilibrium trajectory of distributions to a given target trajectory. This is commonly achieved using a non-local cost function J of the entire trajectory. C) Illustration of the approximate update rule Δ^{app} acting as a descent direction with respect to the “correct” gradient Δ^{neq} . The black arrow has a negative dot product with Δ^{neq} and hence does not act as a descent direction. D) Same as the dynamical learning task in panel A, but illustrating that following the approximate gradient Δ^{app} yields a different route to convergence. E) Four case studies examined in this paper.

approaches to non-equilibrium control yield highly optimized policies, but as a downside they involve biologically implausible steps such as perfect model specification, backpropagation of errors, non-local update rules based on global cost functions, or a long-term memory of previous control attempts. We thus ask whether ideas for training machine learning systems using local, approximate update rules can be brought to bear on the problem of guiding non-equilibrium trajectories. An answer to this question can have biological implications, helping bridge the gap between our current understanding of active matter systems and the types of regulatory feedback network that living organisms use to regulate these systems and carry out physiological functions [25]. Additionally, it can help to generalize recent ideas for training physical materials with decentralized learning and simple, local update rules into non-equilibrium, time-varying settings [3, 11, 26].

Here, we introduce a set of spatiotemporally local learning rules to guide non-equilibrium systems along desired dynamical trajectories. We make minimal use of the knowledge of the system’s dynamics and parameters, instead relying on local comparisons of some (presumed accessible) observable for the system, such as its free energy density or probability density. Our local update rules can be loosely viewed as flowing down an ap-

proximation to the gradient of an optimal control cost function and hence we dub these updates “imperfect,” in analogy to the above mentioned imperfect error signals that can be used in place of backpropagation to train machine learning models (Figure 1C and D). We consider both non-autonomous conservative systems (which obey detailed balance but have parameters varied at finite speed) and non-conservative systems (which break detailed balance), and we use numerical experiments to illustrate the local update rules in several examples of increasing complexity. These include a particle trapped in a moving confining potential, a Helfrich membrane with a time-varying spontaneous curvature field, a driven first-order chemical reaction network, and, finally, an active nematic fluid (Figure 1E). In the last system, we demonstrate that a surprisingly simple update rule based on differences in free energy density can successfully train a spatiotemporal activity protocol to pull nematic defects along a desired trajectory [27]. Taken together, the results in this paper suggest ways for using local learning rules in a broad class of non-equilibrium physical systems and machine learning models.

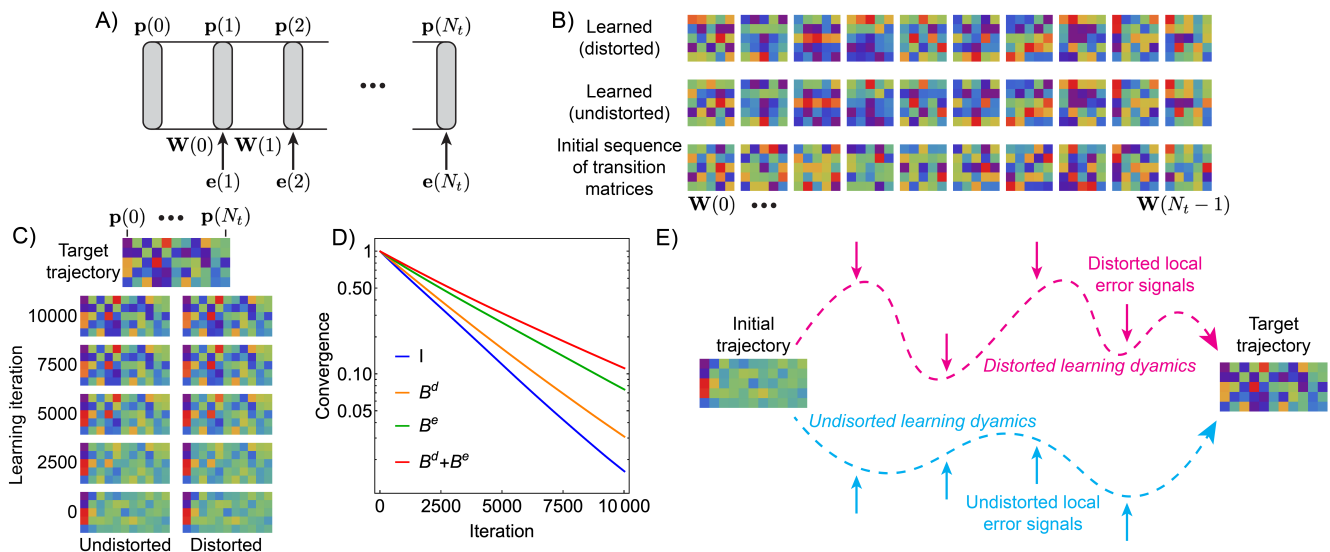


FIG. 2. Learning to control Markovian chain dynamics. A) Illustration of the system in Section II of this paper. Gray columns indicate vectors with labels given above, and lines connecting columns indicate matrices with labels given below. Error signals are provided according to the drawn arrows. B) Depiction of the sequence of transition matrices $\{\mathbf{W}(t)\}_{t=0}^{N_t-1}$, learned using distorted (with \mathbf{B}^d) and undistorted error signals, and starting from the same initial sequence. Colors range from violet to red for increasing values of W_{ij} . Inspection reveals that two learned sequences are not identical even though they start from the same initial sequence. C) Depiction of the trajectory of probability vectors $\{\mathbf{p}^n(t)\}_{t=0}^{N_t}$ obtained along the distorted and undistorted learning trajectories, for the same trial as in panel B. Inspection reveals that the two learning processes produce final trajectories that are nearly identical to each other and match the target. D) Plot of the convergence, defined as $\mathcal{L}_T^n / \mathcal{L}_T^0$, as learning progresses using different error signals. The legend indicates which distortion matrices are used for each protocol, with I indicating undistorted errors. E) Schematic illustration of the different learning trajectories which arrive at the same point of convergence.

II. A PRIMER: LEARNING TO CONTROL NON-EQUILIBRIUM MARKOV CHAIN DYNAMICS WITH LOCAL, DISTORTED FEEDBACK

Many open-loop control techniques rely on cost functions which integrate over the duration of a dynamical trajectory and are hence global in nature [12]. We wish to explore alternative approaches in which temporally local, imperfect feedback is used instead. As a motivating example, we first consider a Markov chain specified by a discrete sequence $\{\mathbf{W}(t)\}_{t=0}^{N_t-1}$ of stochastic transition matrices which transform an initial probability vector $\mathbf{p}(0)$ into a final vector $\mathbf{p}(N_t)$ (Figure 2A). We show that it is possible to learn a Markov chain which produces a given trajectory using temporally local error signals, and we then show that one can go further and systematically distort these local error signals without preventing convergence of the learning algorithm. This problem is inspired by Ref. 4, where imperfect feedback of errors was used to avoid backpropagation when learning the parameters of a shallow neural network model (see SI Section IA).

We aim to learn a trajectory $\{\mathbf{p}^*(t)\}_{t=0}^{N_t}$ through probability space, assuming that $\mathbf{p}^*(0)$ is given. We wish to avoid biologically implausible backpropagation of er-

rors through time, so that during the n^{th} learning iteration at time t we do not use any knowledge of the errors $\mathbf{e}^n(t') = \mathbf{p}^*(t') - \mathbf{p}^n(t')$ for $t' > t + 1$. This causes our learning dynamics to be temporally local, such that each matrix $\mathbf{W}^n(t-1)$ greedily aims to connect $\mathbf{p}^n(t-1)$ to $\mathbf{p}^*(t)$ without consideration of downstream ($t' > t$) losses. We show in SI Section IB that even though $\mathbf{W}^n(t)$ flows down the gradient of these local loss functions $\mathcal{L}^n(t) = \frac{1}{2}(\mathbf{e}^n(t))^\top \mathbf{e}^n(t)$, rather than the global loss function $\mathcal{L}_T^n = \sum_t \mathcal{L}^n(t)$, convergence is still guaranteed over the entire trajectory. Intuitively, this happens as the matrix $\mathbf{W}^n(0)$ first learns to connect the given $\mathbf{p}^*(0)$ to $\mathbf{p}^*(1)$, after which $\mathbf{W}^n(1)$ has the right starting point and can learn to connect $\mathbf{p}^*(1)$ to $\mathbf{p}^*(2)$, and so on. Figures 3C and F of the next section illustrates how in practice convergence happens faster than this “worst-case” scenario, such that later times in the trajectory have useful learning updates even before earlier times have fully converged.

We next consider the effect of systematically distorting these local loss gradients $\nabla_{\mathbf{W}(t-1)} \mathcal{L}^n(t)$ using a set of fixed random matrices $\mathbf{B}^e(t)$ and $\mathbf{B}^d(t)$. We study two ways of doing this: one in which our error vectors are distorted as $\mathbf{e}^n(t) \rightarrow \mathbf{B}^e(t)\mathbf{e}^n(t)$, and one in which our knowledge about the dynamics is distorted as $\nabla_{\mathbf{W}(t-1)} \mathcal{L}^n(t) \rightarrow \mathbf{B}^d(t)\nabla_{\mathbf{W}(t-1)} \mathcal{L}^n(t)$. In SI Sections

IC-E we show analytically and numerically that these distortions to the gradient do not prevent convergence provided that $\mathbf{B}^e(t)$ has positive eigenvalues and $\mathbf{B}^d(t)$ is positive definite. These analytical constraints illustrate, for these Markov chain dynamics, the kinds of conditions under which local learning can work in more general dynamical settings, even in the presence of systematic errors. We further find that these two modes of distorting the gradient have qualitatively different effects on the convergence rate: $\mathbf{B}^e(t)$ affects convergence according to its minimum eigenvalue, which controls the slowest relaxation mode, whereas $\mathbf{B}^d(t)$ affects convergence of all modes uniformly according to its Rayleigh quotient with $\mathbf{p}^n(t-1)$. Figures 2B-E illustrate the fact that the distorted and undistorted learning dynamics both converge to the same solution, but along different paths and with a different final set of degenerate transition matrices $\{\mathbf{W}(t)\}_{t=0}^{N_t-1}$ which both effectively produce the same trajectory $\{\mathbf{p}^N(t)\}_{t=0}^{N_t}$ which matches the target $\{\mathbf{p}^*(t)\}_{t=0}^{N_t}$ (see also Figure 1C). This is similar to how the distorted feedback matrices in Ref. 4 yield different neural network parameters which nevertheless achieve validation results comparable to those obtained from parameters trained without distortion, using full backpropagation.

The Markov chains considered here can encompass many systems of interest and motivate how a to learn dynamics with local, error-prone rules. However, Markov chains are a fairly abstract representation of physical dynamics. We next consider how these principles of imperfect and local feedback can be used to guide dynamical trajectories using more concrete physical models. We first consider in Section III a class of non-equilibrium dynamics in which a conservative system is driven out of equilibrium due to non-autonomous variation of Hamiltonian parameters $\lambda(\mathbf{r}, t)$. After that, in Section IV we consider systems driven by non-conservative forces that are parameterized by an activity protocol $\alpha(\mathbf{r}, t)$. In both classes of non-equilibrium systems we take the same concrete learning problem, in which the goal is to reconstruct a target trajectory of the system $\mathbf{q}^*(\mathbf{r}, t)$ by iteratively running a forward pass through the physical dynamics to generate trial trajectories $\mathbf{q}^n(\mathbf{r}, t)$ and then updating the driving protocol $\lambda^n(\mathbf{r}, t)$ (or $\alpha^n(\mathbf{r}, t)$) using an imperfect, spatiotemporally local update rule.

III. LEARNING TO CONTROL CONSERVATIVE, NON-AUTONOMOUS SYSTEMS

Learning desired dynamics in time-varying environments is a problem that is encountered in many biological and synthetic contexts [25]. For conservative systems (which obey detailed balance), the problem can be generically posed as follows. We consider a system described by a Hamiltonian $H(\mathbf{q}; \lambda(t))$, where \mathbf{q} are the system degrees of freedom and $\lambda(t)$ is a set of non-autonomously controlled parameters. These could represent, for instance,

parameters describing a fitness landscape in an immune or evolutionary context [15, 28, 29], parameters describing molecular interactions in a colloidal self-assembly context [23, 30], or the location and stiffness of an optical trap manipulating a small particle [19, 20]. At equilibrium with fixed λ , the probability of the system obeys the Boltzmann distribution $p_{\lambda}^{\text{eq}}(\mathbf{q}) = Z(\lambda)^{-1} e^{-\beta H(\mathbf{q}; \lambda)}$ where $Z(\lambda)$ is the partition function and $\beta = 1/k_B T$. Viewing λ as learnable parameters, we wish to solve the inverse problem of reconstructing a target probability trajectory. We assume this trajectory $p^*(\mathbf{q}, t) = p_{\lambda^*(t)}(\mathbf{q})$ has been generated by evolving stochastic dynamics of the form

$$\partial_t p(\mathbf{q}, t) = \mu \partial_{\mathbf{q}} \cdot (\partial_{\mathbf{q}} H(\mathbf{q}; \lambda(t)) p(\mathbf{q}, t)) + D \partial_{\mathbf{q}}^2 p(\mathbf{q}, t) \quad (1)$$

under the protocol $\lambda^*(t)$. In these dynamics the mobility μ is related to the diffusion D and inverse thermal energy β by the Einstein relation $\mu = \beta D$. We aim to construct a temporally local rule to iterate our guess for the protocol $\lambda(t)$.

A natural cost function to consider is the Kullback-Leibler (KL) divergence $\mathcal{D}[p_{\lambda^*(t)} || p_{\lambda^n(t)}] \equiv \int d\mathbf{q} p_{\lambda^*(t)} \ln p_{\lambda^*(t)} / p_{\lambda^n(t)}$ between the target trajectory $p_{\lambda^*(t)}$ and the trajectory under the n^{th} learning iteration $p_{\lambda^n(t)}$. The difficulty in computing the gradient of this cost function with respect to the parameters λ is due to the fact that when the system is not at equilibrium with the parameters $\lambda(t)$, then $p_{\lambda(t)}$ deviates from the Boltzmann distribution and the gradient may not have a tractable form. Formally writing the non-equilibrium distribution in a Boltzmann-like form $p_{\lambda^n(t)} \propto e^{-\beta \tilde{H}(\mathbf{q}; \lambda^n(t))}$, the local gradient of the KL divergence can be expressed as

$$\begin{aligned} \Delta^{\text{neq}} &\equiv \frac{\partial \mathcal{D}[p_{\lambda^*(t)} || p_{\lambda^n(t)}]}{\partial \lambda} \\ &= \left\langle \beta \frac{\partial \tilde{H}(\mathbf{q}; \lambda^n(t))}{\partial \lambda} \right\rangle_{p_{\lambda^*(t)}} - \left\langle \beta \frac{\tilde{H}(\mathbf{q}; \lambda^n(t))}{\partial \lambda} \right\rangle_{p_{\lambda^n(t)}} \quad (2) \end{aligned}$$

where $\tilde{H}(\mathbf{q}; \lambda^n(t))$ is the generally unknown exponential weight of $p_{\lambda^n(t)}$. We use the shorthand notation $\partial_{\lambda} H(\mathbf{q}; \lambda^n(t)) \equiv \partial_{\lambda} H(\mathbf{q}; \lambda)|_{\lambda=\lambda^n(t)}$. As elaborated in SI Section IIA, if the protocols are quasi-static then this difficulty of determining \tilde{H} disappears, and the gradient simplifies to

$$\begin{aligned} \Delta^{\text{eq}} &\equiv \frac{\partial \mathcal{D}[p_{\lambda^*(t)}^{\text{eq}} || p_{\lambda^n(t)}^{\text{eq}}]}{\partial \lambda} \\ &= \left\langle \beta \frac{\partial H(\mathbf{q}; \lambda^n(t))}{\partial \lambda} \right\rangle_{p_{\lambda^*(t)}^{\text{eq}}} - \left\langle \beta \frac{H(\mathbf{q}; \lambda^n(t))}{\partial \lambda} \right\rangle_{p_{\lambda^n(t)}^{\text{eq}}} \quad (3) \end{aligned}$$

where \tilde{H} has been replaced with the known Hamiltonian H . The quasi-static assumption thus allows breaking the dynamical problem into a set of independent problems to which one can apply standard contrastive learning tech-

niques based on equilibrated distributions, allowing use of H in the gradient. In SI Section IIB, we illustrate this further using the KL divergence evaluated over path probabilities as an alternative cost function.

If the parameters are changed at finite speed (i.e., not quasi-statically) then a *lag* develops between the non-equilibrium distribution $p_{\lambda(t)}(\mathbf{q})$ and the instantaneous equilibrium distribution $p_{\lambda(t)}^{\text{eq}}(\mathbf{q})$ [31]. Despite this lag, as an approximation to Equation 59 we can replace averages over the quasi-static distributions with averages over the actual non-equilibrium distributions:

$$\Delta^{\text{app}} \equiv \left\langle \beta \frac{\partial H(\mathbf{q}; \boldsymbol{\lambda}^n(t))}{\partial \boldsymbol{\lambda}} \right\rangle_{p_{\boldsymbol{\lambda}^n(t)}} - \left\langle \beta \frac{\partial H(\mathbf{q}; \boldsymbol{\lambda}^n(t))}{\partial \boldsymbol{\lambda}} \right\rangle_{p_{\boldsymbol{\lambda}^*(t)}} \quad (4)$$

This update can also be obtained from Equation 2 by replacing the unknown weight $\tilde{H}(\mathbf{q}; \boldsymbol{\lambda})$ with the Hamiltonian $H(\mathbf{q}; \boldsymbol{\lambda})$. One can view Equation 4 as representing the difference between the thermodynamic force $-\partial H/\partial \boldsymbol{\lambda}$ expected from the target trajectory and that experienced during the n^{th} trial. This difference is used to inform the update to $\boldsymbol{\lambda}^n(t)$, causing the work increment $(\partial H/\partial \boldsymbol{\lambda}) \cdot \dot{\boldsymbol{\lambda}}^n(t) dt$ done during the n^{th} trial to approach that done at the same time during the target trajectory. Although Δ^{app} is imperfect, it has the correct fixed point at $p_{\boldsymbol{\lambda}^*(t)} = p_{\boldsymbol{\lambda}^n(t)}$. If Δ^{app} additionally has a positive overlap with Δ^{neq} , then it will act as a descent direction [32] with respect to Δ^{neq} and will converge to the shared fixed point (Figure 1C). In SI Section IIC we consider a system that is close to equilibrium, so that it can be treated in the framework of linear response theory, to show that flows down Δ^{app} indeed converge to $\boldsymbol{\lambda}^*(t) = \boldsymbol{\lambda}^n(t)$ within a neighborhood of the fixed point.

We emphasize that the gradient Δ^{app} is temporally local, in that no information of the future ($t' > t$) effects of changing $\boldsymbol{\lambda}(t)$ are needed to use the update rule

$$\boldsymbol{\lambda}^{n+1}(t) \leftarrow \boldsymbol{\lambda}^n(t) - \eta \Delta^{\text{app}}, \quad (5)$$

where η is a scalar learning rate. We next demonstrate the feasibility of using this update rule for a simple physical system.

A. Case study: Bead in a time-dependent potential

Here we use Equation 5 to learn a protocol for pulling a bead with a movable harmonic trap at position $\lambda(t)$ with stiffness k (Figure 3A). We non-dimensionalize the Fokker-Planck dynamics using the thermal length scale $l = (\beta k)^{-1/2}$ and the relaxation time $\tau = 1/k\mu$, redefining $pl \rightarrow p$, $q/l \rightarrow q$, $\lambda/l \rightarrow \lambda$, and $t/\tau \rightarrow t$. This 1D system is a simple illustrative example of a broader class of systems whose degrees of freedom \mathbf{q} are subject to linear forces $\mathbf{K}(\mathbf{q} - \mathbf{a})$. Analytical expressions for these linear systems are possible because if the system starts in equilibrium then, due to the linearity of the driving force, the non-equilibrium distribution remains Gaussian

for all time, having a mean and covariance matrix which lag behind their quasi-static counterparts. In SI Section IID we consider this class of systems in detail and evaluate the various updates Δ^{eq} , Δ^{neq} , and Δ^{app} explicitly in terms of these lagged quantities.

We generate a target trajectory in the 1D bead system by moving the trap position $\lambda^*(t)$ as a function of time, and we study several variations of this process (Figure 3B). An example trap trajectory is shown as the black line in Figure 3C, and the purple and green lines represent iterations of the learning process in which the trial trap position $\lambda^n(t)$ is updated locally in time according to Equation 5.

The relaxation time τ controls the degree to which the non-equilibrium distribution $p_{\lambda(t)}(q)$ lags behind the quasi-static distribution $p_{\lambda(t)}^{\text{eq}}(q)$. Because we are not changing the stiffness parameter k , the updates Δ^{neq} and Δ^{app} are in fact equal for this linear system (see SI Section IID). However, convergence slows as τ increases even using the correct update Δ^{neq} , because the typical update step for $\lambda^n(t)$ is smaller when the system is lagging (Figure 3D). Hence for a fixed η , the more the dynamics are out of equilibrium, the slower the convergence.

The thermal length scale l controls the breadth of the probability distributions, and we now argue the effect of this parameter on the learning dynamics is something what we can trivially compensate for and thus neglect. Dimensional analysis suggests that the learning rate η should be divided by l^2 in the non-dimensionalized scheme for updating the trap position $\lambda(t)$. In Figure 3E we illustrate that as l decreases and η correspondingly increases, then the measured convergence rate indeed grows. This growth of the non-dimensional η with decreasing l can be understood from the fact that the KL divergence cost function grows to infinity when comparing two distributions which pass into Dirac delta distributions (as $\beta \rightarrow \infty$) centered on different means. Thus, for lower temperatures our non-dimensional learning step sizes down the gradient of this cost function will be larger because the cost function itself is larger. If, however, we do not scale η by l^2 and we normalize the KL divergence by its value in the first trial to measure convergence, then the dependence of convergence rate on l drops out entirely (inset of Figure 3E). As a result, it is reasonable to neglect the dependence of the learning dynamics on temperature and consider zero-temperature dynamics in which we do not scale η by l^2 .

Finally, we ask whether the approximate update rule Equation 5 works for a more complex non-linear example, when $\Delta^{\text{neq}} \neq \Delta^{\text{app}}$. In place of a pure harmonic potential we use a Morse potential $H(q; \lambda, k) = (1 - e^{-\sqrt{k/2}(q-\lambda)})^2 + \frac{1}{2}k_w(q-\lambda)^2$. We add to this Hamiltonian a harmonic potential with a weak spring constant k_w so that the probability density remains compactly supported. In Figure 3F we show that the learning process in this case also converges, albeit at a slower rate than for the harmonic trap.

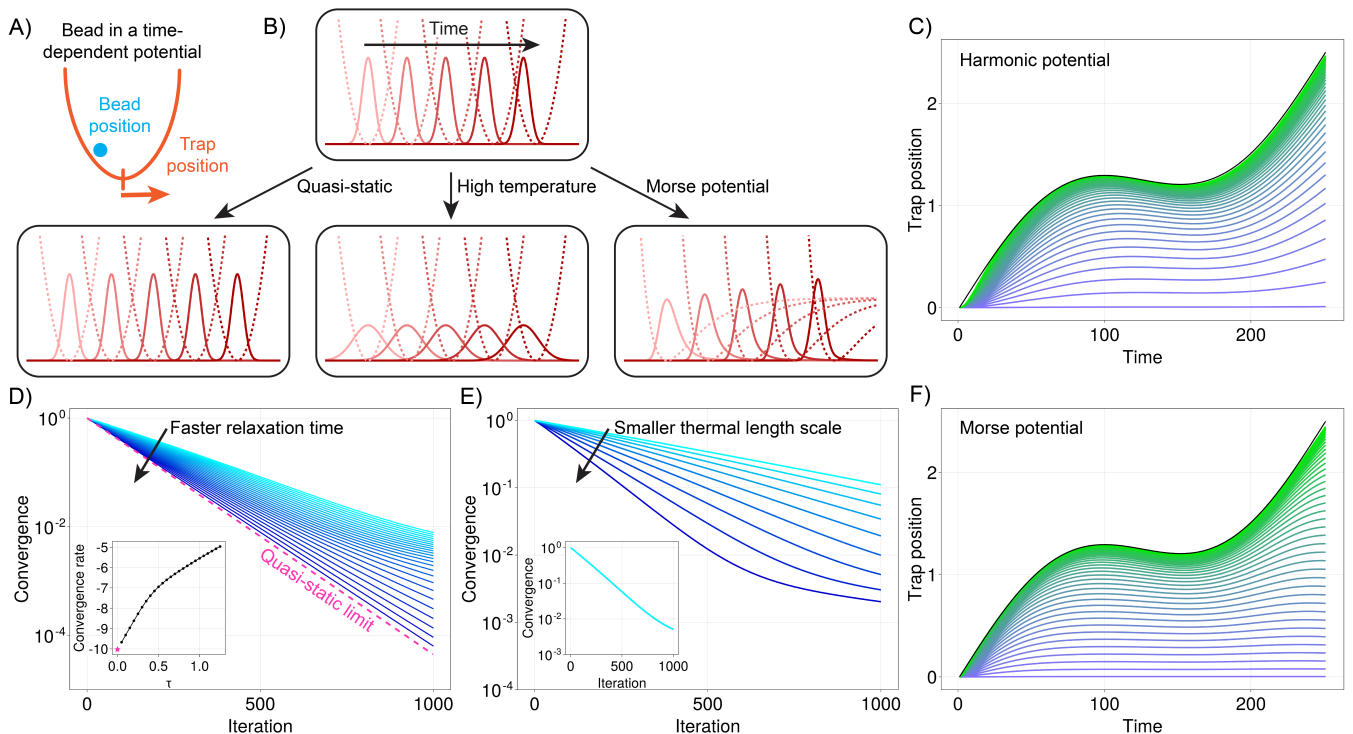


FIG. 3. Imperfect learning for a bead in a time-dependent potential. A) Schematic illustration of the bead-trap system. B) Schematic plots of sequential probability distributions (solid lines) describing the bead location as the trap potentials (dashed lines) are moved to the right at finite speed, creating a lag between the bead and the trap. Variations of this process are illustrated as described in the main text. C) The learned trap position as function of time and learning iteration, with learning rate $\eta = 0.005$ and thermal relaxation time $\tau = 0.2$. Color ranges from purple to green as every 25th learning iteration is shown. The black line indicates the target trajectory. D) Convergence for the n^{th} iteration, defined as the relative KL divergence $\int dt \mathcal{D}[p^*(t)||p^n(t)] / \int dt \mathcal{D}[p^*(t)||p^0(t)]$ is shown as τ is varied from 0.05 (blue) to 1.25 (cyan) in steps of 0.05. The pink dashed line displays the quasi-static limit obtained from learning the parameters of a single equilibrium distribution, rather than of a non-equilibrium trajectory (cf. Figure 1A). The inset shows the exponential convergence rate for each value of τ and the quasi-static limit. E) Convergence as the learning rate is scaled as η/l^2 for thermal length scales l ranging from 0.8 (blue) to 1.6 (cyan) in steps of 0.1. The inset displays the same, for the case when the learning rate is not scaled by l^2 . The nine curves corresponding to different values of l are all overlapping. F) Same as panel C but using the Morse potential and with $\eta = 0.01$.

B. Case study: Helfrich membrane with spontaneous curvature

We next consider a system whose configuration is described by a spatially extended *field* $q(r, t)$, i.e., a function of time t and of a 1D spatial coordinate $r \in [0, L]$. As a concrete example, we study a membrane system whose height $q(r, t)$ evolves to relax a Helfrich Hamiltonian (Figure 4A). In the Monge gauge and for small q , the leading order contribution to the energy is $H[q(r)] = \int_0^L dr h(q(r); \lambda(r))$ where [33, 34]

$$h(q(r); \lambda(r)) = \left(\frac{\sigma}{2} + \frac{\kappa \lambda(r)^2}{4} \right) (\partial_r q)^2 + \frac{\kappa}{2} (\partial_r^2 q - \lambda(r))^2. \quad (6)$$

Here, σ is a surface tension, κ is a bending rigidity, and $\lambda(r, t)$ is a spontaneous curvature field which sets the local rest value of $\partial_r^2 q$. Because of the previously discussed

trivial dependence on temperature (Figure 3E), we neglect noise here in the overdamped dynamics $\partial_t q(r, t) = -\mu \delta H / \delta q$.

We take the spontaneous curvature field $\lambda(r, t)$ to be externally controllable, for example due to a spatiotemporal protocol of curvature-inducing proteins that bind to a lipid membrane [35]. Varying $\lambda(r, t)$ at finite speed drives the membrane out of its initially equilibrated flat configuration $q(r, 0) = 0$ and generates a non-equilibrium height field trajectory $q(r, t)$.

As in the previous example, we specify a target protocol $\lambda^*(r, t)$ and generate its corresponding height field trajectory $q^*(r, t)$ (Figure 4B and C). We then iteratively learn the target protocol starting from an initial guess, $\lambda^0(r, t) = 0$, by incrementing $\lambda^n(r, t)$ using spatiotemporally local updates which are approximations to an inaccessible non-equilibrium gradient. Due to the continuous space dimension of this problem, we use the functional

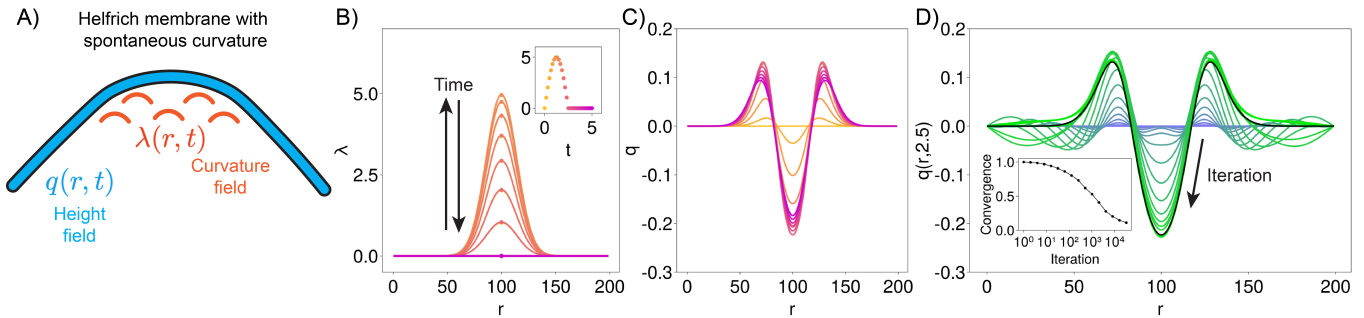


FIG. 4. Imperfect learning for a Helfrich membrane driven by a field of spontaneous curvature. A) Schematic illustration of the Helfrich membrane system. B) Plots of the target spontaneous curvature protocol $\lambda^*(r, t)$ at various times t . The inset displays $\lambda(100, t)$ as a function of t , corresponding to the dots in the main plot. C) Plots of the height field trajectory $q^*(r, t)$ resulting from $\lambda^*(r, t)$ in panel B. D) Plots of the height field $q^*(r, 2.5)$ as the learning iterations increase (from purple to green). The inset shows the convergence (defined as $\int dr dt |q^*(r, t) - q^n(r, t)| / \int dr dt |q^*(r, t) - q^0(r, t)|$) as a function of iteration. We used $\eta = 0.25$, $\beta = 1$, $\mu = 1$, and $\kappa = \sigma = 10$ (in simulation units) for these results.

gradients $\delta H / \delta \lambda$ in Equation 5.

In Figure 4D we illustrate convergence of the imperfect, spatiotemporally local learning rule. To understand how a spatially continuous domain does not prevent learning using local learning rules, we can view the amplitudes $\lambda_m(t)$ of the m^{th} spatial Fourier mode of $\lambda(r, t)$ as separate learning degrees of freedom (see SI Section IIE). In the limit of small $q(r, t)$ and $\lambda(r, t)$, the height field dynamics can be linearized so that the corresponding evolution equations for the amplitudes $q_m(t)$ decouple. These amplitude evolution dynamics can then be mapped onto a discrete system of linear forces, for which we previously demonstrated that convergence is possible. These considerations imply that learning membrane dynamics would be possible over a 2D spatial domain as well.

We have shown it is possible to learn non-autonomous protocols of Hamiltonian parameters driving conservative physical systems by using spatiotemporally local comparisons to a target trajectory. While local rules work trivially in quasi-static conditions, our results demonstrate that local approximations also work in non-quasi-static conditions because they have positive overlap with a “correct” non-local update rule (Figure 1C). We have demonstrated that this principle holds across conditions of relaxation time and temperature, for non-linear potentials, and for spatially continuous degrees of freedom. Having illustrated that imperfect local learning rules can work to control the dynamics of non-autonomous conservative systems, we next consider a more challenging class of systems involving non-conservative forces.

IV. LEARNING TO CONTROL NON-CONSERVATIVE SYSTEMS

A new difficulty for learning to control non-conservative systems is that even at long times the system is not guaranteed to equilibrate with respect to the

current parameters of its Hamiltonian and will instead occupy a non-equilibrium steady-state. This steady-state distribution will be characterized by an exponential weight Φ which is generally unknown, and as a result trying to minimize the KL divergence cost function will involve intractable gradients of Φ (see SI Section IIIA). However, progress can be made by considering alternative cost functions which lead to approximate gradients that involve accessible quantities. We first demonstrate this for the problem of updating a single edge parameter in a chemical reaction network to achieve a desired steady-state node probability. We then consider a complex paradigmatic active matter system, active nematics, and illustrate how an imperfect learning rule there can be used to guide topological defects along desired trajectories.

A. Case study: Dissipative discrete state Markov processes

Here we consider a biophysically relevant problem in which the consumption rate of chemical energy along an edge of a reaction network needs to be learned to achieve a desired steady-state concentration of some species. For instance, the ambient concentration of GTP during the Rho activation cycle [36] can be “learned” in this framework to achieve a target concentration of the activated (GTP-bound) Rho state, which in turn affects downstream signaling (Figure 5A). The general problem can be formulated using a continuous-time rate matrix \mathbf{W} to encode the kinetic rates connecting species which interconvert according to (pseudo)-first order reactions (Figure 5B). We follow Ref. 37 and parameterize the probability rate from state j to i as $W_{ij} = e^{E_j + B_{ij} + \alpha_{ij}/2}$ where $B_{ij} = B_{ji}$ is a symmetric contribution and $\alpha_{ij} = -\alpha_{ji}$ an anti-symmetric contribution which breaks detailed balance and generates steady-state fluxes. We assume that

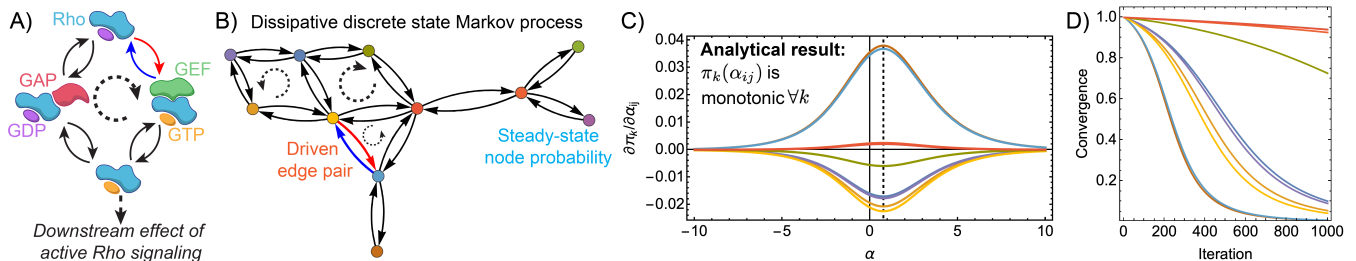


FIG. 5. Imperfect learning for a chemical reaction network’s steady-state. A) Illustration of the Rho activation network, which is driven by hydrolysis of GTP into GDP and is mediated by the exchange factor GEF and the activating protein GAP. B) Schematic illustration of a general discrete state Markov process. As α_{ij} increases, the red edge rate grows exponentially and the blue edge rate decreases exponentially. C) Plots of the derivatives $\partial\pi_k/\partial\alpha_{ij}$ for each of the nodes in the graph in panel A, using randomly drawn values for the parameters E_i , B_{ij} , and α_{ij} . D) Plots of the convergence, defined as $(\pi_k^* - \pi_k^n)^2 / (\pi_k^* - \pi_k^0)^2$, for separate, independent learning processes using each node in the graph as a target, with the same coloring as the other panels.

we have access only to α_{ij} for a given edge $i \leftrightarrow j$ in the network, and we consider how to move the steady-state probability π_k at node k to a target value π_k^* .

As elaborated in SI Section IIIA, this problem is non-trivial for non-equilibrium Markov state networks given the algebraically complicated dependence of steady-state distributions on the transition rates. We consider the simple quadratic cost function $\frac{1}{2}(\pi_k - \pi_k^*)^2$, whose gradient with respect to α_{ij} is $(\partial\pi_k/\partial\alpha_{ij})(\pi_k - \pi_k^*)$. This expression is difficult to handle because computing the prefactor $\partial\pi_k/\partial\alpha_{ij}$ requires detailed knowledge of the network topology and parameters. However, since we are adjusting a scalar quantity, then we would be justified in neglecting this prefactor entirely if we always at least knew its *sign*. Measuring the sign of the derivative once can feasibly be accomplished in practice, but then to continue providing updates in the correct direction we would need to be sure that the sign does not flip as α_{ij} changes during the learning dynamics. In fact, we illustrate numerically in Figure 5B that for a fixed i, j , and k , the derivative $\partial\pi_k/\partial\alpha_{ij}$ does not change sign as α_{ij} is varied from $-\infty$ to ∞ . We mathematically prove this surprising result in SI Section IIIB, using the matrix-tree representation of π_k and a technique called “tree surgery” which was recently introduced in Refs. 37, 38. As a result of the monotonicity of $\pi_k(\alpha_{ij})$, an imperfect gradient can be used to update α_{ij} according to

$$\alpha_{ij}^{n+1} \leftarrow \alpha_{ij}^n \pm \eta(\pi_k^n - \pi_k^*), \quad (7)$$

where we have used the \pm symbol to indicate that the appropriate sign of this update must first be determined but is then guaranteed not to change during learning. We show in SI Section IIIB that the sign of $\partial\pi_k/\partial\alpha_{ij}$ is positive for $k = i$ and negative for $k = j$, but analytically predicting the sign in general is difficult and left for future work. In Figure 5C we demonstrate that learning is possible using Equation 7 for each node in the network, albeit at different rates for each node. This update rule requires no knowledge of the network structure and only

involves measuring the current steady-state node occupation of the node of interest, which is in principle a biologically plausible learning mechanism. In the example of Rho signaling, this implies that global consideration of the network state is not necessary, and the GTP concentration can be adjusted by making local measurements of only the activated state concentration. Although this may be expected given that the Rho network topology is a single cycle, our result implies that this type of local learning scheme is possible for arbitrarily complicated (psuedo)-first order reaction networks.

B. Case study: Nematic defects in activity tweezer

Finally, we consider active nematics, composed of locally extensile or contractile force dipoles that obey a liquid-crystal hydrodynamic theory [39, 40]. Active nematic dynamics describe several systems of biological interest including solutions of short biopolymers mixed with molecular motors [41, 42], bacterial colonies [43, 44], and the epidermal layer of cells in developing organisms [45, 46].

Active nematics can be modeled using an order parameter field $\mathbf{Q}(\mathbf{r}, t)$ (a symmetric and traceless tensor capturing the degree of apolar alignment of force dipoles) and a flow field $\mathbf{v}(\mathbf{r}, t)$. The evolution of $\mathbf{Q}(\mathbf{r}, t)$ involves non-linear coupling to the flow field as well as a relaxational term arising from the Landau de-Gennes free energy function $F = \int d\mathbf{r} f(\mathbf{r})$ (see SI Section IVA) for details. The flow field \mathbf{v} is driven by two stress tensors, an Ericksen stress which the nematic field sets up in response to deviations from its free energy minimum, and an active stress $\sigma^a = \alpha\mathbf{Q}$ which is a non-conservative term resulting from the activity of, for example, molecular motors walking on pairs of filaments.

As a concrete learning problem in this system, we consider the task of manipulating the motion of *defects* in the nematic field (Figure 6A). Defects in active nematics are singular points in the $\mathbf{Q}(\mathbf{r}, t)$ field around which

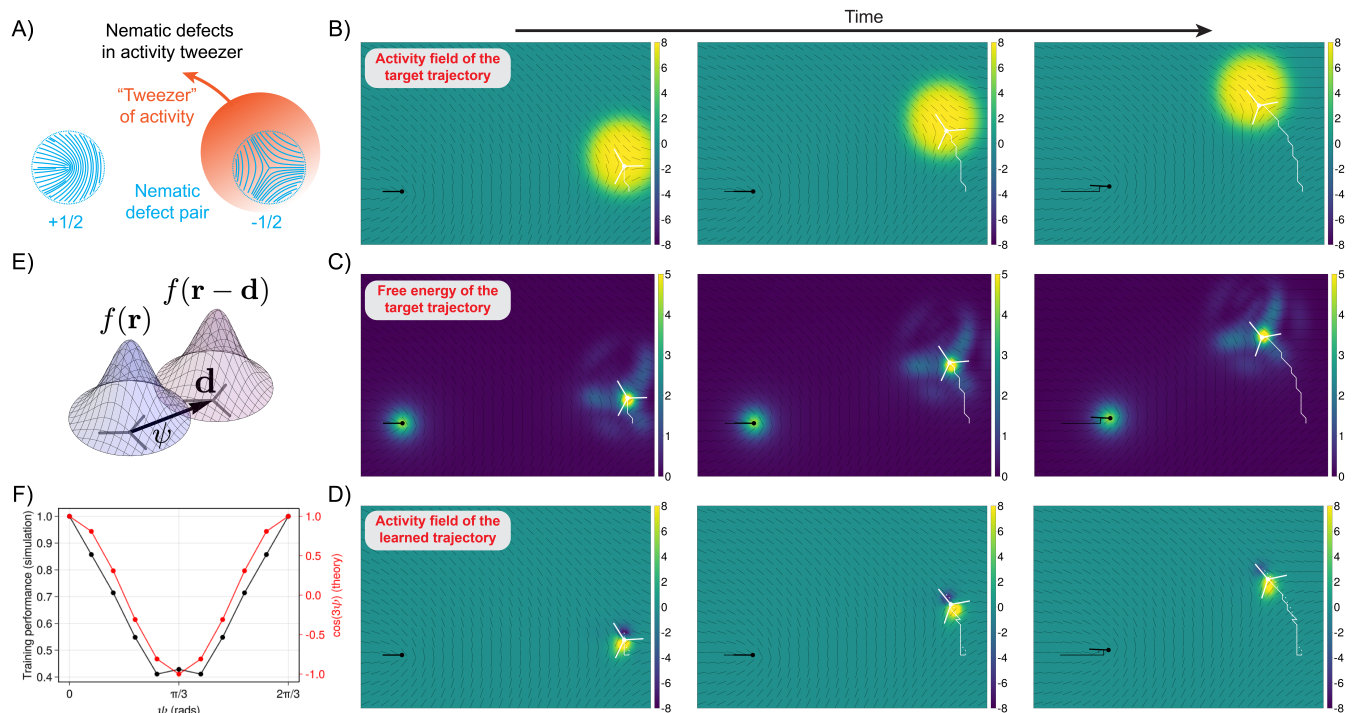


FIG. 6. Imperfect learning for active nematic defect dynamics. A) Schematic illustration of the active nematic system. B) Snapshots of the activity profile used to pull the $-1/2$ defect (white dot and lines) along a partial circular trajectory. The thick black dot and lines represent the $+1/2$ defect. The thin black lines represent the nematic field $\mathbf{Q}(\mathbf{r}, t)$ and color represents $\alpha^*(\mathbf{r}, t)$. C) Snapshots of the free energy density $f(\mathbf{r}, t)$ accompanying the nematic fields in panel B. The free energy is scaled by 10^3 . D) Snapshots of the trained activity protocol $\alpha^N(\mathbf{r}, t)$, showing that the trained defect trajectory (solid white lines) reproduces the target trajectory (dashed white line). The color scheme is the same as panel B. E) Schematic illustration of the free energy profiles under displacement of the $-1/2$ defect by a vector \mathbf{d} . The gray lines indicate the defect orientation, relative to which the angle ψ with respect to which \mathbf{d} is defined. F) Plots of the simulated training performance, defined as $1 - |\mathbf{r}_*^-(T) - \mathbf{r}_-^N(T)| / |\mathbf{r}_*^-(T) - \mathbf{r}_-^0(T)|$, as the angle ψ is varied. The predicted overlap $\sim \cos(3\psi)$ is plotted on the same axis. For this comparison, short target trajectories were obtained by translating the initial nematic field $\mathbf{Q}^*(\mathbf{r}, t) = \mathbf{Q}(\mathbf{r} - vt\mathbf{d}, 0)$ at a speed $v = 0.01$ to allow perfect control of the pulling direction \mathbf{d} . Simulation parameters for these results are provided in SI Section IVA.

the alignment direction rotates by a half-integer multiple of 2π radians [47]. Figure 6A illustrated two types of defects, $+1/2$ and $-1/2$, which form a topologically neutral pair. In confined or periodic systems, defects are topologically protected unless they annihilate with a defect of opposite charge. Positioning these defects within the fluid is thought to be biologically important, as it has been demonstrated that defects in the epidermal nematic field of developing *Hydra* correspond to morphological organizing centers such as the location of the future mouth [45, 46]. Recent work illustrated that the motion of these defects can be manipulated using tightly localized gradients in the activity field $\alpha(\mathbf{r}, t)$ (called “activity tweezers”) [27], similarly to how localized stresses can be created using optical tweezers to manipulate defects in colloidal crystals [48]. The necessary spatial gradients in $\alpha(\mathbf{r}, t)$ can be realized *in vivo* through, e.g., spatial regulation of motor activating proteins [41]. Additionally, it has recently become experimentally possible to exert spatial control over active nematics *in vitro* by using light-

activated motors or cell signaling channels [49–52]. Our method of using imperfect gradients to develop dynamical control over complex non-equilibrium systems can in principle be useful in these experimental contexts.

Using a numerical integrator of the active nematic equations of motion (whose implementation is described in Refs. 53–55), we generate target $-1/2$ defect trajectories using the activity tweezers, i.e., an activity protocol $\alpha^*(\mathbf{r}, t)$, similar to those described in Ref. 27 (Figure 6B). Defects in the nematic field are generically characterized by persistent peaks in the free energy density $f(\mathbf{r})$ (Figure 6C). As a result, it is reasonable to imagine that $f(\mathbf{r})$ can be used as a proxy for defect position and consider a quadratic cost function $\frac{1}{2}(f^n(\mathbf{r}, t) - f^*(\mathbf{r}, t))^2$. The gradient of this cost function with respect to the learnable activity field $\alpha(\mathbf{r}, t)$ involves the difficult prefactor $\partial f^n(\mathbf{r}, t) / \partial \alpha(\mathbf{r}, t)$. Similarly to the manipulations in the previous sections (Equation 7), we first assume that this prefactor can be ignored, and we consider spatiotempo-

rally local learning rule

$$\alpha^{n+1}(\mathbf{r}, t) \leftarrow \alpha^n(\mathbf{r}, t) - \eta(f^*(\mathbf{r}, t) - f^n(\mathbf{r}, t)). \quad (8)$$

Surprisingly, this simple update rule successfully allows reconstructing the target defect trajectory (Figure 6D). Successful implementation of this rule requires practical stabilization measures which we discuss in SI Section IVB. We note that the learned activity protocol differs markedly from the tweezer protocol which was used to create the target trajectory. This hints at the possibility that, while our update rule deterministically produces the same activity protocol for a given condition, there may be a degeneracy of usable activity protocols which can be accessed by alternative update rules. The update rule in Equation 8 produces regions of both negative (extensile) and positive (contractile) activity which is not thought to be biologically realistic because an active nematic is typically either purely extensile or purely contractile, and we aim to refine this in the future. Here we just highlight the fact that a simple free energy comparison $f^*(\mathbf{r}, t) - f^n(\mathbf{r}, t)$ serves as a sufficient feedback signal to learn an activity protocol $\alpha(\mathbf{r}, t)$ in a system with non-trivial physics.

We emphasize that Equation 8 can be viewed as acting like an approximate gradient of a global cost function which is made difficult due to the presence of non-conservative forces, non-autonomous control parameters, and complicated non-linear hydrodynamic equations of motion. Recent studies used top-down, global techniques such as optimal control and computation of exact coherent structures [56, 57] to solve similar active nematic control problems, but they require complete knowledge of the system’s dynamics and parameters. To gain intuition for why our simple local update rule works, in SI Section IVC we adapt recent analytical theory from Ref. 27 describing the effective velocity of a $-1/2$ defect under an activity field $\alpha(\mathbf{r}, t)$. The velocity depends on second order spatial derivatives in $\alpha(\mathbf{r}, t)$ via $\mathbf{v}_- = a\mathbf{\Sigma} : \nabla\nabla\alpha$, where a is a constant prefactor and $\mathbf{\Sigma}$ is a certain rank-three tensor which has the appropriate symmetries to describe the orientation of the $-1/2$ defect (being invariant under a rotation by $2\pi/3$ radians). We treat pulling the defect as a displacement of the original free energy profile $f(\mathbf{r})$ by a small vector \mathbf{d} , producing a new free energy profile $f(\mathbf{r} - \mathbf{d})$ (Figure 6E). We then evaluate the Hessian of the activity $\nabla\nabla\alpha$ produced by iterating Equation 8 under these free energy profiles, find the velocity \mathbf{v}_- which this activity field imparts to the defect, and finally evaluate the dot product between this velocity and the translation direction \mathbf{d} . We find that this overlap depends as $\cos(3\psi)$ on the angle ψ between the defect orientation and \mathbf{d} . To test this approximate theory, we performed learning trials with various initial angles ψ and measured the training performance at each angle. Figure 6F indicates good agreement with theory. This result explains why the approximate update rule Equation 8 works, and it implies that convergence depends

on the orientation of the defect. This also suggests that scalar fields besides the free energy $f(\mathbf{r})$, which might better capture details of the defect orientation, would likely serve as better sources of feedback, but we leave this to future work.

V. DISCUSSION

We have demonstrated in several physical systems the idea that full top-down control is not necessary to guide complex non-equilibrium dynamics. Rather, simple, approximate (and in some cases thermodynamically motivated) update rules which make only spatiotemporally local comparisons can be used instead. As illustrated in Figure 1C, an update rule that at least somewhat aligns with a “correct” gradient can act as a descent direction and allow flowing down the loss landscape. Here, we construct imperfect update rules out of easily measured observables, such as forces averaged over the trial and target distributions (Equation 4), local occupation probabilities (Equation 7), or free energy densities (Equation 8). Ensuring convergence in each case requires some system-specific considerations, but we expect that the broader idea of using easily accessible information to guide complex dynamics in place of top-down control is general.

The results in this paper extend the notion of imperfect gradient descent as a successful optimization strategy to the domain of dynamical control based on local error signals. Another class of techniques in which approximated, temporally local feedback signals are used to inform updates to a control policy is temporal difference RL [58, 59]. Our method bears certain conceptual similarities with this class of techniques, but with the key difference that our method does not learn a value function. The value function in RL encodes expected rewards, and it is commonly estimated using temporally local, approximate error signals obtained through exploration of the environment. To optimize its expected reward, the agent then updates its policy (i.e., its choice of actions) by performing gradient ascent on its estimate of the value function. In a standard RL algorithm, neural networks for both a critic (which learns the value function from experience) and an actor (which optimizes policy based on the critic) need to be trained and stored in memory. By contrast, our method bypasses the need to learn a value function by directly prescribing a simple, physically-motivated approximation to a value function gradient, which we call Δ^{app} . Thus, we leverage physical insight to provide a critic, allowing us to circumvent algorithmic machinery which is typically needed in RL to provide meaningful updates to the agent’s policy. We elaborate on this comparison to RL in SI Section V.

We expect that these methods can be of interest in several domains of research. Relaxing the constraint of having equilibrated distributions could feasibly allow accelerating methods in generative machine learning. For example, similar arguments were previously used

to justify methods like CD-n [60]. Additionally, biological information-processing systems like the immune system operate in dynamic, non-equilibrium environments [28, 29], where the principles explored in this paper might apply. Finally, a current challenge in biology is to identify principles which living organisms might utilize to dynamically control their active mechanochemical machinery and carry out biologically useful tasks [25]. We imagine that imperfect gradients can serve as such a principle, particularly as demonstrated in the task of active nematic defect control. While we considered a specific inverse problem setting, we expect that one can generalize this principle to help study other biologically relevant tasks of non-equilibrium control, such as maintaining homeostasis or searching for optimal trajectories. Additionally, recent advances in training physical materials using simple, local update rules [3, 11, 26] can feasibly be generalized using these results to work in dynamical, non-equilibrium settings.

ACKNOWLEDGMENTS

We wish to thank Jordan Horowitz, Grant Rotskoff, Menachem Stern, Martin Falk, Luca Scharrer, Suraj Shankar, Jeremy Owen, Agnish Kumar Behera, and Matthew Du for helpful discussions. This work was mainly supported by funds from DOE BES Grant DE-SC0019765 (CF and SV). ARD acknowledges support from the University of Chicago Materials Research Science and Engineering Center, which is funded by the National Science Foundation (NSF) under award number DMR-2011854 and NSF award MCB-2313725. CF acknowledges support from the University of Chicago through a Chicago Center for Theoretical Chemistry Fellowship. The authors acknowledge the University of Chicago's Research Computing Center for computing resources.

Supplementary Information

I. FEEDBACK ALIGNMENT FOR TRANSITION MATRICES

In Ref. 4 it is shown that a neural network can be trained without the use of exact backpropagation, in the sense that a transposed weight matrix $(\mathbf{W}^1)^\top$ (which would be required for exactly backpropagating errors to an upstream weight matrix \mathbf{W}^0) can be replaced with a random matrix \mathbf{B} of full rank, and this substitution will not prevent convergence of the learning dynamics. This surprising result is due to the fact that learning dynamics for \mathbf{W}^1 cause it to eventually *align* with \mathbf{B}^\top , such that \mathbf{B} can pass relevant error information to \mathbf{W}^0 . In Ref. 4, this is illustrated numerically using shallow neural networks (with non-linear activation functions) and mathematically proven for shallow linear networks. We first summarize their mathematical analysis, after which we generalize the feedback alignment idea to learn sequences of *transition matrices* from trajectories.

A. Summary of analysis in Ref. 4

The authors of Ref. 4 consider the linear system

$$y_i = W_{ij}^1 h_j \quad (9)$$

$$h_j = W_{jk}^0 x_k \quad (10)$$

where \mathbf{x} is the input data, \mathbf{h} is a hidden layer, and \mathbf{y} is the final output (see Figure 2A of the main text). Summation of repeated indices is implied throughout. The correct output is labeled \mathbf{y}^* , and the error is defined as

$$e_i = y_i^* - y_i = (T_{ik} - W_{ij}^1 W_{jk}^0) x_k \equiv E_{ik} x_k, \quad (11)$$

where T_{ik} is the correct mapping from x_k into y_i^* . From e_i the quadratic loss $\mathcal{L} = \frac{1}{2} e_k e_k$ is computed. To minimize this loss via gradient descent, one updates W_{ij}^0 and W_{ij}^1 using the derivatives

$$\begin{aligned} \Delta W_{ij}^0 &\sim -\frac{\partial \mathcal{L}}{\partial W_{ij}^0} = -\frac{\partial \mathcal{L}}{\partial e_k} \frac{\partial e_k}{\partial W_{ij}^0} \\ &= e_k W_{ki}^1 x_j \end{aligned} \quad (12)$$

and

$$\begin{aligned} \Delta W_{ij}^1 &\sim -\frac{\partial \mathcal{L}}{\partial W_{ij}^1} = -\frac{\partial \mathcal{L}}{\partial e_k} \frac{\partial e_k}{\partial W_{ij}^1} \\ &= e_i W_{jm}^0 x_m. \end{aligned} \quad (13)$$

To compute the product $e_k W_{ki}^1$, i.e. $(\mathbf{W}^1)^\top \cdot \mathbf{e}$, in the derivative with respect to \mathbf{W}^0 , one needs access to the transpose of \mathbf{W}^1 . To avoid this transposition operation, the authors of Ref. 4 replace $(\mathbf{W}^1)^\top$ by a random matrix of full rank, \mathbf{B} , so that

$$\Delta W_{ij}^0 \sim B_{ik} e_k x_j. \quad (14)$$

To understand how this substitution affects the learning process, the authors of Ref. 4 write the continuous gradient descent dynamics of \mathbf{W}^0 and \mathbf{W}^1 :

$$\dot{W}_{ij}^0 = \eta B_{ik} E_{km} X_{mj} \quad (15)$$

and

$$\dot{W}_{ij}^1 = \eta E_{ik} X_{km} W_{jm}^0 \quad (16)$$

where $X_{ij} \equiv x_i x_j$ and the dots denote a derivative with respect to the learning iteration, and η is a learning rate. For an ensemble of scaled inputs x_i which are drawn from $\mathcal{N}(0, 1)$, the matrices $X_{ij} = \delta_{ij}$ in expectation, so that

$$\dot{W}_{ij}^0 = \eta B_{ik} E_{kj} \quad (17)$$

and

$$\dot{W}_{ij}^1 = \eta E_{ik} W_{jk}^0. \quad (18)$$

Next, we imagine freezing \mathbf{W}^1 and consider the evolution of \mathbf{W}^0 . The matrix $E_{kj} = T_{kj} - W_{km}^1 W_{mj}^0$ is linear in W_{mj}^0 , and one can show that the most probable evolution of \mathbf{W}^0 is to grow in magnitude under these dynamics. Hence,

$$\frac{d}{dt} W_{ij}^0 W_{ij}^0 = 2\eta W_{ij}^0 B_{ik} E_{kj} > 0, \quad (19)$$

which implies that W_{ij}^0 comes to align with $B_{ik} E_{kj}$. Next, we freeze \mathbf{W}^0 and evolve \mathbf{W}^1 , and consider the quantity

$$\frac{d}{dt} B_{ik} W_{ki}^1 = \eta B_{ik} E_{kj} W_{ij}^0. \quad (20)$$

Equation 19 implies that $\frac{d}{dt}(B_{ik} W_{ki}^1) > 0$, which means that \mathbf{B} comes to align with $(\mathbf{W}^1)^\top$ as was to be shown.

B. Extension to chains of transition matrices

We now build on this analysis and consider how to leverage feedback alignment to imperfectly learn a chain $\{\mathbf{W}(t)\}_{t=0}^{N_t-1}$ of N_t transition matrices, which act on probability vectors $\mathbf{p}(t)$ as

$$p_i(t) = W_{ij}(t-1)p_j(t-1). \quad (21)$$

As a probability vector over a M dimensional space, $\mathbf{p}(t)$ obeys $\sum_{i=1}^M p_i(t) = 1$, and due to conservation of probability we must have

$$\sum_i W_{ij} = 1 \quad \forall j, \quad (22)$$

i.e., the columns of the transition matrices sum to unity. Furthermore, the entries W_{ij} must be non-negative in order to physically represent the transition probability from state j to state i . See Figure 2B of the main text for an illustration of the transition matrix chain.

We pose the problem of learning a target trajectory in probability space $\{\mathbf{p}^*(t)\}_{t=0}^{N_t}$ through temporally local comparisons to trial trajectories $\{\mathbf{p}^n(t)\}_{t=0}^{N_t}$, and we take the first vector $\mathbf{p}(0)$ as given and fixed. We define the error of the n^{th} trial at each time t during the trajectory as

$$e_i^n(t) = p_i^*(t) - p_i^n(t) = E_{ik}^n(t)p_k(0) \quad (23)$$

where

$$\mathbf{E}^n(t) = \prod_{t'=0}^{t'-1} \mathbf{W}^*(t') - \prod_{t'=0}^{t'-1} \mathbf{W}^n(t') \equiv \mathbf{V}^*(t-1) - \mathbf{V}^n(t-1). \quad (24)$$

The matrix products here are understood to be ordered as $\mathbf{W}^*(t-1)\mathbf{W}^*(t-2)\dots\mathbf{W}^*(0)$.

We define a total loss function as

$$\mathcal{L}_T^n = \sum_{t=1}^{N_t} \mathcal{L}^n(t) = \frac{1}{2} \sum_{t=1}^{N_t} e_k^n(t)e_k^n(t), \quad (25)$$

which sums over local loss functions $\mathcal{L}^n(t)$ defined at each time t . To find transition matrices which minimize this

loss, we consider gradients

$$\frac{\partial \mathcal{L}_T^n}{\partial W_{ij}^n(t-1)} = \sum_{t'=1}^{N_t} \frac{\partial \mathcal{L}^n(t')}{\partial W_{ij}^n(t-1)} = \sum_{t'=t}^{N_t} \frac{\partial \mathcal{L}^n(t')}{\partial W_{ij}^n(t-1)} \quad (26)$$

where the final equality is due to causality. For $t' > t$, we evaluate

$$\begin{aligned} \frac{\partial \mathcal{L}^n(t')}{\partial W_{ij}^n(t-1)} &= -e_k^n(t') \frac{\partial p_k^n(t')}{\partial W_{ij}^n(t-1)} \\ &= -e_k^n(t') \frac{\partial V_{km}^n(t'-1)}{\partial W_{ij}^n(t-1)} p_m(0) \\ &= -e_k^n(t') V_{ki}^n(t'-1:t) V_{jm}^n(t-2) p_m(0) \end{aligned} \quad (27)$$

where

$$\mathbf{V}^n(t'-1:t) \equiv \prod_{t''=t}^{t'-1} \mathbf{W}^n(t''). \quad (28)$$

Now, any updates to W_{ij}^n must preserve its column sum so it remains a stochastic matrix. A sum over i in Equation 27 is not guaranteed to be zero because the row sum for a product of transition matrices is arbitrary. Additionally, the dot product $e_k^n(t') V_{ki}^n(t'-1:t)$, i.e. $(\mathbf{V}^n(t'-1:t))^\top \cdot \mathbf{e}^n(t')$, involves a transposition operation. The term $V_{ki}^n(t'-1:t)$ represents backpropagation of the error signal from future times $t' > t$ to time t , and is hence non-local in time. For these reasons we are motivated to neglect all derivatives $\frac{\partial \mathcal{L}^n(t')}{\partial W_{ij}^n(t-1)}$ for times $t' > t$ and adjust $W_{ij}^n(t-1)$ only according to the *local* gradient at $t' = t$ (cf. Equation 13 above),

$$\frac{\partial \mathcal{L}^n(t)}{\partial W_{ij}^n(t-1)} = -e_k^n(t) \delta_{ik} V_{jm}^n(t-2) p_m(0). \quad (29)$$

To use this expression when $t = 1$ we set $V_{jm}^n(-1) = \delta_{jm}$. We note that summing Equation 29 over i yields zero, because $\sum_k e_k^n(t) = 0$, so this moving along gradient does not affect the column sum of $W_{ij}^n(t-1)$.

We now consider how the error $\mathbf{e}^n(t)$ evolves under the learning dynamics

$$\dot{W}_{ij}^n(t-1) = -\eta \frac{\partial \mathcal{L}^n(t)}{\partial W_{ij}^n(t-1)} = \eta e_i^n(t) V_{jm}^n(t-2) p_m(0) \quad (30)$$

where the dot denotes a derivative with respect to the training iteration n , not with respect to the trajectory time index t . We have that

$$\begin{aligned} \dot{e}_i^n(t) &= \dot{E}_{ik}^n p_k(0) \\ &= -\dot{V}_{ik}^n(t-1) p_k(0) \\ &= -\left(\dot{W}_{im}^n(t-1) V_{mk}(t-2) + W_{im}^n(t-1) \dot{W}_{ml}^n(t-2) V_{lk}^n(t-3) + \dots \right) p_k(0). \end{aligned} \quad (31)$$

To simplify this expression, let us first consider $t = 1$:

$$\begin{aligned} \dot{e}_i^n(1) &= -\dot{W}_{ik}^n(0) p_k(0) \\ &= -\eta e_i^n(1) p_k(0) p_k(0). \end{aligned} \quad (32)$$

Because the scalar quantity $a_1 \equiv p_k(0) p_k(0)$ is positive, this differential equation clearly represents an exponential decay of $e^n(1)$ to zero as $n \rightarrow \infty$ at a rate ηa_1 . Next we consider $t = 2$:

$$\begin{aligned} \dot{e}_i^n(2) &= -\left(\dot{W}_{im}^n(1) W_{mk}^n(0) + W_{im}^n(1) \dot{W}_{mk}^n(0) \right) p_k(0) \\ &= -\eta e_i^n(2) W_{ml}^n(0) p_l(0) W_{mk}^n(0) p_k(0) + W_{im}^n(1) \dot{e}_m^n(1). \end{aligned} \quad (33)$$

We have already shown that after iteration $\sim 1/\eta a_1$ the factor $\dot{e}_m^n(1)$ will be negligible and $\mathbf{W}^n(0) \rightarrow \mathbf{W}^\infty(0)$, so we

can write

$$\dot{e}_i^n(2) \approx -\eta e_i^n(2) W_{ml}^\infty(0) p_l(0) W_{mk}^\infty p_k(0) \equiv -\eta a_2 e_i^n(2). \quad (34)$$

The quantity $a_2 = W_{ml}^\infty(0) p_l(0) W_{mk}^\infty p_k(0)$ is positive because it is of the form $\mathbf{p}^\top \mathbf{A}^\top \mathbf{A} \mathbf{p}$ and the matrix $\mathbf{A}^\top \mathbf{A}$ is positive definite. Thus, the error $\dot{e}_i^n(2)$ will also decay exponentially to zero as $n \rightarrow \infty$. Extrapolating this pattern to arbitrary t , we can therefore neglect all but the leading term in Equation 31 and write

$$\begin{aligned} \dot{e}_i^n(t) &= \dot{W}_{im}^n(t-1) V_{mk}^\infty(t-2) p_k(0) \\ &= -\eta e_i^n(t) V_{jm}^\infty(t-2) p_m(0) V_{mk}^\infty(t-2) p_k(0) = -\eta a_t e_i^n(t). \end{aligned} \quad (35)$$

This convergence process can be viewed as “zippering,” where early times t in the trajectory converge first, after which later times converge as well.

C. Learning chains of transition matrices with imperfect gradients

In the previous subsection, it was assumed that the learning dynamics exactly follow the gradients $\frac{\partial \mathcal{L}^n(t)}{\partial W_{ij}^n(t-1)}$. Somewhat surprisingly, this was shown to be possible even when only considering temporally local loss functions (avoiding backpropagation in time). We now go a step further and consider the conditions under which convergence would still be possible if we systematically *distort* our local feedback signal. Starting from Equation 29, we identify at least two possible ways to introduce a distortion. One is that we distort the error vector:

$$e_k^n(t) \rightarrow B_{kl}^e(t) e_l^n. \quad (36)$$

The other is that we distort our “dynamical knowledge”:

$$\frac{\partial V_{km}^n(t)}{\partial W_{ij}^n(t-1)} = \delta_{ik} V_{jm}^n(t-2) \rightarrow \delta_{ik} B_{jp}^d(t) V_{pm}^n(t-2). \quad (37)$$

Introducing these random matrices \mathbf{B}^e and \mathbf{B}^d , the distorted learning dynamics become (cf. Equation 30)

$$\dot{W}_{ij}^n(t-1) = \eta B_{il}^e(t) e_l^n(t) B_{jk}^d(t) V_{km}^n(t-2) p_m(0). \quad (38)$$

We require that $\sum_i B_{il}^e e_l = 0$ if it is not to affect the column sum of $W_{ij}^n(t-1)$. Considering as before the training dynamics of the first error $e^n(1)$, we have

$$\begin{aligned} \dot{e}_i^n(1) &= -\dot{W}_{ik}^n(0) p_k(0) \\ &= -\eta B_{il}^e(1) e_l^n(1) B_{km}^d(t) p_m(0) p_k(0). \end{aligned} \quad (39)$$

If $\mathbf{B}^d(1)$ is positive definite, then the product $a_1^d \equiv B_{km}^d(t) p_m(0) p_k(0)$ is guaranteed to be positive, so we can write

$$\dot{e}_i^n(1) = -\eta a_1^d B_{il}^e(1) e_l^n(1) \quad (40)$$

with $\eta a_1 > 0$. This differential equation will decay to zero if $\mathbf{B}^e(1)$ has positive eigenvalues (a slightly weaker condition than it being positive definite). For $t = 2$ we have (assuming $\mathbf{e}(1)$ has appreciably decreased)

$$\dot{e}_i^n(2) \approx -\eta B_{il}^e(2) e_l^n(2) B_{mp}^d(2) W_{pl}^\infty(0) p_l(0) W_{mk}^\infty p_k(0) \quad (41)$$

If $\mathbf{B}^d(2)$ is positive definite, then it can be split as $\mathbf{B}^d(2) = (\bar{\mathbf{B}}^d(2))^\top \bar{\mathbf{B}}^d(2)$ for some $\bar{\mathbf{B}}^d(2)$, so that the product $a_2^d = B_{mp}^d(2) W_{pl}^\infty(0) p_l(0) W_{mk}^\infty p_k(0)$ is of the form $\mathbf{p}^\top \mathbf{A}^\top \mathbf{A} \mathbf{p}$ and is hence positive. Thus

$$\dot{e}_i^n(2) = -\eta a_2^d B_{il}^e(2) e_l^n(1) \quad (42)$$

will be guaranteed to converge if $\mathbf{B}^e(2)$ has positive eigenvalues. Continuing this pattern, for arbitrary t we have

$$\dot{e}_i^n(t) = -\eta B_{il}^e(t) e_l^n(t) B_{mp}^d(2) V_{pl}^\infty(t-2) p_l(0) V_{mk}^\infty(t-2) p_k(0) = -\eta a_t^d B_{il}^e(t) e_l^n(1) e_i^n(t) \quad (43)$$

which will also converge if $\mathbf{B}^d(t)$ is positive definite and $\mathbf{B}^e(t)$ has positive eigenvalues.

An alternative illustration of the convergence of these distorted gradients can be given by considering their overlap with the correct gradients. For time t , we evaluate

$$\begin{aligned} \left(\frac{\partial \mathcal{L}^n(t)}{\partial W_{ij}^n(t-1)} \right)_{\text{correct}} & \left(\frac{\partial \mathcal{L}^n(t)}{\partial W_{ij}^n(t-1)} \right)_{\text{distorted}} = e_i^n(t) V_{jm}^n(t-2) p_m(0) B_{il}^e(t) e_l^n(t) B_{jp}^d(2) V_{pl}^n(t-2) p_l(0) \\ & = (e_i^n(t) B_{il}^e(t) e_l^n(t)) (V_{jm}^n(t-2) p_m(0) B_{jp}^d(2) V_{pl}^n(t-2) p_l(0)). \end{aligned} \quad (44)$$

This expression is the product of two terms, each of the form $\mathbf{p}^\top \mathbf{A}^\top \mathbf{A} \mathbf{p}$ provided that $\mathbf{B}^e(t)$ and $\mathbf{B}^d(t)$ are both positive definite. Under these conditions, this overlap is positive and thus the distorted gradient can serve as a descent direction of $\mathcal{L}^n(t)$ [32]. We note that this argument places the more stringent condition on $\mathbf{B}^e(t)$ that it be positive definite rather than have positive eigenvalues.

The simultaneous conditions on \mathbf{B}^e that it have positive eigenvalues and satisfy $\sum_i B_{il}^e e_l = 0$ are not contradictory. For example, such a matrix can be constructed as

$$\mathbf{B}^e = \mathbf{I} + \tilde{\mathbf{C}} \quad (45)$$

where \mathbf{I} is the identity matrix, \mathbf{C} is positive definite, and the tilde operation maps a matrix as

$$\tilde{C}_{ij} = C_{ij} - \frac{1}{M} \sum_{k=1}^M C_{kj} \quad (46)$$

so that its column sums are zero.

D. Effect of imperfect gradients on convergence

The matrices $\mathbf{B}^e(t)$ and $\mathbf{B}^d(t)$ affect the rate of convergence of the error in two qualitatively different ways. For simplicity, we focus on the effect on the first error $\mathbf{e}^n(1)$ due to $\mathbf{B}^e(1)$ and $\mathbf{B}^d(1)$. The undistorted dynamics of $\mathbf{e}^n(1)$ are given in Equation 32, which represents exponential convergence of each component $e_i^n(1)$ to zero at rate ηa_1 . The distorted dynamics are given in Equation 39, which introduce two new features.

First, the scalar quantity a_1^d differs from a_1 by the Rayleigh quotient

$$\frac{a_1^d}{a_1} = \frac{\mathbf{p}^\top(0) \mathbf{B}^d(1) \mathbf{p}(0)}{\mathbf{p}^\top(0) \mathbf{p}(0)} = \frac{\sum_{i=1}^M (y_i^d(1))^2 \lambda_i^d(1)}{\sum_{i=1}^M (y_i^d(1))^2} \quad (47)$$

where λ_i^d are the eigenvalues of $\mathbf{B}^d(1)$ and $y_i^d(1)$ are the components of $\mathbf{p}(0)$ in the eigenbasis of $\mathbf{B}^d(1)$. Clearly the Rayleigh quotient quantity will depend on the the projection of initial point $\mathbf{p}(0)$ onto the eigenmodes of $\mathbf{B}^d(1)$. Assuming random data, we can take these projections to be equal on average, so that $y_i^d(1) = y^d(1)$ for each i . The quotient then simplifies to

$$\frac{a_1^d}{a_1} = \frac{1}{M} \sum_{i=1}^M \lambda_i^d(1) \quad (48)$$

which is the average eigenvalue of $\mathbf{B}^d(1)$. This implies that including a distortion matrix $\mathbf{B}^d(1)$ can in fact accelerate convergence by effectively causing the learning dynamics to take bigger step sizes per iteration, even if the step is not directed exactly down the gradient. If we normalize $\mathbf{B}^d(1) \rightarrow \mathbf{B}^d(1)/\lambda_{\max}^d(1)$ so that its maximum eigenvalue $\lambda_{\max}^d(1)$ is one, then the effect of including $\mathbf{B}^d(1)$ will be to strictly slow down convergence because $a_1^d/a_1 \leq 1$. We emphasize that a_1^d/a_1 affects the convergence rate of each component of $e_i^n(1)$ by the same amount.

By contrast, the effect second effect on the converge rate, caused by $\mathbf{B}^e(1)$, will be different for each component of $e_i^n(1)$. Setting $a_1^d = a_1$ here, we compare

$$\dot{e}_i^n(1) = -\eta a_1 e_i^n(1) \quad (49)$$

and

$$\dot{e}_i^n(1) = -\eta a_1 B_{ik} e_k^n(1). \quad (50)$$

Under Equation 49 each component of $\mathbf{e}^n(1)$ will decay at the same rate, ηa_1 . Under Equation 50, the component of $\mathbf{e}^n(1)$ along the i^{th} eigenvector of $\mathbf{B}^e(1)$ will decay at a rate $\eta a_1 \lambda_i^e$, where λ_i^e associated eigenvalue. At long training times, decay of $\mathbf{e}^n(1)$ will be dominated by the smallest eigenvalue λ_{\min}^e . To summarize, the effect of $\mathbf{B}^d(1)$ is to alter the convergence rate of each component $e_i^n(1)$ by the same factor, equal (under the assumption of random data) to the *average* eigenvalue of $\mathbf{B}^d(1)$. On the other hand, the effect of $\mathbf{B}^e(1)$ is to alter the convergence rate of each component $e_i^n(1)$ differently according to the projection of $\mathbf{e}^n(1)$ on to the eigenbasis of $\mathbf{B}^e(1)$, and this effect will eventually be dominated by the *smallest* eigenvalue of $\mathbf{B}^e(1)$. This qualitative argument extends straightforwardly to arbitrary times t .

E. Numerical results

Here we numerically test the training protocols described above. A remaining issue to address first is that, while the gradients we have introduced will ensure that the column sums of the transition matrices do not differ from one during training, they do not prevent their values from going negative. At least two possibilities exist for handling this. One is to include inequality constraints as Lagrange multipliers in an augmented cost function [32]. The other is to take small steps along the gradient of the unconstrained cost function and then project back onto the manifold of allowed transition matrices. The space of matrices whose entries are in the interval $[0, 1]$ and whose columns sum to one is a simplex, and algorithms exist to project data onto simplices [61]. For simplicity, we use here a crude two-step projection

$$W_{ij} \rightarrow W_{ij}^{\text{clip}} \equiv \max(W_{ij}, 0) \quad (\text{clip to positive values}) \quad (51)$$

$$W_{ij}^{\text{clip}} \rightarrow \frac{W_{ij}^{\text{clip}}}{\sum_{k=1}^M W_{kj}^{\text{clip}}} \quad (\text{renormalize the column sum to one}). \quad (52)$$

We find in practice that this suffices to ensure that W_{ij} remains a legal transition matrix.

We generate target trajectories by creating $N_t + 1$ vectors $\mathbf{p}^*(t)$. We create $\mathbf{p}^*(t)$ by drawing a random number uniformly from $[0, 1]$ for each component $p_i^*(t)$, and then dividing each component by $\sum_{i=1}^M p_i^*(t)$ so that $\mathbf{p}^*(t)$ is a probability vector. We similarly create initial guesses for the N_t transition matrices $\mathbf{W}^0(t)$ by drawing each element uniformly from $[0, 1]$ and then applying Equation 52 to make the column sums equal to one.

To create the N_t matrices $\mathbf{B}^d(t)$, we first create $\bar{\mathbf{B}}^d(t)$ by drawing elements uniformly from $[0, 1]$, and we then set $\mathbf{B}^d(t) = \bar{\mathbf{B}}^d(t) \bar{\mathbf{B}}^d(t)^\top$ to ensure that it is positive definite. We finally normalize $\mathbf{B}^d(t) \leftarrow \mathbf{B}^d(t) / \lambda_{\max}^d(t)$ so that its maximum eigenvalue is equal to one. To create the N_t matrices $\mathbf{B}^e(t)$, we first create $\bar{\mathbf{C}}(t)$ by drawing elements uniformly from $[0, 1]$, and we then set $\mathbf{C}(t) = \bar{\mathbf{C}}(t) \bar{\mathbf{C}}(t)^\top$. We then apply Equations 45 and 46 to form $\mathbf{B}^e(t)$. Finally we set $\mathbf{B}^e(t) \leftarrow \mathbf{B}^e(t) / \lambda_{\max}^e(t)$ so that its maximum eigenvalue is equal to one.

We first set $N_t = 10$, $\eta = 0.025$, and $M = 5$ and run 10 trials of training using different random initial conditions for each trial. We try four protocols: using just $\mathbf{B}^e(t)$, using just $\mathbf{B}^d(t)$, using both, and using neither. For each protocol we use the same initial guesses $\mathbf{W}^0(t)$. The results are shown in SI Figure 7A. The fastest convergence is achieved when no distortion is introduced, but all four protocols show convergence toward zero error. Increasing the space dimensionality to $M = 20$, we find that distortion using $\mathbf{B}^d(t)$ performs much better than using $\mathbf{B}^e(t)$ (SI Figure 7B). This can be explained due to our previous argument that convergence with $\mathbf{B}^e(t)$ depends on its slowest eigenvalue, whereas convergence with $\mathbf{B}^d(t)$ depends on its average eigenvalue. For random matrices of increasing dimensionality M , the minimal eigenvalue falls more sharply with M than its average eigenvalue does, as can be seen numerically (SI Figure 7C).

We find that for later iterations the convergence deviates from pure exponential decay (Figure 7D), which can be due both to set of different relaxation timescales ηa_t for each t and due to the operation of projecting back onto the simplex of legal transition matrices. We further find that, even as both protocols using \mathbf{B}^d and no distortion reach low values of the loss function, they do not learn exactly the same transition matrices (SI Figures 7E and F). There is a manifold of degenerate transition matrices, each of which map $\mathbf{p}^*(t)$ into $\mathbf{p}^*(t + 1)$, and the learning dynamics induced by distortion reach a different final matrix than in the un-distorted dynamics.

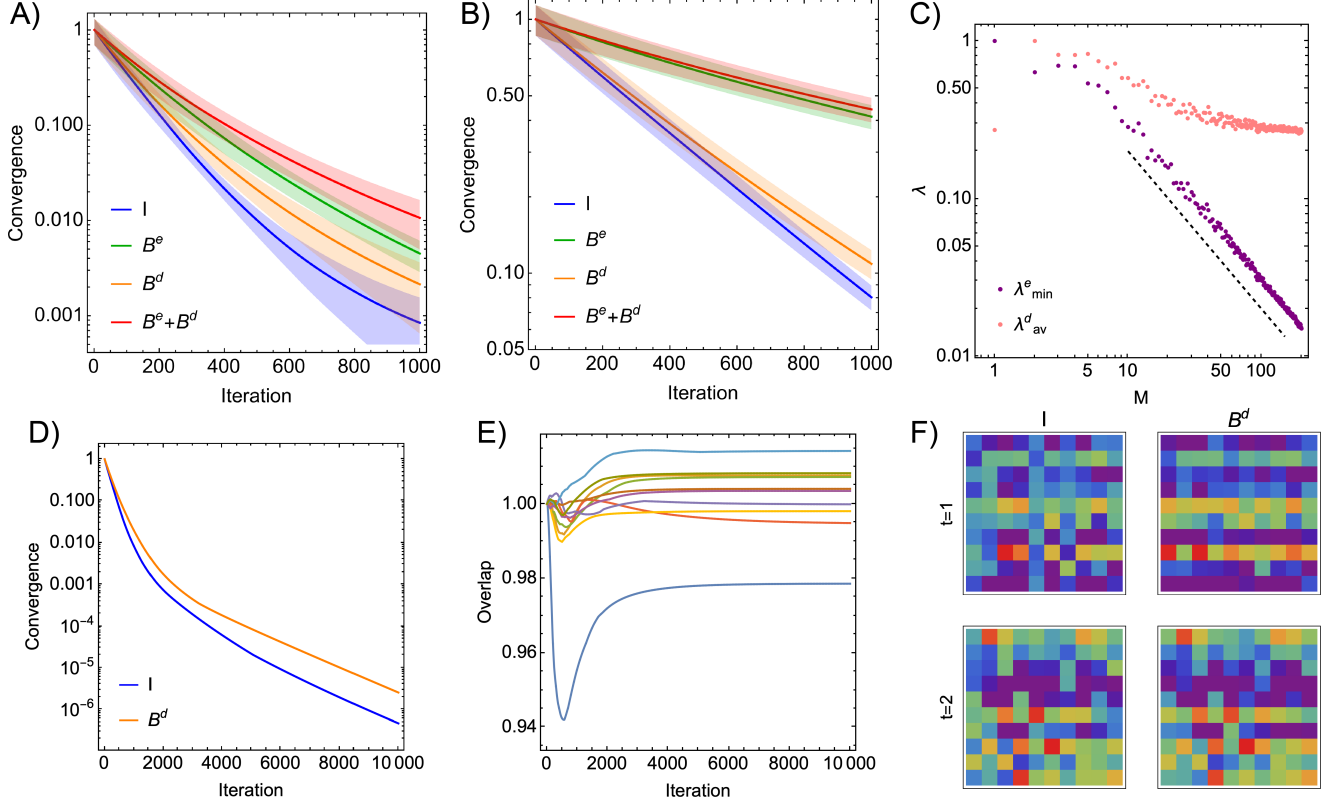


FIG. 7. Numerical results for training transition matrices. A) Convergence of the four protocols with $M = 5$. Convergence is defined as $\mathcal{L}_T^n / \mathcal{L}_T^0$ (cf. Equation 25). Solid lines represent the mean over 10 trials and the filled curves represent the standard deviation. B) Convergence of the four protocols with $M = 20$. C) Samples of the minimum eigenvalue λ_{\min}^e of \mathbf{B}^e and average eigenvalue λ_{av}^d of \mathbf{B}^d as a function of M . The dashed line indicates a scaling of M^{-1} . D) Convergence plots of a single trial with $M = 10$ for 10,000 training steps. E) Overlaps for $t = 1 \dots 10$ shown as different colors, with overlap defined as $W_{ij}^{n,1}(t)W_{ij}^{n,d}(t)/W_{ij}^{n,1}(t)W_{ij}^{n,1}(t)$ for transition matrices under protocols using no distortion (I), and \mathbf{B}^d (d). F) Plots of the final transition matrices $\mathbf{W}^{N,1}(1)$, $\mathbf{W}^{N,d}(1)$, $\mathbf{W}^{N,1}(2)$, $\mathbf{W}^{N,d}(2)$. Colors range from violet to red for increasing values of W_{ij} .

II. IMPERFECT LEARNING OF CONSERVATIVE, NON-AUTONOMOUS DYNAMICS

A. Lagged KL divergences

A standard approach for training generative machine learning models is to minimize the KL divergence between a parameterized trial distribution and a target distribution. Denoting the target distribution $p^*(\mathbf{q})$ and the trial distribution $p_\lambda(\mathbf{q})$, which depends on some parameters λ , one aims to minimize

$$\mathcal{D}[p^*||p_\lambda] \equiv \int d\mathbf{q} p^*(\mathbf{q}) \ln \frac{p^*(\mathbf{q})}{p_\lambda(\mathbf{q})}. \quad (53)$$

If $p_\lambda(\mathbf{q})$ is an equilibrium canonical distribution with respect to a Hamiltonian $H(\mathbf{q}; \lambda)$ with $\beta = 1/k_B T$, we can write

$$p_\lambda(\mathbf{q}) = Z(\lambda)^{-1} e^{-\beta H(\mathbf{q}; \lambda)} \quad (54)$$

where $Z(\lambda)$ is the partition function. After a few lines of algebra one can express the gradient of the KL divergence with respect to λ as

$$\frac{\partial \mathcal{D}[p^*||p_\lambda]}{\partial \lambda} = \left\langle \beta \frac{\partial H(\mathbf{q}; \lambda)}{\partial \lambda} \right\rangle_{p^*} - \left\langle \beta \frac{\partial H(\mathbf{q}; \lambda)}{\partial \lambda} \right\rangle_{p_\lambda}. \quad (55)$$

This expression uses the result $\frac{\partial Z(\boldsymbol{\lambda})^{-1}}{\partial \boldsymbol{\lambda}} = Z(\boldsymbol{\lambda})^{-1} \left\langle \beta \frac{\partial H(\mathbf{q}; \boldsymbol{\lambda})}{\partial \boldsymbol{\lambda}} \right\rangle_{p_{\boldsymbol{\lambda}}}$ but makes no assumption on the form of p^* . Hence, an update rule for the n^{th} update of $\boldsymbol{\lambda}^n$ is

$$\boldsymbol{\lambda}^{n+1} \leftarrow \boldsymbol{\lambda}^n - \eta \left(\left\langle \beta \frac{\partial H(\mathbf{q}; \boldsymbol{\lambda}^n)}{\partial \boldsymbol{\lambda}} \right\rangle_{p^*} - \left\langle \beta \frac{\partial H(\mathbf{q}; \boldsymbol{\lambda}^n)}{\partial \boldsymbol{\lambda}} \right\rangle_{p_{\boldsymbol{\lambda}^n}} \right) \quad (56)$$

where η is a scalar learning rate, and the notation $\frac{H(\mathbf{q}; \boldsymbol{\lambda}^n)}{\partial \boldsymbol{\lambda}}$ indicates the gradient $\frac{H(\mathbf{q}; \boldsymbol{\lambda})}{\partial \boldsymbol{\lambda}}$ evaluated at $\boldsymbol{\lambda} = \boldsymbol{\lambda}^n$ and averaged over the distribution $p^*(\mathbf{q})$. Update rules of this kind are often used to train machine learning models such as restricted Boltzmann machines, where a practical issue is that of sufficiently sampling over the distributions p^* and $p_{\boldsymbol{\lambda}^n}$. Techniques such as CD-n have been proposed to efficiently perform this sampling [60]; we do not concern ourselves with these issues here and assume that necessary averages over these distributions are accessible.

We consider how to learn a target *trajectory* $p^*(\mathbf{q}, t)$, rather than a single static distribution $p^*(\mathbf{q})$. Let us first assume that the target trajectory results from a driving protocol $\boldsymbol{\lambda}^*(t)$ which is quasi-static, so that

$$p^*(\mathbf{q}, t) = p_{\boldsymbol{\lambda}^*(t)}^{\text{eq}}(\mathbf{q}) = Z(\boldsymbol{\lambda}^*(t))^{-1} e^{-\beta H(\mathbf{q}; \boldsymbol{\lambda}^*(t))}. \quad (57)$$

Considering quasi-static trial protocols $\boldsymbol{\lambda}^i(t)$, then one could use standard contrastive learning to learn this trajectory by applying updates to $\boldsymbol{\lambda}^i(t)$ of the form

$$\boldsymbol{\lambda}^{n+1}(t) \leftarrow \boldsymbol{\lambda}^n(t) - \eta \Delta^{\text{eq}} \quad (58)$$

where

$$\begin{aligned} \Delta^{\text{eq}} &= \frac{\partial \mathcal{D}^{\text{eq}}}{\partial \boldsymbol{\lambda}} \equiv \frac{\partial \mathcal{D}[p_{\boldsymbol{\lambda}^*(t)}^{\text{eq}} || p_{\boldsymbol{\lambda}^n(t)}^{\text{eq}}]}{\partial \boldsymbol{\lambda}} \\ &= \left\langle \beta \frac{\partial H(\mathbf{q}; \boldsymbol{\lambda}^n(t))}{\partial \boldsymbol{\lambda}} \right\rangle_{p_{\boldsymbol{\lambda}^*(t)}^{\text{eq}}} - \left\langle \beta \frac{\partial H(\mathbf{q}; \boldsymbol{\lambda}^n(t))}{\partial \boldsymbol{\lambda}} \right\rangle_{p_{\boldsymbol{\lambda}^n(t)}^{\text{eq}}}. \end{aligned} \quad (59)$$

For these updates, we sample the gradients $\partial_{\boldsymbol{\lambda}} H(\mathbf{q}; \boldsymbol{\lambda})$ of the Hamiltonian function in each distribution. The assumption of quasi-staticity allows one to break the dynamical problem into a set of *independent* problems to which standard contrastive learning based on equilibrium distributions can be applied. In SI Section II B, we illustrate this further using as an alternative starting cost function the KL divergence evaluated over path probabilities.

If the driving protocol $\boldsymbol{\lambda}^*(t)$ is not quasi-static then in principle we should not consider quasi-static trial protocols. Away from equilibrium one can still formally write $p_{\boldsymbol{\lambda}}(\mathbf{q})$ as

$$p_{\boldsymbol{\lambda}}(\mathbf{q}) = \tilde{Z}(\boldsymbol{\lambda})^{-1} e^{-\beta \tilde{H}(\mathbf{q}; \boldsymbol{\lambda})} \quad (60)$$

where

$$\tilde{Z}(\boldsymbol{\lambda}) = \int d\mathbf{q} e^{-\beta \tilde{H}(\mathbf{q}; \boldsymbol{\lambda})}. \quad (61)$$

The function exponential weight \tilde{H} is no longer the Hamiltonian function when the system is out of equilibrium. If we knew \tilde{H} , then to minimize Equation 55 we could sample the gradients $\partial_{\boldsymbol{\lambda}} \tilde{H}(\mathbf{q}; \boldsymbol{\lambda})$ in updates of the form

$$\begin{aligned} \Delta^{\text{neq}} &= \frac{\partial \mathcal{D}^{\text{neq}}}{\partial \boldsymbol{\lambda}} \equiv \frac{\partial \mathcal{D}[p_{\boldsymbol{\lambda}^*(t)} || p_{\boldsymbol{\lambda}^n(t)}]}{\partial \boldsymbol{\lambda}} \\ &= \left\langle \beta \frac{\partial \tilde{H}(\mathbf{q}; \boldsymbol{\lambda}^n(t))}{\partial \boldsymbol{\lambda}} \right\rangle_{p_{\boldsymbol{\lambda}^*(t)}} - \left\langle \beta \frac{\partial \tilde{H}(\mathbf{q}; \boldsymbol{\lambda}^n(t))}{\partial \boldsymbol{\lambda}} \right\rangle_{p_{\boldsymbol{\lambda}^n(t)}}. \end{aligned} \quad (62)$$

However, \tilde{H} and its gradients are not known in general for non-equilibrium processes, so this update cannot feasibly be implemented. Instead, we consider the approximation to this update in which \tilde{H} is replaced by the Hamiltonian H :

$$\Delta^{\text{app}} \equiv \left\langle \beta \frac{\partial H(\mathbf{q}; \boldsymbol{\lambda}^n(t))}{\partial \boldsymbol{\lambda}} \right\rangle_{p_{\boldsymbol{\lambda}^*(t)}} - \left\langle \beta \frac{\partial H(\mathbf{q}; \boldsymbol{\lambda}^n(t))}{\partial \boldsymbol{\lambda}} \right\rangle_{p_{\boldsymbol{\lambda}^n(t)}}, \quad (63)$$

In contrast to Δ^{eq} the samples are taken with respect to the non-equilibrium distributions $p_{\lambda^*(t)}$ and $p_{\lambda^n(t)}$ rather than their quasi-static counterparts, and in contrast to Δ^{app} the samples are of gradients of H rather than \tilde{H} .

To motivate why this approximate learning rule might work, we consider the view of non-autonomous dynamics described in Ref. 31 as comprising an inevitable lag which develops between a non-equilibrium distribution and its quasi-static counterpart (in which the $\lambda(t)$ is moved along the same geometrical path at an infinitely slow rate). Schematically, this is depicted as the pair of black lines in SI Figure 8. The KL divergence $\mathcal{D}_{\text{lag}}^* \equiv \mathcal{D}[p^*(t)||p^{*,\text{eq}}(t)]$ is in fact bounded by amount of work dissipated up to time t . Similarly, there is a non-zero lag-related KL divergence $\mathcal{D}_{\text{lag}}^n \equiv \mathcal{D}[p^n(t)||p^{n,\text{eq}}(t)]$ which applies for the n^{th} iteration of our trial process. To close the distance between $p^n(t)$ and $p^*(t)$, we would ideally minimize \mathcal{D}^{neq} , which differs from \mathcal{D}^{eq} due to the two lag-related divergences $\mathcal{D}_{\text{lag}}^*$ and $\mathcal{D}_{\text{lag}}^n$. \mathcal{D}^{neq} and its gradient Δ^{neq} are unfortunately not known, but flow down the Δ^{neq} will have the same fixed point as flow down Δ^{eq} or Δ^{app} . This shared fixed point will occur at $\lambda^n(t') = \lambda^*(t')$ for $t' \leq t$. Among these three gradients, only Δ^{app} can be computed in general as it involves samples over the accessible distributions $p^*(t)$ and $p^n(t)$, (rather than their unknown quasi-static counterparts) and involves the known model Hamiltonian H , rather than the unknown exponential weight \tilde{H} . Even though the vector Δ^{app} will systematically differ from Δ^{neq} , as long as there is a positive projection between the two then Δ^{app} will remain a descent direction and will converge to the correct minimum (see Figure 1C of the main text).

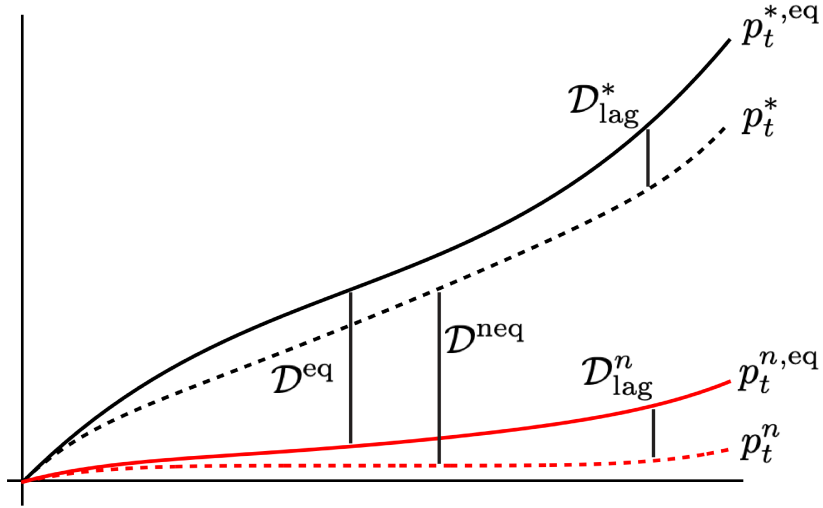


FIG. 8. D) Schematic illustration of learning a non-equilibrium probability trajectory p_t^* which lags behind a quasi-static version $p_t^{*,\text{eq}}$. Similarly the trial trajectory p_t^n lags behind a quasi-static version $p_t^{n,\text{eq}}$. KL divergences can be defined between various pairs of these distributions as discussed in the main text.

B. Path integral formulation

An alternative approach is to consider minimizing over the whole trajectory $\lambda(t)$ using a path-integral formulation of the KL divergence

$$D_{\text{path}} [\mathcal{P}^*[\mathbf{q}(t)]||\mathcal{P}_{\lambda^n(t)}[\mathbf{q}(t)]] \equiv \int \mathcal{D}[\mathbf{q}(t)] \mathcal{P}^*[\mathbf{q}(t)] \ln \frac{\mathcal{P}^*[\mathbf{q}(t)]}{\mathcal{P}_{\lambda^n(t)}[\mathbf{q}(t)]}. \quad (64)$$

We can formally write the path probabilities under a protocol $\lambda(t)$ as

$$\mathcal{P}_{\lambda(t)}[\mathbf{q}(t)] = \mathcal{Z}[\lambda(t)]^{-1} e^{-\beta \mathcal{A}[\mathbf{q}(t); \lambda(t)]} \quad (65)$$

for some action integral $\mathcal{A}[\mathbf{q}(t); \lambda(t)]$ and normalization

$$\mathcal{Z}[\lambda(t)] = \int \mathcal{D}[\mathbf{q}(t)] e^{-\beta \mathcal{A}[\mathbf{q}(t); \lambda(t)]}. \quad (66)$$

The functional derivative of $D_{\text{path}}[\mathcal{P}^*[\mathbf{q}(t)]|\mathcal{P}_{\lambda^n(t)}[\mathbf{q}(t)]]$ with respect to $\lambda(t)$ is (cf. Equation 55)

$$\frac{\delta D_{\text{path}}}{\delta \lambda(t)} = \left\langle \beta \frac{\delta \mathcal{A}}{\delta \lambda(t)} \right\rangle_{\mathcal{P}^*} - \left\langle \beta \frac{\delta \mathcal{A}}{\delta \lambda(t)} \right\rangle_{\mathcal{P}_{\lambda^n(t)}} \quad (67)$$

where the averages are functional integrals using the path probabilities.

In principle, if one knows the action describing the system's evolution and can evaluate samples over path distributions, then Equation 67 can be used to perform gradient descent in path space to optimize $\lambda(t)$. Typical actions, such as the Onsager-Machlup action, involve time derivatives of \mathbf{q} , which will cause Equation 67 to depend on these quantities as well [62]. This approach is thus qualitatively different from optimizing at each time point independently using the non-equilibrium distribution potential \tilde{H} which depends only on \mathbf{q} , not its time derivatives. However, we now show that for quasi-static protocols, Equation 67 implies the same increment as Equation 59.

For a quasi-static case, the path probability can be written as

$$\begin{aligned} \mathcal{P}[\mathbf{q}(t)] &= \lim_{N_t \rightarrow \infty} p(\mathbf{q}_0)p(\mathbf{q}_1|\mathbf{q}_0) \cdots p(\mathbf{q}_N|\mathbf{q}_{N-1}) \\ &= p(\mathbf{q}_0)p(\mathbf{q}_1) \cdots p(\mathbf{q}_N) \end{aligned} \quad (68)$$

where we have discretized the trajectory of length T into N_t intervals. The second line follows because for quasi-static systems the system lacks memory and the conditional probabilities simplify. Each distribution $p(\mathbf{q}_i)$ is given by the Boltzmann distribution under the current value of the work parameter, so that

$$\begin{aligned} \mathcal{P}[\mathbf{q}(t)] &= \lim_{N_t \rightarrow \infty} \left(\prod_{n=0}^{N_t} Z(\lambda_n) \right)^{-1} \exp \left(-\beta \sum_{n=0}^{N_t} H(\mathbf{q}_n; \lambda_n) \right) \\ &= \mathcal{Z}^{\text{eq}}[\lambda(t)]^{-1} \exp \left(-\beta \frac{1}{T} \int_0^T H(\mathbf{q}(t); \lambda(t)) dt \right), \end{aligned} \quad (69)$$

where

$$\mathcal{Z}^{\text{eq}}[\lambda(t)] = \int \mathcal{D}[\mathbf{q}(t)] \exp \left(-\beta \frac{1}{T} \int_0^T H(\mathbf{q}(t); \lambda(t)) dt \right). \quad (70)$$

This result implies that for a quasi-static process, $\mathcal{A}[\mathbf{q}(t); \lambda(t)] = \int_0^T H(\mathbf{q}(t); \lambda(t)) dt$. Evaluating Equation 67 then gives

$$\frac{\delta D_{\text{path}}}{\delta \lambda(t)} = \left\langle \beta \frac{H(\mathbf{q}(t); \lambda(t))}{\partial \lambda} \right\rangle_{\mathcal{P}^*} - \left\langle \beta \frac{H(\mathbf{q}(t); \lambda(t))}{\partial \lambda} \right\rangle_{\mathcal{P}_{\lambda^n(t)}}. \quad (71)$$

This resulting derivative is local in time and can be equivalently expressed as in Equation 59. This result makes precise the statement that quasi-staticity breaks up the global trajectory-level problem into a manifold of independent temporally local problems.

C. Systems under linear response

For systems under weak driving we can use adiabatic perturbation to find expressions for the how the approximate gradient Δ^{app} differs from correct gradients Δ^{neq} and Δ^{eq} . The non-equilibrium distribution in this regime can be written as

$$p_{\lambda(t)}(\mathbf{q}) = p_{\lambda(t)}^{\text{eq}}(\mathbf{q}) + \epsilon p_{\lambda(t)}^1(\mathbf{q}) \quad (72)$$

where the superscript 1 indicates the first order correction to the quasi-static time-dependent distribution $p_{\lambda(t)}^{\text{eq}}$. This correction can be expressed in terms of the inverse of the dynamical evolution operator and the time derivative of the protocol $\lambda(t)$, but we will not use this expression here [63, 64]. Due to normalization of $p_{\lambda(t)}^{\text{eq}}$ and $p_{\lambda(t)}$, the integral over \mathbf{q} of $p_{\lambda(t)}^1$ is zero.

We first rewrite Equation 72 as

$$\begin{aligned}
p_{\lambda(t)}(\mathbf{q}) &= p_{\lambda(t)}^{\text{eq}}(\mathbf{q}) \left(1 + \epsilon \frac{p_{\lambda(t)}^1(\mathbf{q})}{p_{\lambda(t)}^{\text{eq}}(\mathbf{q})} \right) \\
&= Z(\lambda(t))^{-1} e^{-\beta H(\mathbf{q}; \lambda(t)) + m(\mathbf{q}; \lambda(t))} \\
&\equiv Z(\lambda(t))^{-1} e^{-\beta \tilde{H}(\mathbf{q}; \lambda(t))}
\end{aligned} \tag{73}$$

where

$$m(\mathbf{q}; \lambda(t)) \equiv \ln \left(1 + \epsilon \frac{p_{\lambda(t)}^1(\mathbf{q})}{p_{\lambda(t)}^{\text{eq}}(\mathbf{q})} \right). \tag{74}$$

To confirm that $Z(\lambda(t))$ is the proper normalization factor for both the exponential weights $-\beta H(\mathbf{q}; \lambda(t))$ and $-\beta \tilde{H}(\mathbf{q}; \lambda(t))$, we evaluate the integral

$$\begin{aligned}
\int d\mathbf{q} e^{-\beta \tilde{H}(\mathbf{q}; \lambda(t))} &= \int d\mathbf{q} \left(1 + \frac{p_{\lambda(t)}^1(\mathbf{q})}{p_{\lambda(t)}^{\text{eq}}(\mathbf{q})} \right) e^{-\beta H(\mathbf{q}; \lambda(t))} \\
&= Z(\lambda(t)) + Z(\lambda(t)) \int d\mathbf{q} p_{\lambda(t)}^1(\mathbf{q}) \\
&= Z(\lambda(t)).
\end{aligned} \tag{75}$$

Thus, Equation 73 is the correct non-equilibrium distribution in the form of Equation 60 above.

We next evaluate the gradients Δ^{eq} , Δ^{app} , and Δ^{neq} . We have

$$\Delta^{\text{eq}} \equiv \left\langle \beta \frac{\partial H(\mathbf{q}; \lambda^n(t))}{\partial \lambda} \right\rangle_{p_{\lambda^n(t)}^{\text{eq}}} - \left\langle \beta \frac{\partial H(\mathbf{q}; \lambda^n(t))}{\partial \lambda} \right\rangle_{p_{\lambda^n(t)}^{\text{eq}}} \tag{76}$$

which corresponds to the limit $\epsilon \rightarrow 0$. The gradient Δ^{app} is

$$\begin{aligned}
\Delta^{\text{app}} &\equiv \left\langle \beta \frac{\partial H(\mathbf{q}; \lambda^n(t))}{\partial \lambda} \right\rangle_{p_{\lambda^n(t)}} - \left\langle \beta \frac{\partial H(\mathbf{q}; \lambda^n(t))}{\partial \lambda} \right\rangle_{p_{\lambda^n(t)}^{\text{eq}}} \\
&= \Delta^{\text{eq}} + \epsilon \left(\left\langle \beta \frac{\partial H(\mathbf{q}; \lambda^n(t))}{\partial \lambda} \right\rangle_{p_{\lambda^n(t)}^1} - \left\langle \beta \frac{\partial H(\mathbf{q}; \lambda^n(t))}{\partial \lambda} \right\rangle_{p_{\lambda^n(t)}^{\text{eq}}} \right).
\end{aligned} \tag{77}$$

If we set $p_{\lambda^n(t)}^1 = p_{\lambda^n(t)}^{\text{eq}}$ then the correction to $\Delta^{\text{app}} = \Delta^{\text{eq}}$ vanishes. We thus see that the difference between Δ^{app} and Δ^{eq} depends on the degree to which “non-equilibrium components” of the distributions $p_{\lambda^n(t)}$ and $p_{\lambda^n(t)}^{\text{eq}}$ differ.

To evaluate Δ^{neq} , we first need to find (expanding the logarithm for small ϵ)

$$\left\langle \frac{\partial m(\mathbf{q}; \lambda)}{\partial \lambda} \right\rangle_{p_{\lambda(t)}} = \epsilon \left\langle \frac{\partial}{\partial \lambda} \frac{p_{\lambda}^1(\mathbf{q})}{p_{\lambda}^{\text{eq}}(\mathbf{q})} \right\rangle_{p_{\lambda(t)}} + \mathcal{O}(\epsilon^2). \tag{78}$$

The order ϵ term can be expressed as (remembering that integrals over $p_{\lambda}^1(\mathbf{q})$ are zero)

$$\begin{aligned}
\epsilon \int d\mathbf{q} \left(\frac{\partial}{\partial \lambda} \frac{p_{\lambda}^1(\mathbf{q})}{p_{\lambda}^{\text{eq}}(\mathbf{q})} \right) (p_{\lambda}^{\text{eq}}(\mathbf{q}) + \epsilon p_{\lambda}^1(\mathbf{q})) &= \epsilon \int d\mathbf{q} \left(\frac{\partial}{\partial \lambda} \frac{p_{\lambda}^1(\mathbf{q})}{p_{\lambda}^{\text{eq}}(\mathbf{q})} \right) p_{\lambda}^{\text{eq}}(\mathbf{q}) + \mathcal{O}(\epsilon^2) \\
&= \epsilon \left\langle \frac{\partial}{\partial \lambda} \frac{p_{\lambda}^1(\mathbf{q})}{p_{\lambda}^{\text{eq}}(\mathbf{q})} \right\rangle_{p_{\lambda(t)}^{\text{eq}}} + \mathcal{O}(\epsilon^2).
\end{aligned} \tag{79}$$

We can alternatively write the order ϵ term as

$$\begin{aligned}
\epsilon \left\langle \frac{\partial}{\partial \lambda} \frac{p_{\lambda}^1(\mathbf{q})}{p_{\lambda}^{\text{eq}}(\mathbf{q})} \right\rangle_{p_{\lambda^*(t)}^{\text{eq}}} &= -\epsilon \int d\mathbf{q} p_{\lambda}^1(\mathbf{q}) \frac{\partial \ln p_{\lambda}^{\text{eq}}(\mathbf{q})}{\partial \lambda} \\
&= \epsilon \int d\mathbf{q} p_{\lambda}^1(\mathbf{q}) \beta \frac{\partial H(\mathbf{q}; \lambda)}{\partial \lambda} \\
&= \epsilon \left\langle \beta \frac{\partial H(\mathbf{q}; \lambda)}{\partial \lambda} \right\rangle_{p_{\lambda}^1}.
\end{aligned} \tag{80}$$

With this, we can write

$$\begin{aligned}
\Delta^{\text{neq}} &\equiv \left\langle \beta \frac{\partial \tilde{H}(\mathbf{q}; \lambda^n(t))}{\partial \lambda} \right\rangle_{p_{\lambda^*(t)}} - \left\langle \beta \frac{\partial \tilde{H}(\mathbf{q}; \lambda^n(t))}{\partial \lambda} \right\rangle_{p_{\lambda^n(t)}} \\
&\equiv \left\langle \beta \frac{\partial H(\mathbf{q}; \lambda^n(t))}{\partial \lambda} \right\rangle_{p_{\lambda^*(t)}} - \left\langle \beta \frac{\partial H(\mathbf{q}; \lambda^n(t))}{\partial \lambda} \right\rangle_{p_{\lambda^n(t)}} - \left(\left\langle \frac{\partial m(\mathbf{q}; \lambda^n(t))}{\partial \lambda} \right\rangle_{p_{\lambda^*(t)}} - \left\langle \beta \frac{\partial m(\mathbf{q}; \lambda^n(t))}{\partial \lambda} \right\rangle_{p_{\lambda^n(t)}} \right) \\
&= \Delta^{\text{app}} - \epsilon \left(\left\langle \frac{\partial}{\partial \lambda} \frac{p_{\lambda}^1(\mathbf{q})}{p_{\lambda}^{\text{eq}}(\mathbf{q})} \right\rangle_{p_{\lambda^*(t)}^{\text{eq}}} - \left\langle \beta \frac{\partial H(\mathbf{q}; \lambda^n(t))}{\partial \lambda} \right\rangle_{p_{\lambda^n(t)}^1} \right) + \mathcal{O}(\epsilon^2).
\end{aligned}$$

We note that the term $\left\langle \frac{\partial m(\mathbf{q}; \lambda^n(t))}{\partial \lambda} \right\rangle_{p_{\lambda^*(t)}}$ does not simplify like $\left\langle \frac{m(\mathbf{q}; \lambda^n(t))}{\partial \lambda} \right\rangle_{p_{\lambda^n(t)}}$ does, because the average is taken over $p_{\lambda^*(t)}$ while the integrand is evaluated for $p_{\lambda^n(t)}$, which prevents passing from Equation 79 to 80. We can rewrite the term

$$\left\langle \frac{\partial}{\partial \lambda} \frac{p_{\lambda}^1(\mathbf{q})}{p_{\lambda}^{\text{eq}}(\mathbf{q})} \right\rangle_{p_{\lambda^*(t)}^{\text{eq}}} = \int d\mathbf{q} \frac{p_{\lambda^*(t)}^{\text{eq}}(\mathbf{q})}{p_{\lambda^n(t)}^{\text{eq}}(\mathbf{q})} \frac{\partial}{\partial \lambda} p_{\lambda^n(t)}^1(\mathbf{q}) + \int d\mathbf{q} \left(\frac{p_{\lambda^*(t)}^{\text{eq}}(\mathbf{q})}{p_{\lambda^n(t)}^{\text{eq}}(\mathbf{q})} \right) p_{\lambda^n(t)}^1(\mathbf{q}) \left(\frac{\partial}{\partial \lambda} \ln(Z(\lambda^n(t))) + \beta \frac{\partial}{\partial \lambda} H(\mathbf{q}; \lambda^n(t)) \right). \tag{81}$$

If we set $p_{\lambda^*(t)}^{\text{eq}} = p_{\lambda^n(t)}^{\text{eq}}$, Equation 81 simplifies as

$$\begin{aligned}
\left\langle \frac{\partial}{\partial \lambda} \frac{p_{\lambda}^1(\mathbf{q})}{p_{\lambda}^{\text{eq}}(\mathbf{q})} \right\rangle_{p_{\lambda^*(t)}^{\text{eq}}} &= \frac{\partial}{\partial \lambda} \int d\mathbf{q} p_{\lambda^n(t)}^1(\mathbf{q}) + \left(\frac{\partial}{\partial \lambda} \ln(Z(\lambda^n(t))) \right) \int d\mathbf{q} p_{\lambda^n(t)}^1(\mathbf{q}) + \int d\mathbf{q} p_{\lambda^n(t)}^1(\mathbf{q}) \beta \frac{\partial}{\partial \lambda} H(\mathbf{q}; \lambda^n(t)) \\
&= \left\langle \beta \frac{\partial H(\mathbf{q}; \lambda^n(t))}{\partial \lambda} \right\rangle_{p_{\lambda^n(t)}^1}
\end{aligned} \tag{82}$$

which cancels the term $-\left\langle \beta \frac{\partial H(\mathbf{q}; \lambda^n(t))}{\partial \lambda} \right\rangle_{p_{\lambda^n(t)}^1}$ in the order ϵ correction of Δ^{app} to Δ^{neq} in Equation 81. We thus see that the difference between Δ^{app} and Δ^{neq} depends on the degree to which the ‘‘equilibrium components’’ $p_{\lambda^*(t)}^{\text{eq}}$ and $p_{\lambda^n(t)}^{\text{eq}}$ differ from each other.

To go further and demonstrate convergence of the approximate update Δ^{app} , we first recall a result from Refs. 65 and 66 that for a system under linear response

$$\langle X_{\alpha}(\lambda(t)) \rangle_{p_{\lambda(t)}} - \langle X_{\alpha}(\lambda(t)) \rangle_{p_{\lambda(t)}^{\text{eq}}} \approx \zeta_{\alpha\gamma}(\lambda(t)) \frac{d\lambda_{\gamma}(t)}{dt} \tag{83}$$

where

$$X_{\alpha}(\lambda(t)) \equiv -\frac{\partial H(\mathbf{q}; \lambda(t))}{\partial \lambda_{\alpha}} \tag{84}$$

is the thermodynamic force conjugate to the parameter component λ_{α} , and we use the shorthand notation $\frac{d\lambda_{\gamma}(t)}{dt} =$

$\frac{d\lambda_\gamma}{dt}|_{\lambda_\gamma=\lambda_\gamma(t)}$. The time integrated matrix

$$\zeta_{\alpha\gamma}(\boldsymbol{\lambda}) = \beta \int_0^\infty dt'' \langle \Delta X_\alpha(\boldsymbol{\lambda}, t' = 0) \Delta X_\gamma(\boldsymbol{\lambda}, t' = t'') \rangle_{p_{\boldsymbol{\lambda}}^{\text{eq}}} \quad (85)$$

measures the covariance between the stochastic quantities $\Delta X_\alpha(\boldsymbol{\lambda}, t' = 0)$, the fluctuations in X_α under parameter values $\boldsymbol{\lambda}$ measured at time $t' = 0$, and $\Delta X_\gamma(\boldsymbol{\lambda}, t' = t'')$. The matrix $\zeta_{\alpha\gamma}(\boldsymbol{\lambda})$ is also the Kirkwood expression of the friction tensor [67]. Writing the difference between the gradients Δ^{app} and Δ^{eq} as

$$\Delta^{\text{app}} - \Delta^{\text{eq}} = -\beta \left(\left(\langle \mathbf{X}(\boldsymbol{\lambda}^n(t)) \rangle_{p_{\boldsymbol{\lambda}^n(t)}} - \langle \mathbf{X}(\boldsymbol{\lambda}^n(t)) \rangle_{p_{\boldsymbol{\lambda}^*(t)}^{\text{eq}}} \right) - \left(\langle \mathbf{X}(\boldsymbol{\lambda}^n(t)) \rangle_{p_{\boldsymbol{\lambda}^n(t)}} - \langle \mathbf{X}(\boldsymbol{\lambda}^n(t)) \rangle_{p_{\boldsymbol{\lambda}^*(t)}^{\text{eq}}} \right) \right), \quad (86)$$

the final term can be written as

$$\langle \mathbf{X}(\boldsymbol{\lambda}^n(t)) \rangle_{p_{\boldsymbol{\lambda}^n(t)}} - \langle \mathbf{X}(\boldsymbol{\lambda}^n(t)) \rangle_{p_{\boldsymbol{\lambda}^*(t)}^{\text{eq}}} = \xi_{\alpha\gamma}(\boldsymbol{\lambda}^n(t)) \frac{d\lambda_\gamma^n(t)}{dt}. \quad (87)$$

In the vicinity of convergence, when $\boldsymbol{\lambda}^n(t)$ nears $\boldsymbol{\lambda}^*(t)$, we can write

$$\begin{aligned} \frac{\partial H(\mathbf{q}; \boldsymbol{\lambda}^n(t))}{\partial \lambda_\alpha} &= \frac{\partial H(\mathbf{q}; \boldsymbol{\lambda}^*(t))}{\partial \lambda_\alpha} + (\lambda_\gamma^n(t) - \lambda_\gamma^*(t)) \frac{\partial^2 H(\mathbf{q}; \boldsymbol{\lambda}^*(t))}{\partial \lambda_\gamma \partial \lambda_\alpha} \\ &\equiv \frac{\partial H(\mathbf{q}; \boldsymbol{\lambda}^*(t))}{\partial \lambda_\alpha} + \delta \lambda_\gamma(t) \Delta_{\gamma\alpha} H(\mathbf{q}; \boldsymbol{\lambda}^*(t)). \end{aligned} \quad (88)$$

With this we can write the first term on the right of Equation 86 as

$$\begin{aligned} \langle X_\alpha(\boldsymbol{\lambda}^n(t)) \rangle_{p_{\boldsymbol{\lambda}^n(t)}} - \langle X_\alpha(\boldsymbol{\lambda}^n(t)) \rangle_{p_{\boldsymbol{\lambda}^*(t)}^{\text{eq}}} &= \langle X_\alpha(\boldsymbol{\lambda}^*(t)) \rangle_{p_{\boldsymbol{\lambda}^*(t)}} - \langle X_\alpha(\boldsymbol{\lambda}^*(t)) \rangle_{p_{\boldsymbol{\lambda}^*(t)}^{\text{eq}}} \\ &\quad - \delta \lambda_\gamma(t) \left(\langle \Delta_{\gamma\alpha} H(\mathbf{q}; \boldsymbol{\lambda}^*(t)) \rangle_{p_{\boldsymbol{\lambda}^*(t)}} - \langle \Delta_{\gamma\alpha} H(\mathbf{q}; \boldsymbol{\lambda}^*(t)) \rangle_{p_{\boldsymbol{\lambda}^*(t)}^{\text{eq}}} \right) \\ &= \xi_{\alpha\gamma}(\boldsymbol{\lambda}^*(t)) \frac{d\lambda_\gamma^*}{dt} \\ &\quad - \delta \lambda_\gamma(t) \left(\langle \Delta_{\gamma\alpha} H(\mathbf{q}; \boldsymbol{\lambda}^*(t)) \rangle_{p_{\boldsymbol{\lambda}^*(t)}} - \langle \Delta_{\gamma\alpha} H(\mathbf{q}; \boldsymbol{\lambda}^*(t)) \rangle_{p_{\boldsymbol{\lambda}^*(t)}^{\text{eq}}} \right). \end{aligned} \quad (89)$$

We also have that

$$\begin{aligned} \Delta_\alpha^{\text{eq}} &= -\beta \left(\langle X_\alpha(\boldsymbol{\lambda}^n(t)) \rangle_{p_{\boldsymbol{\lambda}^*(t)}^{\text{eq}}} - \langle X_\alpha(\boldsymbol{\lambda}^n(t)) \rangle_{p_{\boldsymbol{\lambda}^n(t)}^{\text{eq}}} \right) \\ &= -\beta \left(\langle X_\alpha(\boldsymbol{\lambda}^*(t)) \rangle_{p_{\boldsymbol{\lambda}^*(t)}^{\text{eq}}} - \langle X_\alpha(\boldsymbol{\lambda}^n(t)) \rangle_{p_{\boldsymbol{\lambda}^n(t)}^{\text{eq}}} - \delta \lambda_\gamma(t) \langle \Delta_{\gamma\alpha} H(\mathbf{q}; \boldsymbol{\lambda}^*(t)) \rangle_{p_{\boldsymbol{\lambda}^*(t)}^{\text{eq}}} \right). \end{aligned} \quad (90)$$

The terms $\langle X_\alpha(\boldsymbol{\lambda}(t)) \rangle_{p_{\boldsymbol{\lambda}(t)}^{\text{eq}}}$ can be expressed in terms of the free energy $F(\boldsymbol{\lambda}) = -\beta^{-1} \ln Z(\boldsymbol{\lambda})$ as

$$\langle X_\alpha(\boldsymbol{\lambda}(t)) \rangle_{p_{\boldsymbol{\lambda}(t)}^{\text{eq}}} = -\frac{\partial F(\boldsymbol{\lambda}(t))}{\partial \lambda_\alpha}, \quad (91)$$

so that

$$\Delta_\alpha^{\text{eq}} = -\beta \left(\frac{\partial F(\boldsymbol{\lambda}^n(t))}{\partial \lambda_\alpha} - \frac{\partial F(\boldsymbol{\lambda}^*(t))}{\partial \lambda_\alpha} - \delta \lambda_\gamma(t) \langle \Delta_{\gamma\alpha} H(\mathbf{q}; \boldsymbol{\lambda}^*(t)) \rangle_{p_{\boldsymbol{\lambda}^*(t)}^{\text{eq}}} \right). \quad (92)$$

The free energy $F(\boldsymbol{\lambda}^n(t))$ can be expanded as

$$F(\boldsymbol{\lambda}^n(t)) = F(\boldsymbol{\lambda}^*(t)) + \delta \lambda_\gamma(t) \frac{\partial F(\boldsymbol{\lambda}^*(t))}{\partial \lambda_\gamma} \quad (93)$$

so that

$$\frac{\partial F(\boldsymbol{\lambda}^n(t))}{\partial \lambda_\alpha} - \frac{\partial F(\boldsymbol{\lambda}^*(t))}{\partial \lambda_\alpha} = \delta \lambda_\gamma(t) \frac{\partial^2 F(\boldsymbol{\lambda}^*(t))}{\partial \lambda_\gamma \partial \lambda_\alpha} \equiv \delta \lambda_\gamma(t) \Delta_{\gamma\alpha} F(\boldsymbol{\lambda}^*(t)). \quad (94)$$

Putting everything together, we can rewrite Equation 86 as

$$\begin{aligned} \Delta_\alpha^{\text{app}} &= \beta \left(-\delta\lambda_\gamma(t) \Delta_{\gamma\alpha} F(\boldsymbol{\lambda}^*(t)) + \delta\lambda_\gamma(t) \langle \Delta_{\gamma\alpha} H(\mathbf{q}; \boldsymbol{\lambda}^*(t)) \rangle_{p_{\boldsymbol{\lambda}^*(t)}^{\text{eq}}} \right. \\ &\quad \left. - \xi_{\alpha\gamma}(\boldsymbol{\lambda}^*(t)) \frac{d\lambda_\gamma^*}{dt} + \delta\lambda_\gamma(t) \left(\langle \Delta_{\gamma\alpha} H(\mathbf{q}; \boldsymbol{\lambda}^*(t)) \rangle_{p_{\boldsymbol{\lambda}^*(t)}} - \langle \Delta_{\gamma\alpha} H(\mathbf{q}; \boldsymbol{\lambda}^*(t)) \rangle_{p_{\boldsymbol{\lambda}^*(t)}^{\text{eq}}} \right) + \xi_{\alpha\gamma}(\boldsymbol{\lambda}^n(t)) \frac{d\lambda_\gamma^n(t)}{dt} \right) \\ &= \beta \left(\xi_{\alpha\gamma}(\boldsymbol{\lambda}^n(t)) \frac{d\lambda_\gamma^n(t)}{dt} - \xi_{\alpha\gamma}(\boldsymbol{\lambda}^*(t)) \frac{d\lambda_\gamma^*}{dt} + \delta\lambda_\gamma(t) \langle \Delta_{\gamma\alpha} H(\mathbf{q}; \boldsymbol{\lambda}^*(t)) \rangle_{p_{\boldsymbol{\lambda}^*(t)}} - \delta\lambda_\gamma(t) \Delta_{\gamma\alpha} F(\boldsymbol{\lambda}^*(t)) \right). \end{aligned} \quad (95)$$

Introducing $\delta\xi_{\alpha\gamma}(t) = \xi_{\alpha\gamma}(\boldsymbol{\lambda}^n(t)) - \xi_{\alpha\gamma}(\boldsymbol{\lambda}^*(t))$, we rewrite this as

$$\Delta_\alpha^{\text{app}} = \beta \left(\xi_{\alpha\gamma}^n \frac{d\delta\lambda_\gamma(t)}{dt} + \delta\xi_{\alpha\gamma} \frac{d\lambda_\gamma^*}{dt} + \delta\lambda_\gamma(t) \left(\langle \Delta_{\gamma\alpha} H(\mathbf{q}; \boldsymbol{\lambda}^*(t)) \rangle_{p_{\boldsymbol{\lambda}^*(t)}} - \Delta_{\gamma\alpha} F(\boldsymbol{\lambda}^*(t)) \right) \right). \quad (96)$$

We can further simplify the last term of this expression by first writing

$$\Delta_{\gamma\alpha} F(\boldsymbol{\lambda}^*(t)) = \frac{\partial}{\partial\lambda_\gamma} \int d\mathbf{q} p_{\boldsymbol{\lambda}^*(t)}^{\text{eq}} \frac{\partial H(\mathbf{q}; \boldsymbol{\lambda}^*(t))}{\partial\lambda_\alpha} = \int d\mathbf{q} \frac{\partial}{\partial\lambda_\gamma} p_{\boldsymbol{\lambda}^*(t)}^{\text{eq}} \frac{\partial H(\mathbf{q}; \boldsymbol{\lambda}^*(t))}{\partial\lambda_\alpha} + \langle \Delta_{\gamma\alpha} H(\mathbf{q}; \boldsymbol{\lambda}^*(t)) \rangle_{p_{\boldsymbol{\lambda}^*(t)}^{\text{eq}}}. \quad (97)$$

Straightforward evaluation gives

$$\frac{\partial}{\partial\lambda_\gamma} p_{\boldsymbol{\lambda}^*(t)}^{\text{eq}} = p_{\boldsymbol{\lambda}^*(t)}^{\text{eq}} \left(\left\langle \beta \frac{\partial H(\mathbf{q}; \boldsymbol{\lambda}^*(t))}{\partial\lambda_\gamma} \right\rangle_{p_{\boldsymbol{\lambda}^*(t)}^{\text{eq}}} - \beta \frac{\partial H(\mathbf{q}; \boldsymbol{\lambda}^*(t))}{\partial\lambda_\gamma} \right) \quad (98)$$

so that

$$\begin{aligned} \int d\mathbf{q} \frac{\partial}{\partial\lambda_\gamma} p_{\boldsymbol{\lambda}^*(t)}^{\text{eq}} \frac{\partial H(\mathbf{q}; \boldsymbol{\lambda}^*(t))}{\partial\lambda_\alpha} &= -\beta \left(\left\langle \frac{\partial H(\mathbf{q}; \boldsymbol{\lambda}^*(t))}{\partial\lambda_\gamma} \frac{\partial H(\mathbf{q}; \boldsymbol{\lambda}^*(t))}{\partial\lambda_\alpha} \right\rangle_{p_{\boldsymbol{\lambda}^*(t)}^{\text{eq}}} - \left\langle \frac{\partial H(\mathbf{q}; \boldsymbol{\lambda}^*(t))}{\partial\lambda_\gamma} \right\rangle_{p_{\boldsymbol{\lambda}^*(t)}^{\text{eq}}} \left\langle \frac{\partial H(\mathbf{q}; \boldsymbol{\lambda}^*(t))}{\partial\lambda_\alpha} \right\rangle_{p_{\boldsymbol{\lambda}^*(t)}^{\text{eq}}} \right) \\ &\equiv -\text{Cov}_{p_{\boldsymbol{\lambda}^*(t)}^{\text{eq}}} \left(\frac{\partial H(\mathbf{q}; \boldsymbol{\lambda}^*(t))}{\partial\lambda_\gamma}, \frac{\partial H(\mathbf{q}; \boldsymbol{\lambda}^*(t))}{\partial\lambda_\alpha} \right) \end{aligned} \quad (99)$$

Additionally using

$$\langle \Delta_{\gamma\alpha} H(\mathbf{q}; \boldsymbol{\lambda}^*(t)) \rangle_{p_{\boldsymbol{\lambda}^*(t)}} = \langle \Delta_{\gamma\alpha} H(\mathbf{q}; \boldsymbol{\lambda}^*(t)) \rangle_{p_{\boldsymbol{\lambda}^*(t)}^{\text{eq}}} + \epsilon \langle \Delta_{\gamma\alpha} H(\mathbf{q}; \boldsymbol{\lambda}^*(t)) \rangle_{p_{\boldsymbol{\lambda}^*(t)}^1} \quad (100)$$

we can rewrite Equation 96

$$\Delta_\alpha^{\text{app}} = \beta \left(\xi_{\alpha\gamma}^n \frac{d\delta\lambda_\gamma(t)}{dt} + \delta\xi_{\alpha\gamma} \frac{d\lambda_\gamma^*}{dt} + \delta\lambda_\gamma(t) \left(\text{Cov}_{p_{\boldsymbol{\lambda}^*(t)}^{\text{eq}}} \left(\frac{\partial H(\mathbf{q}; \boldsymbol{\lambda}^*(t))}{\partial\lambda_\gamma}, \frac{\partial H(\mathbf{q}; \boldsymbol{\lambda}^*(t))}{\partial\lambda_\alpha} \right) + \epsilon \langle \Delta_{\gamma\alpha} H(\mathbf{q}; \boldsymbol{\lambda}^*(t)) \rangle_{p_{\boldsymbol{\lambda}^*(t)}^1} \right) \right). \quad (101)$$

Considering that the quantities $\frac{d\lambda_\gamma^*}{dt}$ and ϵ are small due to the assumption of linear response, and that $\delta\lambda_\gamma(t)$ and $\delta\xi_{\alpha\gamma}$ are small due to the vicinity of convergence, only the term proportional to the covariance matrix survives to first order in Equation 101. Hence, we have

$$\Delta_\alpha^{\text{app}} \approx \beta g_{\alpha\gamma} (\lambda_\gamma^n(t) - \lambda_\gamma^*(t)) \quad (102)$$

where

$$g_{\alpha\gamma} \equiv \text{Cov}_{p_{\boldsymbol{\lambda}^*(t)}^{\text{eq}}} \left(\frac{\partial H(\mathbf{q}; \boldsymbol{\lambda}^*(t))}{\partial\lambda_\alpha}, \frac{\partial H(\mathbf{q}; \boldsymbol{\lambda}^*(t))}{\partial\lambda_\gamma} \right) \quad (103)$$

is shown in Ref. 68 to define a thermodynamic metric tensor which is equal to the Fisher information matrix. Importantly, this tensor is a covariance matrix and hence positive semi-definite. Flowing down Δ^{app} will therefore locally attract $\lambda_\alpha^n(t)$ toward the fixed point $\lambda_\alpha^*(t)$, as desired.

D. Systems with linear forces

Here we treat a class of non-autonomous systems in which linear forces act on the system degrees of freedom. The overdamped stochastic dynamics for a vector \mathbf{q} can be written as

$$\partial_t q_i = -\mu K_{ij} (q_j - a_j) + \xi_i \quad (104)$$

where μ is a mobility, $K_{ij}(\boldsymbol{\lambda}_K(t)) = K_{ji}(\boldsymbol{\lambda}_K(t))$ is a symmetric coupling matrix parameterized by the protocol $\boldsymbol{\lambda}_K(t)$, $a_i(\boldsymbol{\lambda}_a(t))$ is a rest value parameterized by the protocol $\boldsymbol{\lambda}_a(t)$, and η_i is an isotropic white noise obeying

$$\langle \xi_i(t) \xi_j(t') \rangle = 2\mu\beta^{-1} \delta_{ij} \delta(t - t'). \quad (105)$$

The corresponding Fokker-Planck equation is

$$\partial_t p(\mathbf{q}) = \mu K_{ij} \partial_i ((q_j - a_j) p(\mathbf{q})) + D \partial_i \partial_i p(\mathbf{q}) \quad (106)$$

where $D = \mu\beta^{-1}$. For a given value of the protocols $\boldsymbol{\lambda} \equiv (\boldsymbol{\lambda}_K, \boldsymbol{\lambda}_a)$, corresponding to K_{ij} and a_i , there is an equilibrium probability distribution over \mathbf{q} given by the multidimensional Gaussian

$$\begin{aligned} p_{\boldsymbol{\lambda}}^{\text{eq}}(\mathbf{q}) &= \left(\frac{\beta \det(\mathbf{K})}{(2\pi)^n} \right)^{\frac{1}{2}} e^{-\frac{1}{2} \beta (q_i - a_i) K_{ij} (q_j - a_j)} \\ &\equiv Z(\boldsymbol{\lambda})^{-1} e^{-\beta H(\mathbf{q}; \boldsymbol{\lambda})}. \end{aligned} \quad (107)$$

If the system starts in equilibrium with respect to the initial values of the protocol $\boldsymbol{\lambda}(0)$ and is then driven out of equilibrium by executing the protocol at finite speed, the distribution will remain of a Gaussian form due to the linear nature of the forces [69, 70]. The non-equilibrium distribution $p_{\boldsymbol{\lambda}^*}$ can thus be written

$$\begin{aligned} p_{\boldsymbol{\lambda}^*}(\mathbf{q}) &= \left(\frac{\beta \det(\tilde{\mathbf{K}})}{(2\pi)^n} \right)^{\frac{1}{2}} e^{-\frac{1}{2} \beta (q_i - \tilde{a}_i) \tilde{K}_{ij} (q_j - \tilde{a}_j)} \\ &\equiv \tilde{Z}(\boldsymbol{\lambda}^*)^{-1} e^{-\beta \tilde{H}(\mathbf{q}; \boldsymbol{\lambda}^*)} \end{aligned} \quad (108)$$

where $\tilde{K}_{ij} = K_{ij}(\boldsymbol{\lambda}_K^*) + \delta K_{ij}$ and $\tilde{a}_i = a_i(\boldsymbol{\lambda}_a^*) + \delta a_i$ are a ‘‘lagged’’ coupling matrix and mean vector. The non-equilibrium exponential weight $\tilde{H}(\mathbf{q}; \boldsymbol{\lambda})$ can be written as

$$\tilde{H}(\mathbf{q}; \boldsymbol{\lambda}) = H(\mathbf{q}; \boldsymbol{\lambda}) + \delta H(\mathbf{X}; \boldsymbol{\lambda}) \quad (109)$$

where

$$H(\mathbf{q}; \boldsymbol{\lambda}) = \frac{1}{2} ((q_i - a_i) K_{ij} (q_j - a_j)) \quad (110)$$

is the Hamiltonian and

$$\delta H(\mathbf{X}; \boldsymbol{\lambda}) = \frac{1}{2} ((q_i - a_i - \delta a_i) \delta K_{ij} (q_j - a_j - \delta a_j) - (q_i - a_i) K_{ij} \delta a_j - \delta a_i K_{ij} (q_j - a_j) + \delta a_i K_{ij} \delta a_j) \quad (111)$$

is a lagged quantity.

We are interested in the gradients $\partial_{\boldsymbol{\lambda}} H(\mathbf{q}, \boldsymbol{\lambda})$ and $\partial_{\boldsymbol{\lambda}} \tilde{H}(\mathbf{q}, \boldsymbol{\lambda})$ which enter in to Δ^{eq} , Δ^{app} and Δ^{neq} . For an element $\lambda_{\alpha} \in \boldsymbol{\lambda}_a$, we have

$$\frac{\partial H}{\partial \lambda_{\alpha}} = \frac{\partial a_i}{\partial \lambda_{\alpha}} \frac{\partial H}{\partial a_i} = -\frac{\partial a_i}{\partial \lambda_{\alpha}} (K_{ij} (q_j - a_j)) \quad (112)$$

and

$$\frac{\partial \tilde{H}}{\partial \lambda_{\alpha}} = \frac{\partial a_i}{\partial \lambda_{\alpha}} \frac{\partial \tilde{H}}{\partial a_i} = \frac{\partial a_i}{\partial \lambda_{\alpha}} \left(\frac{\partial H}{\partial a_i} + \delta \frac{\partial H}{\partial a_i} \right) \quad (113)$$

where

$$\delta \frac{\partial H}{\partial a_i} \equiv -\delta K_{ij}(q_j - a_j - \delta a_j) + K_{ij} \delta a_j. \quad (114)$$

Similarly, for $\lambda_\alpha \in \boldsymbol{\lambda}_K$ we have

$$\frac{\partial H}{\partial \lambda_\alpha} = \frac{\partial K_{ij}}{\partial \lambda_\alpha} \frac{\partial H}{\partial K_{ij}} = \frac{\partial K_{ij}}{\partial \lambda_\alpha} \left(\frac{1}{2}(q_i - a_i)(q_j - a_j) \right) \quad (115)$$

and

$$\frac{\partial \tilde{H}}{\partial \lambda_\alpha} = \frac{\partial K_{ij}}{\partial \lambda_\alpha} \frac{\partial \tilde{H}}{\partial K_{ij}} = \frac{\partial K_{ij}}{\partial \lambda_\alpha} \left(\frac{\partial H}{\partial K_{ij}} + \delta \frac{\partial H}{\partial K_{ij}} \right) \quad (116)$$

where

$$\delta \frac{\partial H}{\partial K_{ij}} \equiv -\frac{1}{2} ((q_i - a_i)\delta a_j + \delta a_i(q_j - a_j) - \delta a_i \delta a_j). \quad (117)$$

We next use these expressions to evaluate the gradients Δ^{eq} , Δ^{neq} , and Δ^{app} . For $\lambda_\alpha \in \boldsymbol{\lambda}_a$ have

$$\begin{aligned} \Delta^{\text{eq}} &= \left\langle \beta \frac{\partial H(\mathbf{q}; \boldsymbol{\lambda}^n(t))}{\partial \lambda_\alpha} \right\rangle_{p_{\boldsymbol{\lambda}^*(t)}^{\text{eq}}} - \left\langle \beta \frac{\partial H(\mathbf{q}; \boldsymbol{\lambda}^n(t))}{\partial \lambda_\alpha} \right\rangle_{p_{\boldsymbol{\lambda}^n(t)}^{\text{eq}}} \\ &= -\beta \frac{\partial a_i^{n,t}}{\partial \lambda_\alpha} K_{ij}^{n,t} \left(\left(\langle q_j \rangle_{p_{\boldsymbol{\lambda}^*(t)}^{\text{eq}}} - a_j^{n,t} \right) - \left(\langle q_j \rangle_{p_{\boldsymbol{\lambda}^n(t)}^{\text{eq}}} - a_j^{n,t} \right) \right) \\ &= -\beta \frac{\partial a_i^{n,t}}{\partial \lambda_\alpha} K_{ij}^{n,t} (a_j^{*,t} - a_j^{n,t}) \end{aligned} \quad (118)$$

where we have introduced the shorthand notation $K_{ij}^{n,t} \equiv K_{ij}(\boldsymbol{\lambda}_K^n(t))$, $a_i^{n,t} \equiv a_i(\boldsymbol{\lambda}_a^n(t))$, and $\frac{\partial a_i^{n,t}}{\partial \lambda_\alpha} = \partial_{\lambda_\alpha} a_i|_{a_i=a_i^{n,t}}$. We have also used the fact that $\langle q_i \rangle_{p_{\boldsymbol{\lambda}^*(t)}^{\text{eq}}} = a_i^{*,t}$ and $\langle q_i \rangle_{p_{\boldsymbol{\lambda}^n(t)}^{\text{eq}}} = a_i^{n,t}$. We next have

$$\begin{aligned} \Delta^{\text{app}} &= \left\langle \beta \frac{\partial H(\mathbf{q}; \boldsymbol{\lambda}^n(t))}{\partial \lambda_\alpha} \right\rangle_{p_{\boldsymbol{\lambda}^*(t)}} - \left\langle \beta \frac{\partial H(\mathbf{q}; \boldsymbol{\lambda}^n(t))}{\partial \lambda_\alpha} \right\rangle_{p_{\boldsymbol{\lambda}^n(t)}} \\ &= -\beta \frac{\partial a_i^{n,t}}{\partial \lambda_\alpha} K_{ij}^{n,t} \left(\left(\langle q_j \rangle_{p_{\boldsymbol{\lambda}^*(t)}} - a_j^{n,t} \right) - \left(\langle q_j \rangle_{p_{\boldsymbol{\lambda}^n(t)}} - a_j^{n,t} \right) \right) \\ &= -\beta \frac{\partial a_i^{n,t}}{\partial \lambda_\alpha} K_{ij}^{n,t} \left((a_j^{*,t} + \delta a_j^{*,t} - a_j^{n,t}) - (a_j^{n,t} + \delta a_j^{n,t} - a_j^{n,t}) \right) \\ &= \Delta^{\text{eq}} - \beta \frac{\partial a_i^{n,t}}{\partial \lambda_\alpha} K_{ij}^{n,t} (\delta a_j^{*,t} - \delta a_j^{n,t}). \end{aligned} \quad (119)$$

Here, we used the fact that $\langle q_i \rangle_{p_{\boldsymbol{\lambda}^*(t)}} = a_i^{*,t} + \delta a_i^{*,t}$ and $\langle q_i \rangle_{p_{\boldsymbol{\lambda}^n(t)}} = a_i^{n,t} + \delta a_i^{n,t}$. Finally we have

$$\begin{aligned} \Delta^{\text{neq}} &= \left\langle \beta \frac{\partial \tilde{H}(\mathbf{q}; \boldsymbol{\lambda}^n(t))}{\partial \lambda_\alpha} \right\rangle_{p_{\boldsymbol{\lambda}^*(t)}} - \left\langle \beta \frac{\partial \tilde{H}(\mathbf{q}; \boldsymbol{\lambda}^n(t))}{\partial \lambda_\alpha} \right\rangle_{p_{\boldsymbol{\lambda}^n(t)}} \\ &= \Delta^{\text{app}} - \beta \frac{\partial a_i}{\partial \lambda_\alpha} \left(\delta K_{ij}^{n,t} \left(\left(\langle q_j \rangle_{p_{\boldsymbol{\lambda}^*(t)}} - a_j^{n,t} - \delta a_j^{n,t} \right) - \left(\langle q_j \rangle_{p_{\boldsymbol{\lambda}^n(t)}} - a_j^{n,t} - \delta a_j^{n,t} \right) \right) + K_{ij}^{n,t} (\delta a_j^{n,t} - \delta a_j^{n,t}) \right) \\ &= \Delta^{\text{app}} - \beta \frac{\partial a_i}{\partial \lambda_\alpha} \left(\delta K_{ij}^{n,t} (a_j^{*,t} + \delta a_j^{*,t} - a_j^{n,t} - \delta a_j^{n,t}) \right). \end{aligned} \quad (120)$$

We see that if there is no lag in the effective coupling matrix $\delta \mathbf{K}^{n,t}$, then $\Delta^{\text{neq}} = \Delta^{\text{app}}$ for $\lambda_\alpha \in \boldsymbol{\lambda}_a$.

For $\lambda_\alpha \in \boldsymbol{\lambda}_K$, we have

$$\begin{aligned}
\Delta^{\text{eq}} &= \beta \frac{1}{2} \frac{\partial K_{ij}^{n,t}}{\partial \lambda_\alpha} \left(\langle \langle (q_i - a_i^{n,t})(q_j - a_j^{n,t}) \rangle \rangle_{p_{\boldsymbol{\lambda}^*(t)}^{\text{eq}}} - \langle \langle (q_i - a_i^{n,t})(q_j - a_j^{n,t}) \rangle \rangle_{p_{\boldsymbol{\lambda}^n(t)}^{\text{eq}}} \right) \\
&= \beta \frac{1}{2} \frac{\partial K_{ij}^{n,t}}{\partial \lambda_\alpha} \left(\left(\langle q_i q_j \rangle_{p_{\boldsymbol{\lambda}^*(t)}^{\text{eq}}} - a_i^{n,t} \langle q_j \rangle_{p_{\boldsymbol{\lambda}^*(t)}^{\text{eq}}} - a_j^{n,t} \langle q_i \rangle_{p_{\boldsymbol{\lambda}^*(t)}^{\text{eq}}} + a_i^{n,t} a_j^{n,t} \right) \right. \\
&\quad \left. - \left(\langle q_i q_j \rangle_{p_{\boldsymbol{\lambda}^n(t)}^{\text{eq}}} - a_i^{n,t} \langle q_j \rangle_{p_{\boldsymbol{\lambda}^n(t)}^{\text{eq}}} - a_j^{n,t} \langle q_i \rangle_{p_{\boldsymbol{\lambda}^n(t)}^{\text{eq}}} + a_i^{n,t} a_j^{n,t} \right) \right) \\
&= \beta \frac{1}{2} \frac{\partial K_{ij}^{n,t}}{\partial \lambda_\alpha} \left(\langle q_i q_j \rangle_{p_{\boldsymbol{\lambda}^*(t)}^{\text{eq}}} - \langle q_i q_j \rangle_{p_{\boldsymbol{\lambda}^n(t)}^{\text{eq}}} - (a_i^{n,t} a_j^{*,t} + a_j^{n,t} a_i^{*,t}) + 2a_i^{n,t} a_j^{n,t} \right). \tag{121}
\end{aligned}$$

An alternative expression for this gradient can be found using definition of the correlation matrix \mathbf{C}

$$C_{ij} \equiv \langle (q_i - a_i)(q_j - a_j) \rangle = \beta^{-1} (\mathbf{K}^{-1})_{ij} \tag{122}$$

for a multidimensional Gaussian parameterized by mean \mathbf{a} and stiffness \mathbf{K} . One can rewrite this as

$$\langle (q_i - b_i)(q_j - b_j) \rangle = C_{ij} + (b_i - a_i)(b_j - a_j) \tag{123}$$

for arbitrary b_i and b_j . With this can express Δ^{eq} as

$$\Delta^{\text{eq}} = \beta \frac{1}{2} \frac{\partial K_{ij}^{n,t}}{\partial \lambda_\alpha} (C_{ij}^{*,t} - C_{ij}^{n,t} + (a_i^{n,t} - a_i^{*,t})(a_j^{n,t} - a_j^{*,t})). \tag{124}$$

We next have

$$\begin{aligned}
\Delta^{\text{app}} &= \beta \frac{1}{2} \frac{\partial K_{ij}^{n,t}}{\partial \lambda_\alpha} \left(\langle \langle (q_i - a_i^{n,t})(q_j - a_j^{n,t}) \rangle \rangle_{p_{\boldsymbol{\lambda}^*(t)}} - \langle \langle (q_i - a_i^{n,t})(q_j - a_j^{n,t}) \rangle \rangle_{p_{\boldsymbol{\lambda}^n(t)}} \right) \\
&= \beta \frac{1}{2} \frac{\partial K_{ij}^{n,t}}{\partial \lambda_\alpha} \left(\tilde{C}_{ij}^{*,t} + (a_i^{n,t} - a_i^{*,t} - \delta a_i^{*,t})(a_j^{n,t} - a_j^{*,t} - \delta a_j^{*,t}) - \tilde{C}_{ij}^{n,t} - \delta a_i^{n,t} \delta a_j^{n,t} \right) \\
&= \Delta^{\text{eq}} + \beta \frac{1}{2} \frac{\partial K_{ij}^{n,t}}{\partial \lambda_\alpha} (\delta C_{ij}^{*,t} - \delta C_{ij}^{n,t} - (a_i^{n,t} - a_i^{*,t}) \delta a_j^{*,t} - \delta a_i^{*,t} (a_j^{n,t} - a_j^{*,t})) \tag{125}
\end{aligned}$$

where we have introduced $\tilde{C}_{ij} \equiv \beta^{-1} (\tilde{\mathbf{K}}^{-1})_{ij} = C_{ij} + \delta C_{ij}$, with δC_{ij} being the lag induced in the correlation matrix \mathbf{C} . We note that the relation between δK_{ij} and δC_{ij} can be obtained using the Woodbury matrix identity (assuming that all matrices are invertible as necessary)

$$\begin{aligned}
(\mathbf{K} + \delta \mathbf{K})^{-1} &= \mathbf{K}^{-1} - \mathbf{K}^{-1} (\mathbf{K}^{-1} + (\delta \mathbf{K})^{-1})^{-1} \mathbf{K}^{-1} \\
&= \beta \mathbf{C} - \beta^2 \mathbf{C} (\beta \mathbf{C} + (\delta \mathbf{K})^{-1})^{-1} \mathbf{C} \\
&\equiv \beta (\mathbf{C} + \delta \mathbf{C}). \tag{126}
\end{aligned}$$

Assuming that the lag $\delta \mathbf{K}$ is small compared to \mathbf{K} , we can expand $(\beta \mathbf{C} + (\delta \mathbf{K})^{-1})^{-1} \approx \delta \mathbf{K}$ and obtain

$$\delta \mathbf{C} = -\beta \mathbf{C} (\delta \mathbf{K}) \mathbf{C}. \tag{127}$$

Finally, we have

$$\begin{aligned}
\Delta^{\text{neq}} &= \Delta^{\text{app}} - \beta \frac{1}{2} \frac{\partial K_{ij}^{n,t}}{\partial \lambda_\alpha} \left(\langle \langle (q_i - a_i^{n,t}) \delta a_j^{n,t} + \delta a_i^{n,t} (q_j - a_j^{n,t}) - \delta a_i^{n,t} \delta a_j^{n,t} \rangle \rangle_{p_{\boldsymbol{\lambda}^*(t)}} \right. \\
&\quad \left. - \langle \langle (q_i - a_i^{n,t}) \delta a_j^{n,t} + \delta a_i^{n,t} (q_j - a_j^{n,t}) - \delta a_i^{n,t} \delta a_j^{n,t} \rangle \rangle_{p_{\boldsymbol{\lambda}^n(t)}} \right) \\
&= \Delta^{\text{app}} - \beta \frac{1}{2} \frac{\partial K_{ij}^{n,t}}{\partial \lambda_\alpha} ((a_i^{*,t} - a_i^{n,t}) \delta a_j^{n,t} + \delta a_i^{n,t} (a_j^{*,t} - a_j^{n,t}) + \delta a_i^{*,t} \delta a_j^{n,t} + \delta a_i^{n,t} \delta a_j^{*,t} - 2\delta a_i^{n,t} \delta a_j^{n,t}). \tag{128}
\end{aligned}$$

We see that if there is no lag in the effective mean $\delta \mathbf{a}^{n,t}$, then $\Delta^{\text{neq}} = \Delta^{\text{app}}$ for $\lambda_\alpha \in \boldsymbol{\lambda}_K$.

E. Fourier analysis of Helfrich membrane dynamics

As described in the main text, the overdamped relaxational dynamics of the height field $q(r, t)$ of a Helfrich membrane are

$$\partial_t q(r, t) = -\mu \frac{\delta H[q(r, t)]}{\delta q(r, t)} = \mu \left(\left(\sigma + \frac{\kappa \lambda^2}{2} \right) \partial_r^2 q + \partial_r q \partial_r \lambda - \kappa (\partial_r^4 q - \partial_r^2 \lambda) \right). \quad (129)$$

We expand $q(r, t)$ in Fourier modes as

$$q(r, t) = \sum_{m=-\infty}^{\infty} q_m(t) e^{imkr} \quad (130)$$

where $k = 2\pi/L$. Similarly, the protocol $\lambda(r, t)$ is expanded as

$$\lambda(r, t) = \sum_{m=-\infty}^{\infty} \lambda_m(t) e^{imkr}. \quad (131)$$

For small values of $\lambda(r, t)$ and $q(r, t)$, we neglect the nonlinear terms in Equation 129 and write the equation of motion for the amplitude of the m^{th} mode as

$$\begin{aligned} \partial_t q_m(t) &= -\mu m^2 k^2 \left((\sigma + m^2 k^2 \kappa) q_m(t) + \kappa \lambda_m(t) \right) \\ &= -\mu K_m (q_m(t) - a_m(t)) \end{aligned} \quad (132)$$

where

$$K_m \equiv m^2 k^2 (\sigma + m^2 k^2 \kappa) \quad (133)$$

and

$$a_m(t) \equiv -\frac{\kappa}{\sigma + m^2 k^2 \kappa} \lambda_m(t). \quad (134)$$

Comparing Equations 104 and 132 see that the m^{th} modes acts like a particle in a harmonic trap whose position $a_m(t)$ but not stiffness K_m is altered as a function of time. The coupling matrix K_{ij} in this case is diagonalized due to the neglected non-linear terms in the membrane dynamics, and we have also neglected the noise; these extensions to the theory of trainable membranes could be treated in future work.

III. STEADY STATES OF CHEMICAL REACTION NETWORKS

A. Cost function for learning steady-states

Here we study linear chemical reaction networks driven by out-of-equilibrium chemical potentials that drive non-conservative reaction fluxes. Such a system is described by N_s species which interact (through first-order or pseudo-first-order kinetics) through a $N_s \times N_s$ transition rate matrix \mathbf{W} . The probability of observing species i at time t is denoted $p_i(t)$, and the vector of these probabilities evolves according to the master equation

$$\partial_t \mathbf{p}(t) = \mathbf{W} \mathbf{p}(t). \quad (135)$$

At long times these dynamics will settle into a steady-state distribution $\boldsymbol{\pi}$ for which $\mathbf{W} \boldsymbol{\pi} = \mathbf{0}$. We note that, in contrast to the \mathbf{W} matrices in SI Section I, the \mathbf{W} matrices in this section are continuous-time rate matrices (with column sums of zero), not discrete-time transition matrices (with column sums of one).

Viewing the rate matrix \mathbf{W} as the weighted adjacency matrix of a graph connecting N_s nodes, the matrix tree

theorem gives an exact expression π_i in terms of the spanning trees of the graph rooted at node i :

$$\pi_i = \frac{\sum_{T \in \mathcal{T}} w(T_i)}{\sum_i \sum_{T \in \mathcal{T}} w(T_i)} \quad (136)$$

where

$$w(T_i) = \prod_{\{jk\} \in T_i} W_{jk} \quad (137)$$

is the product of all transition rates W_{jk} leading from k to j in the directed spanning tree T_i . The spanning tree T belongs to the set of all such trees \mathcal{T} in the transition graph, and T_i represents the unique directed version of the tree T in which each edge is directed so as to point toward node i .

Equation 136 can be expressed in the Boltzmann-like form

$$\pi_i = Z^{-1} e^{\Phi_i} \quad (138)$$

where

$$\Phi_i = \ln \sum_{T \in \mathcal{T}} w(T_i) \quad (139)$$

is the “non-equilibrium potential” and

$$Z = \sum_{i=1}^N e^{\Phi_i} \quad (140)$$

is the “partition function.”

We can formally compute the gradient of the KL divergence between a trial distribution π^n and a target steady-state distribution π^* :

$$\frac{\partial D[\pi^* || \pi^n]}{\partial W_{ij}} = - \left\langle \frac{\partial \Phi}{\partial W_{ij}} \right\rangle_{\pi^*} + \left\langle \frac{\partial \Phi}{\partial W_{ij}} \right\rangle_{\pi^n} \quad (141)$$

where

$$\left\langle \frac{\partial \Phi}{\partial W_{ij}} \right\rangle_{\pi^*} \equiv \sum_k \pi_k^* \frac{\partial \Phi_k}{\partial W_{ij}}. \quad (142)$$

The gradient $\frac{\partial \Phi_k}{\partial W_{ij}}$ can be written as

$$\frac{\partial \Phi_k}{\partial W_{ij}} = \left(\sum_{T \in \mathcal{T}} w(T_k) \right)^{-1} \sum_{T \in \mathcal{T}} \frac{\partial w(T_k)}{\partial W_{ij}}. \quad (143)$$

Although in principle this expression can be computed given knowledge of \mathbf{W} , the gradient $\frac{\partial \Phi_k}{\partial W_{ij}}$ is non-local (in k) and more difficult to handle than the corresponding term which appears when minimizing the KL divergence for Hamiltonian systems, $\frac{\partial H}{\partial \lambda}$. We thus consider an alternative problem, and instead of the KL divergence $D[\pi^* || \pi^n]$ we aim to minimize the quadratic cost function

$$C(\pi_k^*, \pi_k^n) = \frac{1}{2} (\pi_k^* - \pi_k^n)^2. \quad (144)$$

In the next section we show that approximate gradients of this cost function can be expressed in a simple local form.

B. Fixed sign derivatives

The transition rates W_{ij} in chemical kinetics are exponential functions of the energy barrier heights and one cannot generally directly vary them. A convenient way to parameterize W_{ij} is as [37]

$$W_{ij} = e^{E_j - B_{ij} + F_{ij}(\alpha_{ij})/2}, \quad (145)$$

where $B_{ij} = B_{ji}$ and $F_{ij} = -F_{ji}$. The parameters $F_{ij}(\alpha_{ij})$ represent non-conservative driving which violates detailed balance. We set $F_{ij}(\alpha_{ij}) = \alpha_{ij}$ for simplicity. Assuming that we have access to the parameter α_{ij} across edge $i \leftrightarrow j$, we are interested in the gradient

$$\frac{\partial C(\pi_k^*, \pi_k^n)}{\partial \alpha_{ij}} = -\frac{\partial \pi_k^n}{\partial \alpha_{ij}} (\pi_k^* - \pi_k^n). \quad (146)$$

We next show that the prefactor $\frac{\partial \pi_k^n}{\partial \alpha_{ij}}$ is a non-local function, requiring knowledge of parameters at all nodes in the network. However, we further show that updates based on Equation 146 can be considerably simplified into a local rule due to this prefactor having a fixed sign across the range of α_{ij} .

Varying α_{ij} affects both W_{ij} and W_{ji} , so that (dropping the superscript n)

$$\begin{aligned} \frac{\partial \pi_k}{\partial \alpha_{ij}} &= \frac{\partial W_{ij}}{\partial \alpha_{ij}} \frac{\partial \pi_k}{\partial W_{ij}} + \frac{\partial W_{ji}}{\partial \alpha_{ij}} \frac{\partial \pi_k}{\partial W_{ji}} \\ &= \frac{1}{2} \left(W_{ij} \frac{\partial \pi_k}{\partial W_{ij}} - W_{ji} \frac{\partial \pi_k}{\partial W_{ji}} \right) \end{aligned} \quad (147)$$

since $\frac{\partial W_{ij}}{\partial \alpha_{ij}} = \frac{1}{2} W_{ij}$ and $\frac{\partial W_{ji}}{\partial \alpha_{ij}} = -\frac{1}{2} W_{ji}$. We can pull out the dependence of π_k on the rates W_{ij} and W_{ji} as follows:

$$\pi_k = \frac{a_k W_{ij} + b_k W_{ji} + c_k}{\bar{a} W_{ij} + \bar{b} W_{ji} + \bar{c}} \quad (148)$$

where

$$a_k = \sum_T^{(ij)} w^-(T_k) \geq 0 \quad (149)$$

is the sum over all directed spanning trees rooted at node k which contain the directed edge $j \rightarrow i$. The quantity $w^-(T_k)$ is the product of all rates in this tree excluding W_{ij} , which has been factored out (denoted by the $-$ superscript). Similarly, we have

$$b_k = \sum_T^{(ji)} w^-(T_k) \geq 0 \quad (150)$$

for the spanning trees which include $i \rightarrow j$. Note that the directed spanning trees which include $i \rightarrow j$ necessarily exclude $j \rightarrow i$, so the sums in a and b are over separate terms. Finally, the sum over spanning trees in which neither $i \rightarrow j$ nor $j \rightarrow i$ appear is

$$c_k = \sum_T^{(-)} w(T_k) \geq 0 \quad (151)$$

where the path weights $w(T_k)$ have no terms factored out. The coefficients in the denominator of Equation 148 include

sums over all nodes k' :

$$\bar{a} = \sum_{k'} a_{k'} > a_k \quad (152)$$

$$\bar{b} = \sum_{k'} b_{k'} > b_k \quad (153)$$

$$\bar{c} = \sum_{k'} c_{k'} > c. \quad (154)$$

From the form in Equation 148, we can write Equation 147 as the non-local function

$$\frac{\partial \pi_k}{\partial \alpha_{ij}} = \frac{x_1 W_{ij} + x_2 W_{ji} + 2x_3 W_{ij} W_{ji}}{2(\bar{a} W_{ij} + \bar{b} W_{ji} + \bar{c})^2} \quad (155)$$

where

$$x_1 = a_k \bar{c} - c_k \bar{a} \quad (156)$$

$$x_2 = c_k \bar{b} - b_k \bar{c} \quad (157)$$

$$x_3 = a_k \bar{b} - b_k \bar{a}. \quad (158)$$

Clearly the sign of Equation 155 is determined by the numerator, which in turn depends on the factors x_1 , x_2 , and x_3 . We will show that these factors are either all non-negative or all non-positive, implying that the sign of the numerator is fixed for any values of W_{ij} and W_{ji} (which as rate matrix elements must be non-negative). Dividing each of these factors by $\bar{a}\bar{b}\bar{c}$, we see that this can happen if either

$$\frac{a_k}{\bar{a}} \leq \frac{c_k}{\bar{c}} \leq \frac{b_k}{\bar{b}} \rightarrow x_1, x_2, x_3 < 0 \quad (159)$$

or

$$\frac{a_k}{\bar{a}} \geq \frac{c_k}{\bar{c}} \geq \frac{b_k}{\bar{b}} \rightarrow x_1, x_2, x_3 > 0. \quad (160)$$

In SI Figure 9A we show numerically that one of these two orderings always holds by plotting a histogram of the quantity $\omega_k \equiv (a_k/\bar{a} - c_k/\bar{c})(c_k/\bar{c} - b_k/\bar{b})$, which will be positive if either of the two orderings holds.

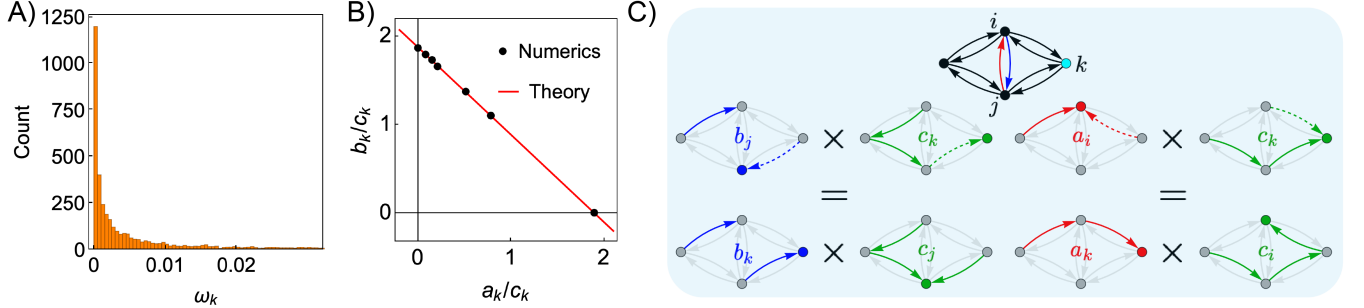


FIG. 9. A) Histogram of ω_k for each node k of 50 randomly generated graphs with 8 nodes and 11 edges. D) Numerical verification of the theoretical result $\frac{b_k}{c_k} = \frac{b_j}{c_j} - \frac{b_j c_i a_k}{a_i c_j c_k}$, which is implied by Equation 163, for the a node in the graph in SI Figure 5 of the main text. C) Illustration in a four state graph of the correspondence between terms on both sides of Equation 164. Two schematic equations, on the left and right side are depicted. On the left, it is shown how a term from the sum $b_j c_k$ can be mapped into a term from $b_k c_j$, while on the right it is shown how a term from the sum $a_i c_k$ can be mapped into a term from $a_k c_i$.

To prove these inequalities, we first note that (recall that these quantities are related to edge W_{ij})

$$a_i = b_j. \quad (161)$$

The term a_i represents the sum of all directed trees which flow into node i and which involve the edge $j \rightarrow i$. These trees thus include the flows into node j . Similarly, b_j represents all directed trees which flow into node j and involve the edge $i \rightarrow j$. The weights W_{ij} and W_{ji} are excluded from a_i and b_j , respectively, and thus these terms represent the weights for the same collection of flows into nodes i and j . We also have that

$$a_j = b_i = 0 \quad (162)$$

since no directed spanning trees rooted at node j can contain the edge $j \rightarrow i$, and no directed spanning trees rooted at node i can contain the edge $i \rightarrow j$.

Next, we prove the following formula which is our key result (numerically verified in SI Figure 9B):

$$a_i c_k = b_j c_k = c_i a_k + c_j b_k, \quad (163)$$

where the first equality is due to Equation 161. Inserting the definitions of these quantities, Equation 163 reads

$$\begin{aligned} \sum_T \sum_{T'}^{ij} w^-(T_i) w(T'_k) &= \sum_T \sum_{T'}^{ji} w^-(T_j) w(T'_k) \\ &= \sum_S^{ij} \sum_{S'} w^-(S_k) w(S'_i) + \sum_U^{ji} \sum_{U'} w^-(U_k) w(U'_j). \end{aligned} \quad (164)$$

Let $N_{[ij]}$ denote the number of undirected spanning trees containing the edge $i \leftrightarrow j$ and N_- denote the number of undirected spanning trees without the undirected edge $i \leftrightarrow j$. Further let N_{ij}^k denote the number of directed spanning trees rooted at node k which contain the directed edge $j \rightarrow i$, and similarly for N_{ji}^k . We have $N_{ij}^k + N_{ji}^k = N_{[ij]}$ for any k . The double sum on the left hand side of Equation 164 has $N_{[ij]} N_-$ terms, while the first double sum on the right hand side has $N_{ij}^k N_-$ and the second has $N_{ji}^k N_-$. Hence, there are the same number of terms on both sides the equation. If we can find a one-to-one correspondence between the terms on each side of this equation, the equality would be proved. Fortunately, just such a correspondence was illustrated in Ref. 37 using a procedure called ‘‘tree surgery.’’ This procedure algorithmically takes as input a pair of directed spanning trees T_m , which is rooted at node m and contains either the edge $i \leftarrow j$ or $j \leftarrow i$, and T'_n , which is rooted at node n does not contain either edge. The procedure converts this pair into a new pair \tilde{T}_n and \tilde{T}'_m , where \tilde{T}_n contains edge $i \leftarrow j$ or $j \leftarrow i$, and \tilde{T}'_m does not. It was further shown that the weight products $w(T_m)w(T'_n)$ and $w(\tilde{T}_n)w(\tilde{T}'_m)$ will be equal if, during the conversion procedure, the edge $i \leftarrow j$ or $j \leftarrow i$ is not flipped. Using this procedure, it is possible to convert each of the $N_{[ij]} N_-$ terms on the left hand side of Equation 164 into either a term of the form $w^-(S_k)w(S'_i)$, or one of the form $w^-(U_k)w(U'_j)$. This is illustrated in SI Figure 9C. In our case, one can ignore the effect of flipping the distinguished edge $i \leftrightarrow j$ because doing so would simply convert a tree T_i rooted at i into a tree T_j rooted at j , or vice versa. The weights of interest $w^-(T_i) = w^-(T_j)$ for two such trees must be the same because the term W_{ij} in $w(T_i)$ and W_{ji} in $w(T_j)$, which would change during the edge flip, have been factored out in $w^-(T_i)$ and $w^-(T_j)$. As a result, flipping the edge $i \leftarrow j$ does not affect the equality of edge weights between the left and right hand sides of Equation 164. We can therefore establish the desired one-to-one correspondence between the terms on both sides of Equation 164, implying equality.

The linear relation between a_k , b_k and c_k in Equation 163 implies two interesting properties of the derivative $\frac{\partial \pi_k}{\partial \alpha_{ij}}$. First, one of the two orderings in Equations 160 or 159 holds. To see this, we consider

$$\frac{c_k}{\bar{c}} = \frac{c_i a_k + c_j b_k}{c_i \bar{a} + c_j \bar{b}}. \quad (165)$$

Let us first assume that $c_k/\bar{c} \leq b_k/\bar{b}$, which means

$$c_i a_k + c_j b_k \leq \frac{b_k}{\bar{b}} (c_i \bar{a} + c_j \bar{b}), \quad (166)$$

or

$$b_k \geq \frac{a_k \bar{b}}{\bar{a}}. \quad (167)$$

This means that

$$\begin{aligned} \frac{c_k}{\bar{c}} &\geq \frac{c_i a_k + c_j \frac{a_k \bar{b}}{a}}{c_i \bar{a} + c_j \bar{b}} \\ &= \frac{a_k}{\bar{a}} \frac{c_i + c_j \frac{\bar{b}}{a}}{c_i + c_j \frac{\bar{b}}{\bar{a}}} = \frac{a_k}{\bar{a}} \end{aligned} \quad (168)$$

which is the ordering in Equation 159. If, instead, $c_k/\bar{c} \leq a_k/\bar{a}$, then similar reasoning implies that $c_k/\bar{c} \geq b_k/\bar{b}$ which is the ordering in Equation 160. We note that a recent set of results for gradients of π_k in Ref. 71, obtained using linear algebraic manipulations on the rate matrix \mathbf{W} , also imply the fixed sign derivative result obtained here and can hence be viewed as a complementary derivation. One can show that Equation 163 further implies that $\frac{\partial \pi_k}{\partial B_{ij}}$ will have a fixed sign across the range of B_{ij} , which is not implied by Ref. 71.

Equation 163 yields another interesting property of $\frac{\partial \pi_k}{\partial \alpha_{ij}}$, which is that the extrema of this derivative occur at precisely the same value of α_{ij} for each node k . Omitting the formulas here, this can be shown by computing the second derivative $\frac{\partial^2 \pi_k}{\partial \alpha_{ij}^2}$ and substituting the linear relations $c_k = (c_j/a_i)a_k + (c_j/a_i)b_k$ and $\bar{c} = (c_j/a_i)\bar{a} + (c_j/a_i)\bar{b}$. One then finds that the zeros of this expression depend on W_{ij} , W_{ji} , (c_i/a_i) , (c_j/a_i) , \bar{a} , and \bar{b} , but not on a_k or b_k . Hence, the solution of $\frac{\partial^2 \pi_k}{\partial \alpha_{ij}^2} = 0$ is independent of k , meaning that every node k in the network has the greatest sensitivity (in the effect of varying α_{ij} on π_k) at the same value of α_{ij} . Because each derivative $\frac{\partial \pi_k}{\partial \alpha_{ij}}$ is of the same functional form for each k and they have extrema at the same location, these curves must be non-intersecting.

Additionally, one can ask the effect of perturbing the edge by directly varying W_{ij} , rather than the anti-symmetric contribution α_{ij} . From Equation 148 we compute (cf. Equation 155)

$$\frac{\partial \pi_k}{\partial W_{ij}} = \frac{x_1 + x_3 W_{ji}}{(\bar{a}W_{ij} + \bar{b}W_{ji} + \bar{c})^2} \quad (169)$$

Because $W_{ji} \geq 0$, the sign of this derivative is determined by x_1 and x_3 and is hence fixed across the range of W_{ij} because x_1 and x_3 are either both positive or both negative. Similar arguments apply to the derivative $\frac{\partial \pi_k}{\partial W_{ji}}$.

C. Finding the derivative signs when $k = i, j$

We have shown that the sign of the derivative $\frac{\partial \pi_k}{\partial \alpha_{ij}}$ is fixed for a given choice of i , j , and k , but in general it is not clear how to find what the fixed sign is. However, for the special case when $k = i$ or $k = j$ (so that the node of interest is part of the controlled edge $j \leftrightarrow i$), it is possible to determine the sign.

If $k = i$, then the ordering in Equation 160 must hold. To show this, we first remember that $b_i = 0$ and that a_i/\bar{a} and c_i/\bar{c} must be non-negative, and hence greater than or equal to b_i/\bar{b} . We also have (cf. Equation 165, no summation of repeated indices implied)

$$\frac{c_i}{\bar{c}} = \frac{c_i a_i + c_j b_i}{c_i \bar{a} + c_j \bar{b}} = \frac{c_i a_i}{c_i \bar{a} + c_j \bar{b}} \leq \frac{a_i}{\bar{a}}, \quad (170)$$

which satisfies the ordering in Equation 160. Hence, $\frac{\partial \pi_k}{\partial \alpha_{ij}} > 0$ if $k = i$. Similar arguments hold to show that $\frac{\partial \pi_k}{\partial \alpha_{ij}} < 0$ if $k = j$. Intuitively this agrees with the idea that increasing the flux directly into node i (out of node j) should increase (decrease) its steady-state probability.

IV. ACTIVE NEMATIC DEFECT CONTROL

A. Equations of motion

Nematic systems are described by a symmetric and traceless tensor

$$\mathbf{Q} = q(\hat{\mathbf{n}}\hat{\mathbf{n}} - \frac{1}{d}\mathbf{I}) \quad (171)$$

where $\hat{\mathbf{n}}$ is a unit director, q quantifies the polarization of the nematic, d is the system dimensionality, and \mathbf{I} is the identity tensor. This order parameter \mathbf{Q} couples to a flow field \mathbf{v} and relaxes along the gradient of a free energy function. We study a simplified version of these physics, taking the overdamped limit and the limit of high substrate friction [47]. We have the equations of motion

$$\partial_t Q_{ij} = S_{ij}(\mathbf{v}) + \Gamma_H H_{ij} \quad (172)$$

$$v_i = \gamma_v^{-1} \partial_k (\sigma_{ik}^a(\mathbf{Q}) + \sigma_{ik}^E(\mathbf{Q})). \quad (173)$$

Here, H_{ij} is the symmetric traceless part of $-\frac{\delta F}{\delta Q_{ij}}$ with F the free energy, S_{ij} is a flow-coupling term, and γ_v is a friction coefficient. In these overdamped dynamics, \mathbf{v} is given instantaneously in terms of \mathbf{Q} so that Equation 172 is closed in \mathbf{Q} . The active and Ericksen stress tensors are [50]

$$\sigma_{ij}^a = -\alpha Q_{ij} \quad (174)$$

$$\begin{aligned} \sigma_{ij}^E = & f \delta_{ij} - \lambda H_{ik} \left(Q_{kj} + \frac{1}{3} \delta_{kj} \right) - \lambda \left(Q_{ik} + \frac{1}{3} \delta_{ik} \right) H_{kj} \\ & + 2\lambda \left(Q_{ij} + \frac{1}{3} \delta_{ij} \right) H_{kl} Q_{kl} - \partial_j Q_{kl} \frac{\delta F}{\delta \partial_i Q_{kl}} \\ & + Q_{ik} H_{kj} - H_{ik} Q_{kj}. \end{aligned} \quad (175)$$

The Landau-de Gennes free energy is

$$F = \int d\mathbf{r} f(\mathbf{r}) \quad (176)$$

where

$$\begin{aligned} f = & \frac{A_0}{2} \left(1 - \frac{U}{3} \right) \text{Tr}(\mathbf{Q}^2) - \frac{A_0 U}{3} \text{Tr}(\mathbf{Q}^3) \\ & + \frac{A_0 U}{4} \text{Tr}(\mathbf{Q}^2)^2 + \frac{L}{2} (\partial_k Q_{lm})^2. \end{aligned} \quad (177)$$

Finally, the flow coupling term is

$$S_{ij}(\mathbf{v}) = -v_k \partial_k Q_{ij} + \Phi_{ik} Q_{kj}^+ + Q_{ik}^+ \Phi_{kj} - 2\lambda Q_{ij}^+ (Q_{kl} \partial_k v_l),$$

where

$$Q_{ij}^+ = Q_{ij} + \frac{1}{3} \delta_{ij}, \quad (178)$$

$$\Psi_{ij} = \frac{1}{2} (\partial_i v_j + \partial_j v_i), \quad (179)$$

$$\Omega_{ij} = \frac{1}{2} (\partial_i v_j - \partial_j v_i), \quad (180)$$

and

$$\Phi_{ij} = \xi \Psi_{ij} - \Omega_{ij}. \quad (181)$$

In these equations, ξ , A_0 , U , Γ_H , γ_v are parameters whose meaning is described in Ref. 50. We set $\xi = 0.7$, $A_0 = 0.1$, $U = 3.5$, $\Gamma_H = 1.5$, and $\gamma_v = 10$ (all in simulation units).

B. Stabilization

Although the update in Equation 8 of the main text provides sufficient information to reconstruct a target defect trajectory, it can also lead to unwanted behavior if not stabilized. In particular, large activity and nematic gradients can cause nucleation of new defects, which we treat as a terminal condition in which the learning dynamics have failed. To prevent this, we stabilize the learning dynamics in three ways:

- We encourage updates to $\alpha(\mathbf{r}, t)$ only in the near vicinity of the defect through an eligibility trace-like field [58] $z(\mathbf{r}, t)$, which evolves during learning as

$$z^{n+1}(\mathbf{r}, t) \leftarrow \lambda_z z^{n+1}(\mathbf{r}, t) + f^n(\mathbf{r}, t)/\bar{f} \quad (182)$$

where $\lambda_z \leq 1$ is a decay factor and $\bar{f} = 0.01$ is scale factor for the free energy density. This eligibility trace multiplies the term $(f^*(\mathbf{r}, t) - f^n(\mathbf{r}, t))$ in Equation 8 of the main text. Because defects correspond to persistent peaks in $f(\mathbf{r}, t)$, the eligibility z will continually be supported near defects and will otherwise decay to zero at a rate $\sim 1/\lambda_z$. We set $\lambda_z = 0.75$ for the results in the main text.

- We only allow learning when the trial defect position is within a certain spatial window of the target defect position. In principle the “zippering” mechanism discussed in SI Section I guarantees convergence for the whole trajectory, because eventually the first part of the trajectory will be learned, after which the second part has the correct starting configuration and can in turn converge, and so on. However, during early learning iterations the activity updates for later parts of the trajectory (when the defect is not close to its target) can lead to unstable spots which can nucleate new defects. On the other hand, when the learning has successfully brought the defect position close to its target, the activity fields can still evolve in general because the two free energy profiles do not match exactly. This effect can also destabilize learning. We thus turn off learning when the defect position is too far (> 5 lattice units) or too close ($< \sqrt{2}$ lattice units) to the target defect position.
- We clamp the local absolute value of activity at $|\alpha(\mathbf{r}, t)|_{\max} = 12$, and we turn off learning when the total absolute activity in the system has passed $\int d\mathbf{r} |\alpha(\mathbf{r}, t)| = 150$.

It remains to explore whether all of these stabilization methods are strictly necessary or whether they could be further refined; we simply found that this combination seems to work well for our test cases.

C. Explanation of the update rule

Here we draw on recent theoretical work [27] to justify the efficacy of Equation 8 in the main text. The authors of Ref. 27 have shown that the approximate velocity of $-1/2$ defect due to a spatially inhomogenous activity field is

$$v_i^- = a \Theta_{ijk} \partial_j \partial_k \alpha. \quad (183)$$

Here,

$$\Theta_{ijk} = \hat{t}_i \hat{t}_j \hat{t}_k - \frac{1}{4} (\delta_{ij} \hat{t}_k + \delta_{kj} \hat{t}_i + \delta_{ik} \hat{t}_j) \quad (184)$$

is a rank-three tensor describing the orientation of a defect which has one of its three legs directed along $\hat{\mathbf{t}} = (\cos(\theta), \sin(\theta))$. The orientation tensor is invariant under $\theta \leftarrow \theta + m2\pi/3$ for any integer m , and it is equal to zero under contraction of any two of its indices. Denoting $g_{ij} = \partial_i \partial_j \alpha$, we can express Equation 183 as

$$\mathbf{v}^- = \mathbf{M} \cdot \mathbf{c} \quad (185)$$

where

$$\mathbf{M} = \frac{1}{4} \begin{pmatrix} g_{xx} - g_{yy} & g_{xy} + g_{yx} \\ -(g_{xy} + g_{yx}) & g_{xx} - g_{yy} \end{pmatrix} \quad (186)$$

and $\mathbf{c} = (\cos(3\theta), \sin(3\theta))$.

Referring to Figure 6E of the main text, if we slightly displace a defect, whose free energy profile is $f(\mathbf{r})$, along a

vector \mathbf{d} , it will have an approximate free energy profile

$$f^*(\mathbf{r}) = f(\mathbf{r} - \mathbf{d}) \approx f(\mathbf{r}) - d_i \partial_i f(\mathbf{r}) + \frac{1}{2} d_i d_j \partial_i \partial_j f(\mathbf{r}). \quad (187)$$

Considering an activity update

$$\alpha(\mathbf{r}, t) \leftarrow \alpha(\mathbf{r}, t) - \eta(f^*(\mathbf{r}, t) - f(\mathbf{r}, t)) \quad (188)$$

we can write for the first iteration (following the initial guess $\alpha(\mathbf{r}, t) = 0$)

$$\alpha(\mathbf{r}, t) = \eta \left(d_i \partial_i f(\mathbf{r}) - \frac{1}{2} d_i d_j \partial_i \partial_j f(\mathbf{r}) \right). \quad (189)$$

Evaluating g_{ij} , we have (setting $\eta = 1$ for simplicity)

$$g_{ij} = d_k \partial_i \partial_j \partial_k f(\mathbf{r}) - \frac{1}{2} d_k d_l \partial_l \partial_k \partial_i \partial_j f(\mathbf{r}). \quad (190)$$

We will evaluate this expression at the location of the defect $\mathbf{r} = \mathbf{0}$ where the free energy profile is maximal and assume that the free energy profile is approximately isotropic [72]. The third order derivatives of $f(\mathbf{r})$ consequently vanish, so that

$$g_{ij}(\mathbf{0}) = -\frac{1}{2} d_k d_l \partial_l \partial_k \partial_i \partial_j f(\mathbf{0}). \quad (191)$$

The only terms which can contribute to this sum are those having even numbers of derivatives with respect to x and y (i.e. $\partial_x^3 \partial_y f(\mathbf{0}) = 0$ but $\partial_x^2 \partial_y^2 f(\mathbf{0}) \neq 0$). For an isotropic function $f(\mathbf{r}) = f(r)$ one can show that $\partial_x^4 f(\mathbf{0}) = \partial_y^4 f(\mathbf{0}) = 3\partial_x^2 \partial_y^2 f(\mathbf{0})$. Denoting $\partial_x^2 \partial_y^2 f(\mathbf{0}) \equiv f'' > 0$ and $\mathbf{d} = d(\cos(\phi), \sin(\phi))$, we evaluate Equation 185

$$\mathbf{v}^- = \frac{1}{4} d^2 f'' \begin{pmatrix} -\cos(2\phi - 3\theta) \\ \sin(2\phi - 3\theta) \end{pmatrix}. \quad (192)$$

Finally, we are interested in the overlap of this defect velocity with the displacement vector \mathbf{d} . We thus compute

$$\mathbf{d} \cdot \mathbf{v}^- = -\frac{1}{4} d^3 f'' \cos(3\psi). \quad (193)$$

where $\psi = \phi - \theta$ is the relative angle between the defect orientation and \mathbf{d} . As f'' is negative, we have that the overlap is proportional to $\cos(3\psi)$.

V. CONNECTION TO IDEAS IN REINFORCEMENT LEARNING

Reinforcement learning (RL) refers to a class of methods in which an agent learns through trial and error how to exert actions on its environment in order to maximize a user-defined reward [58]. Here, we briefly outline the conceptual similarities and differences between techniques which are utilized in standard RL algorithms and those discussed in this paper.

A. States, actions, rewards, and value functions

The standard setting of RL comprises a set of states, a learner which can exert actions on the system, a dynamical rule for the system which maps a state and an action into a new state (either deterministically or stochastically), and a reward function. The reward is determined by the user and in principle is completely arbitrary, although in practice a judicious specification of the reward structure is crucial to a successful RL implementation. Rewards are often chosen to satisfy some criterion of the system, such as to balance a pole against gravity in the famous cart-pole task.

In this paper we consider deterministic dynamics, either operating on probability distributions or on individual average configurations of the system. Actions correspond to time-dependent control fields which drive the system

through non-equilibrium trajectories. In the language of RL, our “reward functions” pose an open-loop, inverse problem in which we want to minimize the difference between the current system trajectory and a given target trajectory. We use both KL divergences and quadratic cost functions in this paper to quantify this difference.

B. Learning the value function

The agent chooses an action according to its current policy, which can be either a stochastic or deterministic function of the current state. RL algorithms optimize the expected reward during training by incrementally improving the policy using new experiences. A standard algorithm for updating a deterministic policy was introduced in Ref. 59. Specifically, for a policy $\mu_{\theta}(s)$, which is a function that maps a state s into an action a and has learnable parameters θ , updates happen according to

$$\theta^{n+1} \leftarrow \theta^n + \eta \nabla_{\theta} Q(s_t, a_t)|_{\theta=\theta^n}. \quad (194)$$

Here, the current state is s_t and the agent has taken action a_t . The function $Q(s, a)$ is called the value function, which reflects the agent’s current estimate of the cumulative reward that it will receive if it takes action a while in state s . It depends implicitly on the parameters θ via the action selection $a = \mu_{\theta}(s)$, and as a result the gradient $\nabla_{\theta} Q(s_t, a_t)$ can be expanded using the chain rule.

Equation 194 is a simple learning rule which increments θ so that it will increase expected reward (as estimated through its learned value function). Clearly, the success of RL will depend on how well $Q(s, a)$ can be learned by the agent. A common approach is to represent $Q(s, a)$ by a parameterized function $Q^{\mathbf{w}}(s, a)$ and to increment its parameters \mathbf{w} , in addition to θ , according to a separate update rule. A standard rule for \mathbf{w} is the semi-gradient temporal difference (TD) scheme [58, 59]

$$\mathbf{w}^{n+1} \leftarrow \mathbf{w}^n + \eta_w (r_t + \gamma Q^{\mathbf{w}}(s_{t+1}, a_{t+1}) - Q^{\mathbf{w}}(s_t, a_t)) \nabla_{\mathbf{w}} Q^{\mathbf{w}}(s_t, a_t)|_{\mathbf{w}=\mathbf{w}^n} \quad (195)$$

where γ is a discount factor, η_w is a learning rate, and r_t is the reward received at time t . The TD approximation in this update rule results from truncating the Bellman equation one timestep into the future (see SI Section V C), and the approximation leading to semi-gradient methods results from neglecting the dependence of $Q^{\mathbf{w}}(s_{t+1}, a_{t+1})$ on the current value of \mathbf{w} . Using this update rule works well in practice, but a practical downside is that it requires separate storage for the parameters \mathbf{w} .

In this context, our methods can be loosely viewed as bypassing the need to separately learn the value function $Q(s, a)$, by replacing $\nabla_{\theta} Q(s_t, a_t)$ in Equation 194 with a prescribed, physically approximated error signal $\sim \Delta^{\text{app}}$. In Equation 195, approximations are used to update the current estimate of the value function, whereas in our approach approximations are used in writing down the gradient of the value function directly. We do assume knowledge of the target trajectory in writing down Δ^{app} , but this information is used in Equation 195 to determine the rewards r_t .

C. Exploiting temporal locality

Both our learning rules and those based on the TD method are temporally local, in that they consider at most a few timesteps and not the entire system trajectory. As mentioned above, updates to the parameters \mathbf{w} of a learned value function $Q^{\mathbf{w}}(s, a)$ exploit temporal locality through the TD error $\delta_t = r_t + \gamma Q^{\mathbf{w}}(s_{t+1}, a_{t+1}) - Q^{\mathbf{w}}(s_t, a_t)$, which will be small if $Q^{\mathbf{w}}(s_t, a_t) \approx r_t + \gamma Q^{\mathbf{w}}(s_{t+1}, a_{t+1})$. This condition is a statement of the Bellman equation, which roughly says that the cumulative expected reward starting at time t is equal to the reward accrued at t plus the discounted cumulative expected reward starting at time $t + 1$. Thus, a converged estimate for the value function will satisfy the Bellman equation and lead to small TD errors.

The justification of temporally local update rules in our method is reminiscent of but slightly different from the Bellman equation. In our inverse problem setup, a perfect gradient would include the effect of updating actions at time $t - 1$ on the loss both at time t and at all future times $t' \geq t$ (cf. Equation 26 above). We avoid the latter contribution because it is non-local and involves backpropagation of errors through time. This is justified because of the zipper mechanism of convergence, outlined in SI Section I. One can view this mechanism as endowing the inverse problem with so-called “optimal substructure,” in which a complex optimality problem (learning the whole trajectory) can be decomposed into a set of optimality sub-problems (learning individual time points or successive differences). By a similar token, the Bellman equation gives optimal substructure to the problem of maximizing the cumulative expected reward, which justifies the TD method of RL. Whereas in TD the optimal substructure allows updating the estimate of the value function using temporally local information, for us the optimal substructure allows

following a physically prescribed value function gradient in a temporally local manner.

-
- [1] Yann LeCun, Yoshua Bengio, and Geoffrey Hinton. Deep learning. *nature*, 521(7553):436–444, 2015.
 - [2] Timothy P Lillicrap, Adam Santoro, Luke Marris, Colin J Akerman, and Geoffrey Hinton. Backpropagation and the brain. *Nature Reviews Neuroscience*, 21(6):335–346, 2020.
 - [3] Menachem Stern and Arvind Murugan. Learning without neurons in physical systems. *Annual Review of Condensed Matter Physics*, 14:417–441, 2023.
 - [4] Timothy P Lillicrap, Daniel Cownden, Douglas B Tweed, and Colin J Akerman. Random synaptic feedback weights support error backpropagation for deep learning. *Nature communications*, 7(1):13276, 2016.
 - [5] Logan G Wright, Tatsuhiro Onodera, Martin M Stein, Tianyu Wang, Darren T Schachter, Zoey Hu, and Peter L McMahon. Deep physical neural networks trained with backpropagation. *Nature*, 601(7894):549–555, 2022.
 - [6] Menachem Stern, Matthew B Pinson, and Arvind Murugan. Continual learning of multiple memories in mechanical networks. *Physical Review X*, 10(3):031044, 2020.
 - [7] Menachem Stern, Daniel Hexner, Jason W Rocks, and Andrea J Liu. Supervised learning in physical networks: From machine learning to learning machines. *Physical Review X*, 11(2):021045, 2021.
 - [8] Sam Dillavou, Menachem Stern, Andrea J Liu, and Douglas J Durian. Demonstration of decentralized physics-driven learning. *Physical Review Applied*, 18(1):014040, 2022.
 - [9] Benjamin Scellier and Yoshua Bengio. Equilibrium propagation: Bridging the gap between energy-based models and backpropagation. *Frontiers in computational neuroscience*, 11:24, 2017.
 - [10] Benjamin Scellier, Anirudh Goyal, Jonathan Binas, Thomas Mesnard, and Yoshua Bengio. Extending the framework of equilibrium propagation to general dynamics. 2018.
 - [11] Menachem Stern, Sam Dillavou, Marc Z Miskin, Douglas J Durian, and Andrea J Liu. Physical learning beyond the quasistatic limit. *Physical Review Research*, 4(2):L022037, 2022.
 - [12] John Bechhoefer. *Control theory for physicists*. Cambridge University Press, 2021.
 - [13] Suraj Shankar, Vidya Raju, and L Mahadevan. Optimal transport and control of active drops. *Proceedings of the National Academy of Sciences*, 119(35):e2121985119, 2022.
 - [14] Grant M Rotskoff, Gavin E Crooks, and Eric Vanden-Eijnden. Geometric approach to optimal nonequilibrium control: Minimizing dissipation in nanomagnetic spin systems. *Physical Review E*, 95(1):012148, 2017.
 - [15] Shamreen Iram, Emily Dolson, Joshua Chiel, Julia Pelesko, Nikhil Krishnan, Özenç Güngör, Benjamin Kuznets-Speck, Sebastian Deffner, Efe Ilker, Jacob G Scott, et al. Controlling the speed and trajectory of evolution with counterdiabatic driving. *Nature Physics*, 17(1):135–142, 2021.
 - [16] Shriram Chennakesavalu and Grant M Rotskoff. Unified, geometric framework for nonequilibrium protocol optimization. *Physical Review Letters*, 130(10):107101, 2023.
 - [17] Todd R Gingrich, Grant M Rotskoff, Gavin E Crooks, and Phillip L Geissler. Near-optimal protocols in complex nonequilibrium transformations. *Proceedings of the National Academy of Sciences*, 113(37):10263–10268, 2016.
 - [18] Avishek Das and David T Limmer. Variational control forces for enhanced sampling of nonequilibrium molecular dynamics simulations. *The Journal of chemical physics*, 151(24), 2019.
 - [19] Tim Schmiedl and Udo Seifert. Optimal finite-time processes in stochastic thermodynamics. *Physical review letters*, 98(10):108301, 2007.
 - [20] Alexandre P Solon and Jordan M Horowitz. Phase transition in protocols minimizing work fluctuations. *Physical review letters*, 120(18):180605, 2018.
 - [21] Luke K Davis, Karel Proesmans, and Étienne Fodor. Active matter under control: Insights from response theory. *Physical Review X*, 14(1):011012, 2024.
 - [22] Megan C Engel, Jamie A Smith, and Michael P Brenner. Optimal control of nonequilibrium systems through automatic differentiation. *Physical Review X*, 13(4):041032, 2023.
 - [23] Shriram Chennakesavalu and Grant M Rotskoff. Probing the theoretical and computational limits of dissipative design. *The Journal of Chemical Physics*, 155(19), 2021.
 - [24] Martin J Falk, Vahid Alizadehyazdi, Heinrich Jaeger, and Arvind Murugan. Learning to control active matter. *Physical Review Research*, 3(3):033291, 2021.
 - [25] Herbert Levine and Daniel I Goldman. Physics of smart active matter: integrating active matter and control to gain insights into living systems. *Soft Matter*, 2023.
 - [26] Nidhi Pashine, Daniel Hexner, Andrea J Liu, and Sidney R Nagel. Directed aging, memory, and nature’s greed. *Science advances*, 5(12):eaax4215, 2019.
 - [27] Suraj Shankar, Luca VD Scharrer, Mark J Bowick, and M Cristina Marchetti. Spatiotemporal control of active topological defects. *arXiv preprint arXiv:2212.00666*, 2022.
 - [28] Andreas Mayer, Vijay Balasubramanian, Aleksandra M Walczak, and Thierry Mora. How a well-adapting immune system remembers. *Proceedings of the National Academy of Sciences*, 116(18):8815–8823, 2019.
 - [29] Oskar H Schnaack, Luca Peliti, and Armita Nourmohammad. Learning and organization of memory for evolving patterns. *Physical Review X*, 12(2):021063, 2022.
 - [30] Avishek Das and David T Limmer. Variational design principles for nonequilibrium colloidal assembly. *The Journal of*

chemical physics, 154(1), 2021.

- [31] Suriyanarayanan Vaikuntanathan and Christopher Jarzynski. Dissipation and lag in irreversible processes. *Europhysics Letters*, 87(6):60005, 2009.
- [32] Jorge Nocedal and Stephen J Wright. *Numerical optimization*. Springer, 1999.
- [33] WT Gózdź and G Gompper. Shape transformations of two-component membranes under weak tension. *Europhysics Letters*, 55(4):587, 2001.
- [34] Neeraj J Agrawal and Ravi Radhakrishnan. Calculation of free energies in fluid membranes subject to heterogeneous curvature fields. *Physical Review E*, 80(1):011925, 2009.
- [35] Joshua Zimmerberg and Michael M Kozlov. How proteins produce cellular membrane curvature. *Nature reviews Molecular cell biology*, 7(1):9–19, 2006.
- [36] Harvey F Lodish. *Molecular cell biology*. Macmillan, 2008.
- [37] Jeremy A Owen, Todd R Gingrich, and Jordan M Horowitz. Universal thermodynamic bounds on nonequilibrium response with biochemical applications. *Physical Review X*, 10(1):011066, 2020.
- [38] Gabriela Fernandes Martins and Jordan M. Horowitz. Topologically constrained fluctuations and thermodynamics regulate nonequilibrium response. *Phys. Rev. E*, 108:044113, Oct 2023.
- [39] Amin Doostmohammadi, Jordi Ignés-Mullol, Julia M Yeomans, and Francesc Sagués. Active nematics. *Nature communications*, 9(1):3246, 2018.
- [40] M Cristina Marchetti, Jean-François Joanny, Sriram Ramaswamy, Tanniemola B Liverpool, Jacques Prost, Madan Rao, and R Aditi Simha. Hydrodynamics of soft active matter. *Reviews of modern physics*, 85(3):1143, 2013.
- [41] Shiladitya Banerjee, Margaret L Gardel, and Ulrich S Schwarz. The actin cytoskeleton as an active adaptive material. *Annual review of condensed matter physics*, 11:421–439, 2020.
- [42] Stephen J DeCamp, Gabriel S Redner, Aparna Baskaran, Michael F Hagan, and Zvonimir Dogic. Orientational order of motile defects in active nematics. *Nature materials*, 14(11):1110–1115, 2015.
- [43] Katherine Copenhagen, Ricard Alert, Ned S Wingreen, and Joshua W Shaevitz. Topological defects promote layer formation in myxococcus xanthus colonies. *Nature Physics*, 17(2):211–215, 2021.
- [44] Yusuf Ilker Yaman, Esin Demir, Roman Vetter, and Askin Kocabas. Emergence of active nematics in chaining bacterial biofilms. *Nature communications*, 10(1):2285, 2019.
- [45] Yonit Maroudas-Sacks, Liora Garion, Lital Shani-Zerbib, Anton Livshits, Erez Braun, and Kinneret Keren. Topological defects in the nematic order of actin fibres as organization centres of hydra morphogenesis. *Nature Physics*, 17(2):251–259, 2021.
- [46] Pau Guillamat, Carles Blanch-Mercader, Guillaume Pernellet, Karsten Kruse, and Aurélien Roux. Integer topological defects organize stresses driving tissue morphogenesis. *Nature materials*, 21(5):588–597, 2022.
- [47] Suraj Shankar, Anton Souslov, Mark J Bowick, M Cristina Marchetti, and Vincenzo Vitelli. Topological active matter. *Nature Reviews Physics*, 4(6):380–398, 2022.
- [48] William TM Irvine, Andrew D Hollingsworth, David G Grier, and Paul M Chaikin. Dislocation reactions, grain boundaries, and irreversibility in two-dimensional lattices using topological tweezers. *Proceedings of the National Academy of Sciences*, 110(39):15544–15548, 2013.
- [49] Ian Linsmeier, Shiladitya Banerjee, Patrick W Oakes, Wonyeong Jung, Taeyoon Kim, and Michael P Murrell. Disordered actomyosin networks are sufficient to produce cooperative and telescopic contractility. *Nature communications*, 7(1):12615, 2016.
- [50] Rui Zhang, Steven A Redford, Paul V Ruijgrok, Nitin Kumar, Ali Mozaffari, Sasha Zemsky, Aaron R Dinner, Vincenzo Vitelli, Zev Bryant, Margaret L Gardel, et al. Spatiotemporal control of liquid crystal structure and dynamics through activity patterning. *Nature materials*, 20(6):875–882, 2021.
- [51] Linnea M Lemma, Minu Varghese, Tyler D Ross, Matt Thomson, Aparna Baskaran, and Zvonimir Dogic. Spatio-temporal patterning of extensile active stresses in microtubule-based active fluids. *PNAS nexus*, 2(5):pgad130, 2023.
- [52] Shreya Chandrasekar, Jordan R Beach, and Patrick W Oakes. Shining a light on rhoa: Optical control of cell contractility. *The International Journal of Biochemistry & Cell Biology*, 161:106442, 2023.
- [53] Carlos Floyd, Suriyanarayanan Vaikuntanathan, and Aaron R Dinner. Simulating structured fluids with tensorial viscoelasticity. *The Journal of Chemical Physics*, 158(5), 2023.
- [54] Carlos Floyd, Aaron R Dinner, and Suriyanarayanan Vaikuntanathan. Signatures of odd dynamics in viscoelastic systems: From spatiotemporal pattern formation to odd rheology. *arXiv preprint arXiv:2210.01159*, 2022.
- [55] Steven Redford, Jonathan Colen, Jordan L Shivers, Sasha Zemsky, Mehdi Molaei, Carlos Floyd, Paul Ruijgrok, Vincenzo Vitelli, Zev Bryant, Aaron Dinner, et al. Motor crosslinking augments elasticity in active nematics. *Soft Matter*, 2024.
- [56] Michael M Norton, Piyush Grover, Michael F Hagan, and Seth Fraden. Optimal control of active nematics. *Physical review letters*, 125(17):178005, 2020.
- [57] Caleb G Wagner, Michael M Norton, Jae Sung Park, and Piyush Grover. Exact coherent structures and phase space geometry of preturbulent 2d active nematic channel flow. *Physical Review Letters*, 128(2):028003, 2022.
- [58] Richard S Sutton and Andrew G Barto. *Reinforcement learning: An introduction*. MIT press, 2018.
- [59] David Silver, Guy Lever, Nicolas Heess, Thomas Degris, Daan Wierstra, and Martin Riedmiller. Deterministic policy gradient algorithms. In *International conference on machine learning*, pages 387–395. Pmlr, 2014.
- [60] Miguel A Carreira-Perpinan and Geoffrey Hinton. On contrastive divergence learning. In *International workshop on artificial intelligence and statistics*, pages 33–40. PMLR, 2005.
- [61] Yunmei Chen and Xiaojing Ye. Projection onto a simplex. *arXiv preprint arXiv:1101.6081*, 2011.
- [62] Lars Onsager and Stefan Machlup. Fluctuations and irreversible processes. *Physical Review*, 91(6):1505, 1953.

- [63] Juan MR Parrondo. Reversible ratchets as brownian particles in an adiabatically changing periodic potential. *Physical Review E*, 57(6):7297, 1998.
- [64] Ken Funo, Neill Lambert, Franco Nori, and Christian Flindt. Shortcuts to adiabatic pumping in classical stochastic systems. *Physical Review Letters*, 124(15):150603, 2020.
- [65] David A Sivak and Gavin E Crooks. Thermodynamic metrics and optimal paths. *Physical review letters*, 108(19):190602, 2012.
- [66] Patrick R Zulkowski, David A Sivak, Gavin E Crooks, and Michael R DeWeese. Geometry of thermodynamic control. *Physical Review E*, 86(4):041148, 2012.
- [67] John G Kirkwood. The statistical mechanical theory of transport processes I. General theory. *The Journal of Chemical Physics*, 14(3):180–201, 1946.
- [68] Gavin E Crooks. Measuring thermodynamic length. *Physical Review Letters*, 99(10):100602, 2007.
- [69] O Mazonka and C Jarzynski. Exactly solvable model illustrating far-from-equilibrium predictions. *arXiv preprint cond-mat/9912121*, 1999.
- [70] R Van Zon and EGD Cohen. Stationary and transient work-fluctuation theorems for a dragged Brownian particle. *Physical Review E*, 67(4):046102, 2003.
- [71] Timur Aslyamov and Massimiliano Esposito. Nonequilibrium response for markov jump processes: Exact results and tight bounds. *Physical Review Letters*, 132(3):037101, 2024.
- [72] Shuang Zhou, Sergij V Shiyankovskii, Heung-Shik Park, and Oleg D Lavrentovich. Fine structure of the topological defect cores studied for disclinations in lyotropic chromonic liquid crystals. *Nature Communications*, 8(1):14974, 2017.